POLISH MARITIME RESEARCH

No 4(67)   2010   Vol 17

CONTENTS

POLISH MARITIME RESEARCH

in internet
www.bg.pg.gda.pl/pmr/pmr.php

Editorial

POLISH MARITIME RESEARCH is a scientific journal of worldwide circulation. The journal appears as a quarterly four times a year. The first issue of it was published in September 1994. Its main aim is to present original, innovative scientific ideas and Research & Development achievements in the field of :

Engineering, **Computing & Technology**, **Mechanical Engineering**,

which could find applications in the broad domain of maritime economy. Hence there are published papers which concern methods of the designing, manufacturing and operating processes of such technical objects and devices as : ships, port equipment, ocean engineering units, underwater vehicles and equipment as well as harbour facilities, with accounting for marine environment protection.

The Editors of POLISH MARITIME RESEARCH make also efforts to present problems dealing with education of engineers and scientific and teaching personnel. As a rule, the basic papers are supplemented by information on conferences , important scientific events as well as cooperation in carrying out international scientific research projects.

Scientific Board

The modeling of seakeeping qualities of Floating Production, Storage and Offloading (FPSO) sea-going ships in preliminary design stage

Tomasz Cepowski, Assoc. Prof.
Szczecin Maritime University

ABSTRACT

This paper presents an analysis of a presently applied approach to accounting for seakeeping qualities of FPSO sea-going ships and possible using it in preliminary design stage. Approximations of heaving, pitching, green water ingress on the deck and slamming of FPSO ships, based on main ship design and wave parameters, are presented. The approximations were elaborated with the use of the linear regression method and theory of artificial neural networks for a very wide range of FPSO ship dimensions and hull forms. In the investigations ship operational conditions were limited to those occurring in real service of FPSO ships, described by means of the so called operational scenario. Such approach made it possible to reach simultaneously high approximation accuracy and simple structure of mathematical model.

Keywords: Floating Production; Storage and Offloading (FPSO) unit; offshore; design; preliminary design stage; seakeeping qualities; green water ingress on the deck; slamming; heaving; pitching; main ship hull dimensions

INTRODUCTION

In [10] a classification of transport ships with accounting for their seakeeping qualities has been proposed. According to it transport ships can be split into the following groups [10]:
- ships which are to fulfil their mission irrespective of weather conditions,
- ships of design features which increase their susceptibility to weather conditions,
- passenger carrying ships,
- transport ships for which seakeeping qualities are only one of their limitations.

For each of the groups crucial seakeeping qualities can be determined and on their basis a type of ship which represents a given group can be selected. In [10] attention has been focussed on the group of passenger carrying ships, and design guidelines which account for selected seakeeping qualities possible to be applied in the preliminary design stage of car passenger ferries, have be described.

However in this publication was considered only the group of ships which are to fulfil their mission irrespective to weather conditions, that constitute characteristic feature of the group of ships.

The following kinds of ships can be numbered among the group in question:
1. naval ships (surface ones),
2. sea bed mining industry units such as:
   a. FPSO (Floating Production, Storage and Offloading) units,
   b. FSO (Floating Storage and Offloading) units,
   c. underwater pipe laying ships,
   d. auxiliary servicing ships,
3. research ships,
4. servicing ships:
   a. floating bases,
   b. rescue ships,
5. fishing ships:
   a. fish factory trawlers.

From the point of view of design problems ships of the group are to be characterized by suitable seakeeping qualities in heavy weather and such operational conditions in which the ships have to operate.

The design problems of the group of ships result from functions assigned to them, and seakeeping qualities are only technical limitations to be satisfied by them. From the point of view of modeling seakeeping qualities the crucial problem for ships of the kind is:
- to minimize ship hull vertical motions,
- to minimize rolling motions.

Out of all oscillating motions of ships of the kind, pitching and heaving is first of all controlled since the motions are main cause of ship hull vertical motions.

The necessity of limiting the ship hull vertical motions results from other detrimental phenomena accompanying them, among which the following can be numbered:

1. green water ingress on the deck, causing failure to deck gear,
2. slamming - causing failure to hull bottom elements and generating ship hull shocks and vibrations,
3. accelerations which have influence on:
   - worsened operational effectiveness of devices on the deck (helicopter, production equipment, cranes, sounds, drilling rigs etc),
   - ship weapon systems,
   - operation of weapon monitoring and control systems,
   - underwater operations, e.g. lowering the diving bell,
4. sea-sickness of crew members.

Moreover for some ships of the group, rolling motions which may cause worsening operational effectiveness of certain shipboard devices (helicopter, deck gear etc) are of importance.

For all ships of the group seakeeping qualities usually constitute only a design limitation, however for naval and FPSO ships the qualities are an important design problem. For such ships, in accordance with **[36]**, wave intensity is classified with a view of possibility of fulfiling selected functions of the ships.

For naval ships three levels of sea wave conditions are defined [36]:

1. the conditions in which the ship is capable of operating with ultimate effectiveness at maximum speed,
2. heavy weather conditions in which reduction of ship speed occurs but helicopter landing pad and weapon systems are still capable of operating,
3. the conditions in which the ship should only to survive.

And, for FPSO ships two levels of sea wave conditions are defined [36]:

1. the conditions in which operation (production) is possible,
2. the conditions in which operation is not possible (production is stopped).

From the point of view of ship design problems this is FPSO ship which represents the group of ships.

SEAKEEPING QUALITIES OF FPSO SHIPS

FPSO ships are to operate in arbitrary environmental conditions without possibility of avoidance of storm zone and to be towed for repair. Therefore FPSO ships are required to have a.o. good seakeeping qualities that favourably influence the following [34]:

- crew comfort and safety,
- operational efectiveness of production systems,
- operational effectiveness of process of reloading to shuttle tanker,
- possibility of using helicopter.

Out of all seakeeping qualities important for the considered group of ships the following may be numbered among the crucial ones for FPSO ships:

- pitching and heaving,
- slamming,
- green water ingress on the deck.

Factors conductive to ocurrence of such phenomena are first of all the following:

- large vertical motions resulting from ship length and unfavourable angle of wave encounter with ship,
- continuously changeable draught and trim of FPSO ship,
- heavy weather conditions.

Formal requirements for designing FPSO ships concern first of all problems associated with their construction and are formulated in [34]:

- NORSOK standards (initiated by Norwegian mining industry), first of all NORSOK Standard N-004: *Design of Steel Structures* [29],
- ISO /WD 19904 Standard: *Offshore Structures - Floating Systems*,
- rules of the classification institutions:
  - Lloyds Register of Shipping (LR): *Rules and Regulations for the Classification of a Floating Installation at a Fixed Location*, July 1999 [25],
  - American Bureau of Shipping: *Guide for Building and Classing Facilities on Offshore Installations*, June 2000 [1]
  - Det Norske Veritas (DNV): *Offshore 2000 Rules for Classification of Floating Production and Storage Units*, OSS -102, January 2001 [13].

The above mentioned requirements are compared to each other in the report [22]. The classification rules which deal with the accounting for seakeeping qualities are very general and do not make it possible to take into account sea wave conditions. As results a. o. from the report [30] the formal design reccomendations dealing with green water ingress on the deck and slamming on FPSO ships are not sufficient.

Data and research results on modeling seakeeping qualities of FPSO ships are very scarce. The research results given in [4, 5, 6, 9, 3, 15, 18, 19, 20, 21, 22, 26, 27, 28, 31, 32, 34, 37, 38, 39] cover only a small group of ships and deal first of all with influence of form of selected hull parts of FPSO ships on a given phenomenon.

The classification institutions reccommend to determine seakeeping qualities of FPSO ships on the basis of model tests [1, 13, 25, 34]. If to perform such tests is not possible the institutions propose to apply simplified methods to calculation of selected seakeeping qualities.

Informal design reccommendations are limited first of all to performing the tests on slamming and green water ingress on the deck for a given ship. In the tests a relation is searched for between waving, ship's hull form parameters and e.g. freeboard height and loads resulting from slamming or green water ingress on the deck. Results of the tests do not take into account impact of general geometrical parameters on the phenomena hence they cannot be accounted for in the preliminary stage of ship design.

On the basis of [4, 5, 6, 9, 3, 15, 18, 19, 20, 21, 22, 26, 27, 28, 31, 32, 34, 37, 38, 39] it can be stated that the performed research investigations and formal design reccommendations (given in the classification rules):

- can be used for modeling FPSO ship's hull form and construction in the design stage when ship's dimensions and general hull form (its over and under water parts) have been already determined,
- are not applicable in the preliminary design stage,
- only partly take into account operational conditions in which ship operates (sea waving, motion parameters),

- do not make it possible to predict occurrence probability or frequency of a given phenomenon depending on main ship design parameters and wave parameters occurring in a given water area in heavy weather conditions.

There is a particularly scarce amount of information (or even lack of it) on guidelines concerning calculations of occurrence frequency of green water ingress on the deck and excessive slamming.

The existing design guidelines make it possible to calculate only natural heave and pitch frequencies and to estimate on the basis seakeeping qualities of FPSO ship sailing in a given water area.

AIM OF THE INVESTIGATIONS

The investigations in question have been aimed at elaboration of novel methods of modeling seakeeping qualities of FPSO sea-going ships in the preliminary design stage, i.e. elaboration of approximation functions of:
1. significant amplitudes of heave and pitch motions and occurrence probability of bow slamming and green water ingress on the deck fore on the basis of design parameters avaliable in the preliminary (parametrical) design stage, and sea wave parameters as well,
2. characteristic wave periods at which maximum significant amplitudes of heave and pitch motions as well as occurrence frequencies of slamming and green water ingress on the deck occur depending on FPSO ship's design parameters available in the preliminary design stage, under assumed ship operation conditions.

It was assumed that the above mentioned aim will be reached by analyzing results obtained from numerical calculations of ship motions in waves in conventional operational conditions described by means of operational scenarios. In order to make it possible a supplementary aim of the research, consisting in determination of an appropriate operational scenario for FPSO ship, has been formulated.

RESEARCH METHOD

The general research method covered the following items (Fig. 1):
1. Elaboration of model ship hull variants covering a wide range of their forms and dimensions,
2. Elaboration of operational scenarios describing the most characteristic operational conditions of the ships in service,
3. Simplification of a physical model and its parametrization,
4. Calculation of model values of seakeeping qualities by using numerical methods based on the plane flow hypothesis,
5. Choice of approximation functions for the set of discrete results from numerical model,
6. Verification and assessment of definite modeling methods,
7. Determination of applicability range and limitations for particular models.

OPERATIONAL SCENARIO

The following operational scenario was assumed in the investigations:

A FPSO ship stays on oil field in storm conditions and production process is under way on it (the ship's draught is permanently changing).
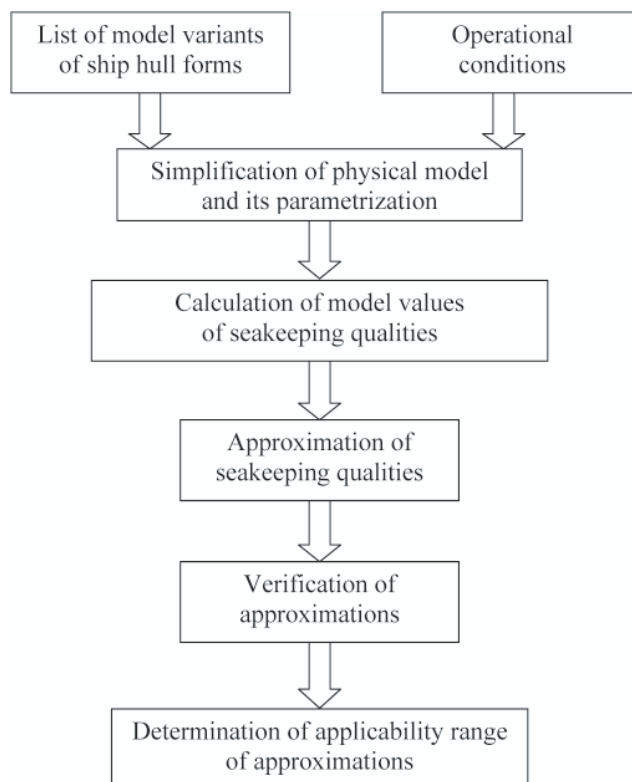
Fig. 1. *General algorithm of modeling ship seakeeping qualities*

Because of possible change in course angle the ship heads the wave (180° wave encounter angle). In such position influence of waves on loads exerted to mooring system and mining installation is the smallest.

The occurring sea waves is not fully developed and can be desrcied by means of the JONSWAP wave spectrum of the highest amplification factor. The wave complies with the so called design wave conditions decribed in [29]. The wave is of the most unfavourable characteristic period and generates maximum values of heave and pitch motions, slamming and green water ingress on the deck fore.

The above defined scenario can be described by the following parameters:
- ship speed: $v = 0$ m/s,
- wave encounter angle: $\beta = 180^\circ$ (head wave),
- wave spectrum: JONSWAP with amplification factor: $\gamma = 3.3$,
- significant wave height $H_s = 12 \div 17$ m,
- characteristic wave period generating maximum values of heave and pitch motions, slamming and green water ingress on the deck fore,
- ship draught $d = \frac{1}{4} d_{max} \div d_{max}$, every $\frac{1}{4} d_{max}$.

The model values of seakeeping qualities were calculated by means of numerical methods and the SEAWAY software based on the plane flow theory. To calculate hydrodynamical coeffcients the method described in [16] was applied. The accuracy tests of the SEAWAY software presented in the report [23] show high accuracy of calculations made with its help.

To approximate maximum significant amplitudes or occurrence frequencies of assumed seakeeping qualities the following set of explicating variables was assumed; it was consisted of:
- ship hull design parameters within a wide range of its dimensions,
- wave parameters resulting from the assumed operational scenario.
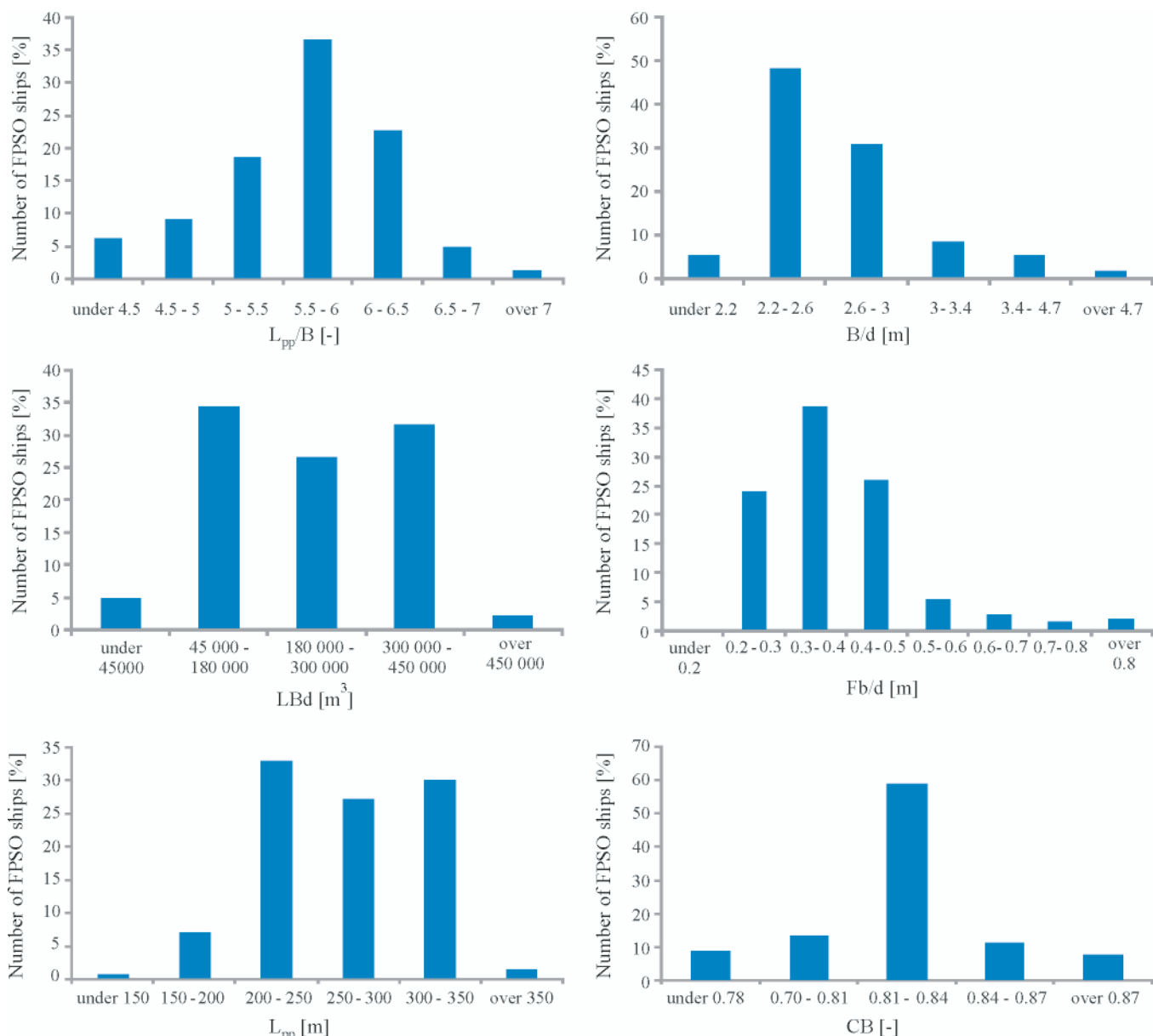
Fig. 2. *Percentage number of new-built FPSO ships depending on the hull block coefficient CB[2], length between perpendiculars L$_{pp}$, freeboard height – ship draught ratio Fb/d, volume LBd, ship breadth – draught ratio B/d, ship length b.p. – breadth ratio Lpp/B, respectively*

SHIP HULL DESIGN PARAMETERS

In Fig. 2 are presented histograms of percentage amounts of new-built FPSO ships of determined geometrical parameters, elaborated with the use of the Lloyd Register[1] data base. The histograms concern only FPSO ships under building, i.e. in the design, production or operational stage.

In the modeling of seakeeping qualities the following ranges for hull geometrical parameters were assumed in accordance with Fig. 2:

- for LBd volume = 45 000, 176 667, 308 333, 440 000 m³,
- for L/B ratio = 4, 5, 6, 7,
- for B/d ratio = 2.18, 3.02, 3.86, 4.7.

Also, the hull forms typical for FPSO ship, characterized by the block coefficient values in the range CB = 0.81 ÷ 0.87, were assumed. The hull forms are presented in Fig. 3, and the general hull form coefficients - in Tab. 1.

Tab. 1. *Hull form variants of FPSO ship, where: **CB** – block coefficient of hull underwater part, **CB$_{(L)}$** – longitudinal prismatic coefficient of hull underwater part, **CB$_{(V)}$** – vertical prismatic coefficient of hull underwater part, **CWL** – waterplane coefficient, **XF** – distance from waterplane geometrical centre to aft perpendicular, related to ship length b.p., **XB** – distance from buoyancy centre to aft perpendicula, r related to ship length b.p., **WC** – percentage length of midship body, related to ship length b.p., **CBA** – block coefficient of hull aft underwater part, **CBF** – block coefficient of fore underwater part*

Variant No.	CBA [-]	CBF [-]	WC [%]	CWL [-]	XF [%]	CB [-]	XB [%]	CB$_{(L)}$ [-]	CB$_{(V)}$ [-]
1	0.73	0.78	35	0.91	50.3	0.83	52.5	0.84	0.92
2	0.74	0.73	55	0.93	46.9	0.87	49.2	0.88	0.94
3	0.74	0.50	55	0.88	44.1	0.81	46.4	0.82	0.93

---

[1] [2] www.sea-web.com, Lloyds Register of Shipping: Sea-web's Ships Database

Variant 1
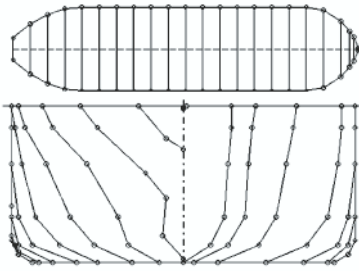
Variant 2
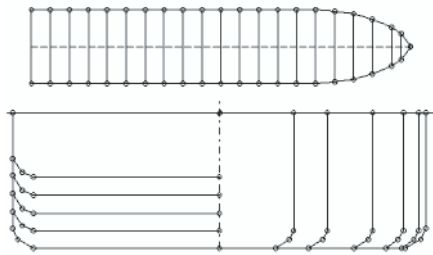
Variant 3
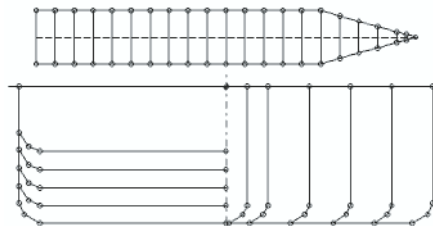
Fig. 3. Variants of FPSO ship's hull form

As results from subject-matter literature, the freeboard height F_b greatly influences intensity of green water ingress on the deck. Therefore it has been decided to examine the freeboard influence on green water ingress on the deck for the wide range of the freeboard height – ship draught ratio: $F_b/d = 0.25, 0.5, 0.75, 1.0, 1.5$.

A specially characteristic feature of FPSO ships is permanently changeable loading state resulting first of all from changeable mass of loads and ballast in consequence of conducted production and reloading processes. This generates changes in buoyancy, draught, trim and hydrostatic parameters of ship's hull.

Since the assumed seakeeping qualities are first of all influenced by ship draught, only mean draught change was taken into account out of all parameters which describe ship loading state. Change in the mean draught d was expressed in the form of its relation to the design draught d_k: $d/d_k = 0.25$, 0.5, 0.75.

Change in draught affects change in freeboard height.

On the basis of the above given assumptions was elaborated a set of 192 variants of forms and dimensions of underwater hull part, for which hull body lines were designed. For each of the hull variants four loading states described by mean draught values and five additional variants accounting for the effect of the freeboard height – ship draught ratio, were prepared.

WAVE PARAMETERS

To calculate the model seakeeping qualities the following wave parameters resulting from the assumed operational scenario, were taken:
- JONSWAP wave spectrum, and amplification factor $\gamma = 3.3$,

- values of the significant wave height H_s = 12, 15, 17 m,
- values of the characteristic wave period $\bar{T}_l$ in the range from 2 to 20 s, every 0,5 s.

In the operational scenario it was assumed to account for occurrence of maximum values of seakeeping qualities depending on characteristic wave period. In consequence of such assumption the characteristic wave period has been eliminated from the set of explicating variables. Hence to approximate significant amplitudes and occurrence frequencies of the assumed seakeeping qualities only the significant wave height H_s was selected out of all the wave parameters.

ELABORATION OF APPROXIMATION FUNCTIONS FOR THE ASSUMED SEAKEEPING QUALITIES OF FPSO SHIPS AND ASSESSMENT OF THEIR ACCURACY

By making use of statistical methods and the theory of artificial neural networks a set of approximation functions was elaborated for the assumed seakeeping qualities of FPSO ships. At first approximations were searched for in the form of analytical functions elaborated with the use of linear regression in the domain of functions of the simplest forms. In the case when an elaborated model has appeared too little accurate analytical relationships were searched for by using the theory of artificial neural networks. As results from the investigations the approximations of heaving, pitching and occurrence frequencies of green water ingress on the deck fore, elaborated with the use of linear regression were rather accurate. Consequently was elaborated a set of analytical relationships which make it possible to approximate the following quantities:
- the maximum significant heave amplitudes:

$$z_{1/3max} = H_S \left(0.668 - 1.71 \cdot 10^{-6} \cdot L_{pp}^{\;2} + \right.$$
$$\left. + 1.8 \cdot 10^{-9} \cdot L_{pp}^{\;3} + 0.001 \cdot d - \frac{0.23}{CBF^2} + \frac{0.09}{CBF^3} \right) \quad (1)$$

where:
$x_{1/3\,max}$ – maximum significant heave amplitudes [m],
H_S – significant wave height [m],
L_{pp} – ship length between perpendiculars [m],
d – ship draught [m],
CBF – block coeffcient of fore part of underwater hull [-],

- the maximum significant pitch amplitudes:

$$\Psi_{1/3max} = H_S \left(0.007 + \frac{136.3}{L_{pp}} - 15.09 \frac{CBF}{d} + \right.$$
$$\left. + 11.28 \frac{CBF^2}{d} + 0.09 \frac{L_{pp}}{d^2} \right) \quad (2)$$

where:
$\Psi_{1/3\,max}$ – maximum significant pitch amplitudes [°].

- the maximum occurrence frequency of green water ingress on the deck fore:

$$n_{zp.max} = \exp \left[6.71 + \left(-0.122 - \frac{19.3}{H_s^{\;2}} \right) \cdot Fb \right] \quad (3)$$

where:
$n_{zp.max}$ – maximum occurrence frequency of green water ingress on the deck fore per one hour [l/h],
Fb – freeboard height at bow [m],
H_s – significant wave height [m].

In Tab. 2 are presented selected statistical parameters describing the above given relationships, and in Fig. 4 through 7 – the approximations are compared with the model values. As results from the above given data the elaborated approximations are very accurate. The seakeeping qualities described by the relationships (1) and (2) are greatly influenced by the ship length between perpendiculars, L_{pp}, and significant wave height H_s. Hence they were simplified to the following form:

$$z_{1/3max} = H_S\left(0.47 - 8.33 \cdot 10^{-7} \cdot L_{pp}^2\right) \quad (4)$$

$$\Psi_{1/3max} = H_S\left(-0.043 + \frac{92.15}{L_{pp}}\right) \quad (5)$$

In Tab. 2 are presented selected statistical parameters decribing the above given relationships, and in Fig. 4 through 8 the approximations are compared with the model values. The approximations (4) and (5) are characterized by a lower accuracy as compared with the approximations (1) and (2), but they are based only on the significant wave height and ship's length between perpendiculars.

And, the approximation (3) is characterized by a high correlation, but large values of the frequency of green water ingress on the deck produce a relatively large value of estimation standard error. To solve the problem was elaborated an artificial neural network which predicts occurrence probability of green water ingress on the deck, expressed in the form of the two-state variable Ω_n of the two values:
- „1" – assigned when the occurrence probability of green water ingress on the deck exceeds its dangerous threshold equal to 0.05 (acc. the recommendations given in [24]),
- „2" – assigned when the occurrence probability of green water ingress on the deck does not exceed its dangerous threshold equal to 0.05.

The above described network is presented graphically in Fig. 12c, and analytically expressed by means of the following relationship:

$$\Omega_{zp} = \frac{1}{1+e^{-\left(\left(\left[F_b \cdot \frac{100 \cdot F_b}{d} \cdot L_{pp} \cdot C_B \cdot H_S\right] \times S + P\right) \times A - B\right)}} \times$$
$$\times C + 0.05 \quad (6)$$

where:
Ω_{zp} – two-state nominal variable which describes occurrence probability of green water ingress on the deck: „1" – if the green water ingress on the deck exceeds its dangerous threshold, and „2" – if it does not exceed its dangerous threshold,
d – ship draught [m],
C_B – block coefficent of hull underwater part,

A – matrix of weighing factors:

$$\begin{bmatrix} 0.616 & 13.521 & -19.178 & -18.131 & 16.863 \\ 4.472 & -0.799 & 3.924 & -0.412 & 2.459 \\ 3.038 & -0.144 & 4.114 & -4.835 & -1.001 \\ -1.695 & -9.208 & 6.682 & 2.450 & 0.476 \\ -1.684 & -2.051 & 0.956 & 2.240 & -4.404 \end{bmatrix}$$

S – matrix of coefficients:

$$\begin{bmatrix} 0.024 & 0 & 0 & 0 & 0 \\ 0 & 0.008 & 0 & 0 & 0 \\ 0 & 0 & 0.003 & 0 & 0 \\ 0 & 0 & 0 & 5.931 & 0 \\ 0 & 0 & 0 & 0 & 0.200 \end{bmatrix}$$

B – vector of threshold values:
[1.956 -3.126 7.385 -5.794 5.793],
C – column vector of weighing factors:
[7.772 -12.540 -14.094 -11.717 6.419],
P – vector of displacement values:
[-0.010 -0.198 -0.332 -4.201 -2.400].

The classifying statistics presented in Tab. 3 indicate that the network is of very high capability of predicting.

Tab. 2. Statistical parameters of the elaborated relationships, where: $z_{1/3\,max}$ – maximum significant heave amplitude, $\Psi_{1/3\,max}$ – maximum significant pitch amplitude, $n_{zp.max}$ – maximum occurrence frequency of green water ingress on the deck, per one hour

Parameter	No. of equation	Determination coefficient R^2	Estimation standard error
$z_{1/3\,max}$	(1)	0.98	0.07 [m]
$\Psi_{1/3\,max}$	(2)	0.92	0.51 [°]
$n_{zp.max}$	(3)	0.98	31 [l/h]
$z_{1/3\,max}$	(4)	0.94	0.12 [m]
$\Psi_{1/3\,max}$	(5)	0.84	0.69 [°]

Tab. 3. Statistics for artificial neural network classification problems in predicting the function values Ω_{zp}

Number of	Teaching set		Validating set		Testing set	
	$\Omega_{zp}=1$	$\Omega_{zp}=2$	$\Omega_{zp}=1$	$\Omega_{zp}=2$	$\Omega_{zp}=1$	$\Omega_{zp}=2$
Total	7280	720	1616	144	1614	146
correct cases	7026	694	1567	141	1564	141
erroneous cases	254	26	49	3	50	5
Erroneous cases [%]	3.49	3.61	3.03	2.08	3.10	3.42
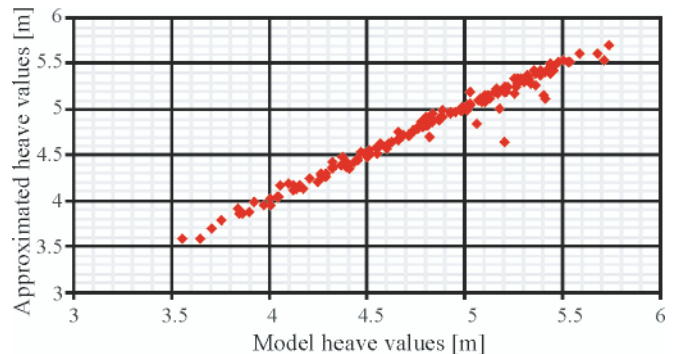
Fig. 4. Comparison of approximations of maximum significant heave amplitudes calculated by using Eq. 1, with their model values, for the significant wave height Hs = 12 m
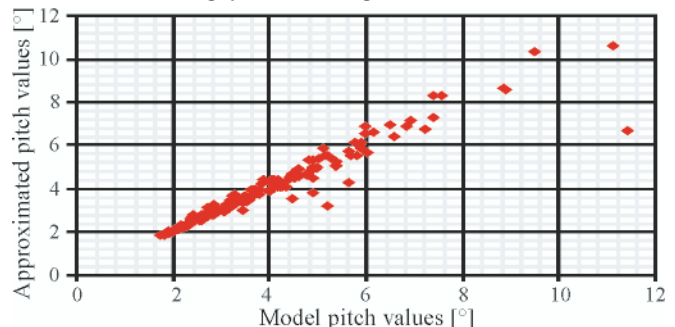
Fig. 5. Comparison of approximations of maximum significant pitch amplitudes calculated by using Eq. 2, with their model values, for the significant wave height Hs = 12 m
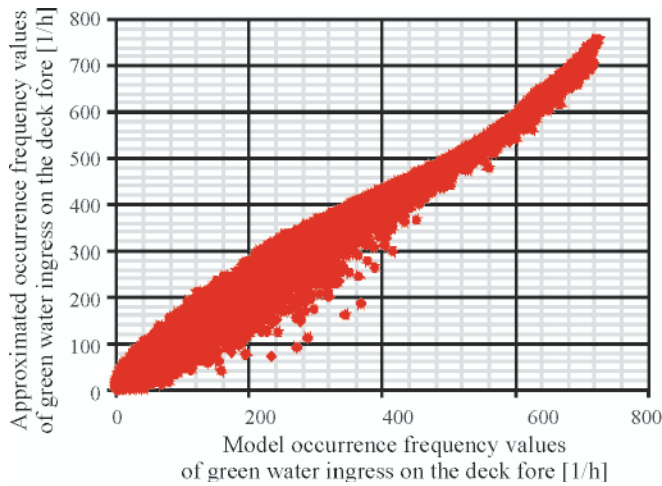
Fig. 6. Comparison of maximum occurrence frequencies of green water ingress on the deck fore with their model values
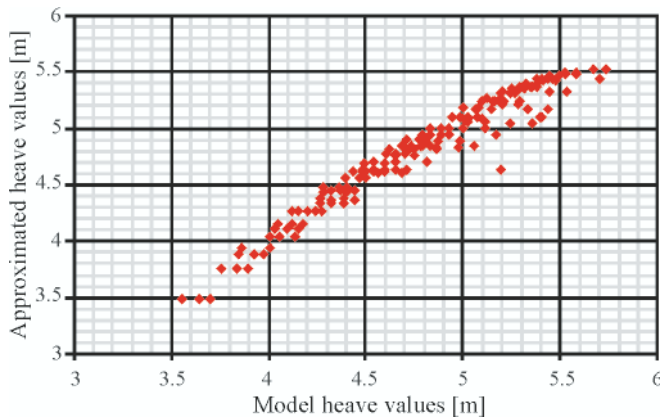
Fig. 7. Comparison of approximations of maximum significant heave amplitudes calculated by using Eq. 4, with their model values, for the significant wave height Hs = 12 m
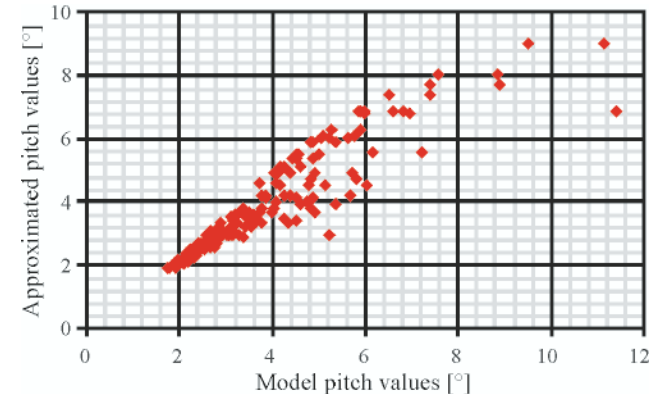
Fig. 8. Comparison of approximations of maximum significant pitch amplitudes calculated by using Eq. 5, with their model values, for the significant wave height Hs = 12 m

The approximations of:
- slamming occurrence frequencies,
- characteristic wave period at which maximum frequency of green water ingress on the deck occurs,
- characteristic wave period at which maximum slamming frequency occurs, elaborated by using the linear regression method, appeared not sufficiently accurate.

Just the use of the theory of artificial neural networks enabled to solve the problem. As a result of the investigations were elaborated the artificial neural networks of multi-layer perceptron structure, which made it possible to approximate:
- maximum occurrence frequencies of bow slamming:

$$n_{sl.max} = \qquad (7)$$

$$= H_S \cdot \frac{\dfrac{1}{1 + e^{-\left(\left(\left[d. \; CBF. \; L_{pp}\right] \times S + P\right) \times A - B\right)}} \times C + 0.009}{3.72 \cdot 10^{-3}}$$

where:
$n_{sl.max}$ – maximum occurrence frequency of bow slamming per one hour [l/h],
CBF – block coefficient of hull fore underwater part,
A – matrix of weighing factors values:

$$\begin{bmatrix} -0.489 & -1.994 & -4.747 \\ 0.180 & 7.268 & -4.653 \\ -6.218 & -8.546 & -7.206 \end{bmatrix}$$

S – matrix of coefficients:

$$\begin{bmatrix} 0.046 & 0 & 0 \\ 0 & 3.571 & 0 \\ 0 & 0 & 0.003 \end{bmatrix}$$

B – vector of threshold values:
$$[1.542 \quad 7.755 \quad 0.385]$$
C – column vector of weighing factors values:
$$[-1.268 \quad 5.999 \quad 4.581]$$
P – vector of displacement values:
$$[-0.324 \quad -1.786 \quad -0.390]$$
- characteristic wave period at which maximum frequency of green water ingress on the deck fore occurs:

$$T_{nzp} = \qquad (8)$$

$$= 10.5 \left(\frac{1}{1 + e^{-\left(\left(\left[WC. \; L_{pp}. \; \frac{XF \cdot 100}{L_{pp}}. \; CB. \; CM. \; GM_L\right] \times S + P\right) \times A - B\right)}} \times \right.$$

$$\left. \times C - 0.379 \right)$$

where:
T_{nzp} – characteristic wave period at which maximum frequency of green water ingress on the deck occurs [s],
CB – block coefficient of hull underwater part [-],
CM – midship section coefficient [-],
GM_L – initial longitudinal metacentric height [m],
XF – abscissa of logitudinal centre of floatation relative to aft perpendicular [m],

A – matrix of weighing factors values:

$$\begin{bmatrix} 0.650 & -0.632 & -0.506 & 0.650 & -0.632 & -0.506 \\ -0.076 & 2.127 & 0.894 & -0.076 & 2.127 & 0.894 \\ -0.428 & 1.090 & 0.964 & -0.428 & 1.090 & 0.964 \\ -0.270 & -0.799 & -1.208 & -0.270 & -0.799 & -1.208 \end{bmatrix}$$

S – matrix of coeffcients:

$$\begin{bmatrix} 0.005 & 0 & 0 & 0 & 0 & 0 \\ 0 & 0.003 & 0 & 0 & 0 & 0 \\ 0 & 0 & 0.106 & 0 & 0 & 0 \\ 0 & 0 & 0 & 5.931 & 0 & 0 \\ 0 & 0 & 0 & 0 & 54.945 & 0 \\ 0 & 0 & 0 & 0 & 0 & 3.26 \; 10^{-4} \end{bmatrix}$$

B – vector of threshold values:
[-1.435   0.467   -0.378]

C – column vector of weighing factors values:
[2.260   2.510   -2.920]

P – vector of displacement values:
[-0.189   -0.332   -4.689   -4.201   -53.670   -0.024].

- characteristic wave period at which maximum slamming frequency occurs:

$$T_{nsl} = \qquad (9)$$

$$=8.5\left(\frac{1}{1+e^{-\left(\left(\left[L_{pp}. \quad B. \quad \frac{XF\cdot100}{L_{pp}}. \quad CM. \quad BM_L\right]\times S+P\right)\times A-B\right)}}\times\right.$$

$$\left.\times\,C + 0.795\right)$$

where:

T_{nsl} – characteristic wave period at which maximum slamming frequency occurs [s],

BM_L – longitudinal metacentric radius [m],

A – matrix of weighing factors values:

$$\begin{bmatrix} 1.328 & -1.701 & 0.452 & 1.311 & 1.328 \\ 0.483 & 1.538 & -1.757 & -0.836 & 0.483 \\ 1.002 & 1.360 & 2.847 & 3.509 & 1.002 \\ -5.255 & 1.152 & 2.192 & 2.470 & -5.255 \\ -3.132 & -1.427 & 7.693 & 4.662 & -3.132 \end{bmatrix}$$

S – matrix of coefficients:

$$\begin{bmatrix} 0.0029 & 0 & 0 & 0 & 0 \\ 0 & 0.018 & 0 & 0 & 0 \\ 0 & 0 & 0.106 & 0 & 0 \\ 0 & 0 & 0 & 54.645 & 0 \\ 0 & 0 & 0 & 0 & 2.65\ 10^{-4} \end{bmatrix}$$

B – vector of threshold values:
[3.012   3.507   2.824   2.641],

C – column vector of weighing factors values:
[-1.950   -2.366   -2.464   2.335],

P – vector of displacement values:
[-0.332   -0.429   -4.688   -53.372   -0.021].

Structures of the above given networks are presented in Fig. 12, statistical parameters - in Tab. 4, and in Fig. 9 though 11 – comparison of the approximated values with the relevant model values. As results from the above specified data the

elaborated approximations are of simple structure and very good accuracy, simultaneously.
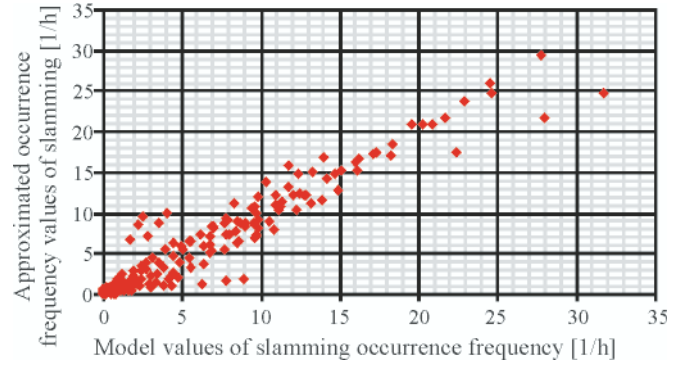
Fig. 9. Comparison of approximations of maximum occurrence frequencies of slamming with their model values, for Hs = 12 m
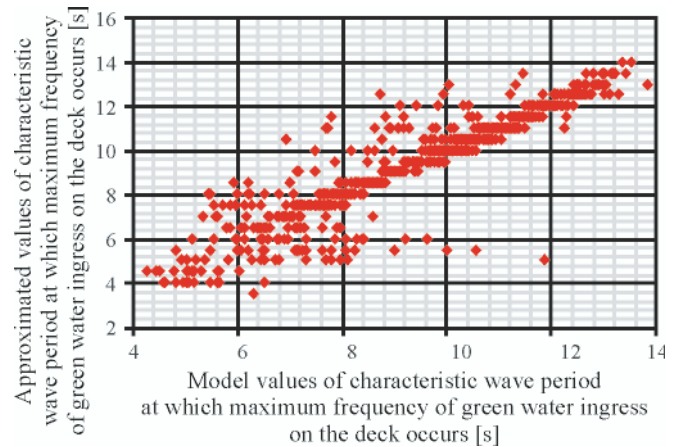
Fig. 10. Comparison of approximations of characteristic wave period at which maximum frequency of green water ingress on the deck occurs, with their model values
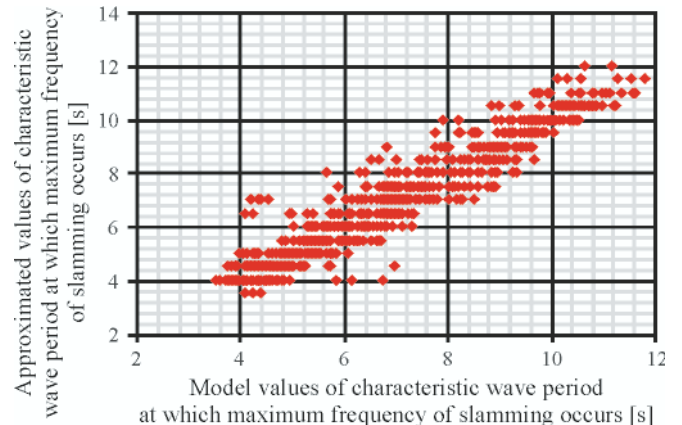
Fig. 11. Comparison of approximations of characteristic wave period at which maximum frequency of slamming occurs, with their model values

Tab. 4. Statistical parameters of the elaborated artificial neural networks, where: U – teaching set, W – validating set, T – testing set, $n_{sl.max}$ – maximum occurrence frequency of bow slamming per one hour [l/h], T_{nzp} – characteristic wave period at which maximum frequency of green water ingress on the deck occurs [s], T_{nsl} – characteristic wave period at which maximum slamming frequency occurs [s]

	$n_{sl.max}$			T_{nzp}			T_{nsl}		
	U	W	T	U	W	T	U	W	T
Standard deviation	4.33 [l/h]	4.30 [l/h]	3.63 [l/h]	2.29 [s]	2.26 [s]	2.34 [s]	2.20 [s]	2.04 [s]	1.95 [s]
Mean absolute error	0.60 [l/h]	0.30 [l/h]	0.38 [l/h]	0.47 [s]	0.52 [s]	0.46 [s]	0.46 [s]	0.47 [s]	0.53 [s]
Correlation	0.96	0.99	0.98	0.93	0.92	0.91	0.96	0.95	0.92
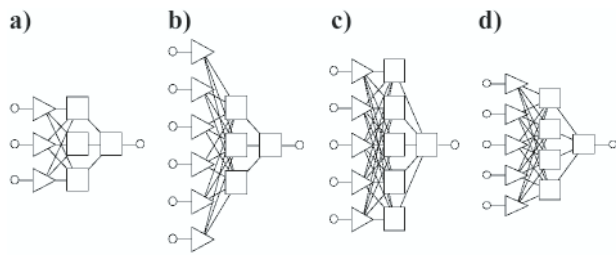
*Fig. 12. Structures of the artificial neural networks: **a)** approximating maximum slamming occurrence frequencies, **b)** approximating characteristic wave period at which maximum frequencies of green water ingress on the deck occur, **c)** predicting either safe or dangerous green water ingress on the deck, **d)** approximating characteristic wave period at which maximum frequencies of slamming occur.*

SUMMARY

The presented approximations of seakeeping qualities of FPSO ships, described by Eq. (1) through (9), can be used for:
- the determining of crucial design parameters which affect pitching, heaving, slamming and green water ingress on the deck, at an assumed significant wave height,
- the predicting of the characteristic wave height which causes increasing intensity of green water ingress on the deck and slamming, on the basis of ship design parameters,
- the predicting of the phenomena of heaving, pitching, slamming and green water ingress on the deck, on the basis of ship design parameters,
- the assessing of ship seakeeping qualities,
- the optimizing of ship design parameters with a view of assumed seakeeping qualities.

By narrowing ship operational conditions with the use of a deterministic scenario it was possible to obtain a high approximation accuracy in the wide range of values of design parameters and relatively simple structure of the considered model, simultaneously.

The elaborated approximation functions may find application to the modeling of seakeeping qualities of FPSO ships in the domain as follows:
- the assumed ranges of ship hull geometrical parameters on the basis of which model values of seakeeping qualities have been calculated, in particular, of:
  - the ratio of ship length b.p. and breadth: $L_{pp}/B = 4 \div 7$,
  - the ratio of ship breadth and draught:
    $$B/d = 2.18 \div 4.7,$$
  - the block coefficient of hull underwater part:
    $$CB = 0.71 \div 0.87,$$
  - the midship section coeffcient: $CM = 0.97 \div 0.99$,
  - the block coefficient of hull fore underwater part:
    $$CBF = 0.5 \div 0.78,$$
  - the midship body length: $WC = 40 \div 256$ m,
  - the distance from waterplane centre to aft perpendicular:
    $$XF = 50 \div 250 \text{ m}$$
  - the ship length between perpendiculars:
    $$L_{pp} = 116 \div 466 \text{ m},$$
  - the ship breadth: $B = 24 \div 80$ m,
  - the ship draught: $d = 6.5 \div 28.5$ m,
  - the underwater hull volumetric displacement:
    $$V = 36\ 829 \div 385\ 908 \text{ m}^3.$$
  - the waterplane area: $Fw = 3000 \div 29\ 000$ m^2
  - the freeboard height: $Fb = 0.4 \div 42.75$ m;
- the assumed wave conditions:
  - the significant wave height:
    - for predicting maximum occurrence frequency of green water ingress on the deck: $Hs = 12 \div 17$ m,

- for the remaining seakeeping qualities Hs value - unlimited, however wave effects are non-linearly changing along with Hs value increasing,
  - JONSWAP wave spactrum,
  - the characteristic wave period: $T = 2 \div 20$ s;
- the assumed ship motion parameters:
  - the ship speed: $V = 0$ m/s,
  - the wave encounter angle $\beta = 180°$ (head wave).

The calculations of model seakeeping qualities were performed on the basis of the linear oscillating motion theory. In [4] have been presented results of the model tests aimed at determining effects of a.o. form parameters of ship hull over-water and under-water parts on the phenomenon of green water ingress on the deck. The tests have revealed some non-linearities in the wave effects, which result from:
1. influence of water entering forcastle deck,
2. influence of ship hull over-water part on green water ingress on the deck at large values of wave height and oscillating motions,
3. inaccuracies in the linear model of calculating relative motions at large values of significant wave height.

As results from [4] it is not possible to consider particular non-linearities separately. In the investigations in order to account for the above mentioned non-linearities, were introduced the additional general coefficients α and β which take into account differences between experimentally obtained and computed values (Fig. 4.12), as follows:

$$r_p = \alpha r + \beta r^2 \qquad (10)$$

where:
r_p – predicted value,
r – measured value,
α, β – coefficients.
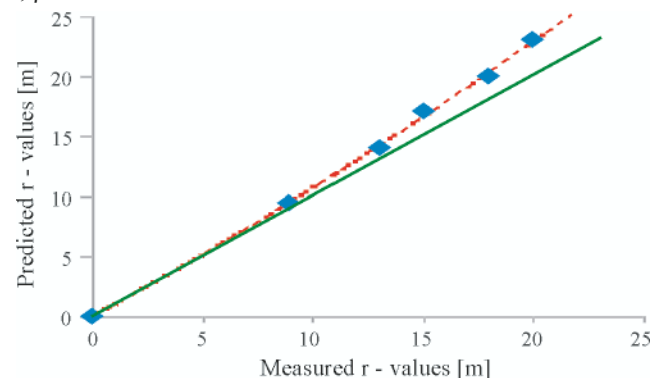
Fig. 13. Non-linearity between values calculated by using linear methods and experimetally measured ones [4]

It is not possible to determine values of the coefficients by using analytical methods but only by model tests for definite hulls. It means that to account for the above mentioned non-linearities in the parametric design stage, is not possible.

Many approximations have been elaborated by using linear regression method, that has resulted in a great simplification of approximation function's form. In the case when linear models have appeared inaccurate the theory of artificial neural networks has been applied.

Approximating occurrence frequency of green water ingress on the deck constituted the greatest difficulty in modeling seakeeping qualities of FPSO ships. In some cases as a result of numerical calculations very large model values of the frequency were achieved. It was a consequence of the assumed operational conditions (large values of significant

wave height) and the wide range of freeboard height values. Therefore despite the elaborated approximations appeared rather accurate, the standard error was rather large. To solve the problem the theory of artificial neural networks was applied to recognizing (classifying) seakeeping qualities. The artificial neural network applicable to assessing occurence frequency of green water ingress on the deck on the basis of both ship design and wave parameters, was prepared. In consequence was obtained the solution showing high accuracy in estimating occurrence frequency of green water ingress on the deck.

In the subject-matter literature there are no data which could be used for verifying the approximations presented in this paper, in the range of the made assumptions. Therefore the verification of the elaborated approximations was performed only on the basis of model values used for elaborating the approximations. As results from the relationships the approximations show trends which are in line with literature sources.

BIBLIOGRAPHY

1. Almeida J., Vasconcelos A., Neves C., Oliveira E., Goulart M., Gomes R.: *The Preliminary Design of the FPSO Maracana.* (FPSO - Floating production storage and offloading unit) International Student Offshore Design Competition, Rio de Janeiro Federal University Team, Rio de Janeiro 2002

2. Banda E., Belton R., Faleye W., Holmes B., Ogah N., Spencer A.: *Design of a Floating Production, Storage, and Offloading (FPSO) System and Oil Offtake System For Offshore West Africa Ocean Engineering Program.* Civil Engineering Department, Texas A&M University, 2003

3. BOMEL Ltd: *Analysis of green water susceptibility of FPSO/FSU's on the UKCS* (United Kingdom Continental Shelf). Offshore Technology Report No. 2001/005, 2001

4. Buchner B.: *Green Water on Ship-type Offshore Structures.* Grafisch Bedrijf Ponsen & Looijen bv, Wageningen, The Netherlands, 2002

5. Buchner B.: *The Impact of Green Water on FPSO Design.* Offshore Technology Conference, Houston, Texas, 1995

6. Buchner B.: *The Influence of the Bow Shape of FPSOs on Drift Forces and Green Water.* Offshore Technology Conference, Houston, Texas, 1996

7. Buchner B., Garcia J.L.C.: *Design Aspects of Green Water Loading on FPSOs.* The 22nd International Conference on Offshore Mechanics & Arctic Engineering, Cancun, Mexico, 8÷13 June, 2003

8. Buchner B.,Voogt A.J.: *Wave impacts due to steep fronted waves.* Rogue Waves 2004, Brest, France 2004

9. Buchner B.,Voogt A.J.: *Wave Slamming on External Turrets of FPSOs.* Proceedings of the ASME 28th International Conference on Ocean, Offshore and Arctic Engineering, Honolulu, Hawaii, 2009

10. Cepowski T.: *Influence analysis of changes of design parameters of passenger-car ferries on their selected sea-keeping qualities.* Polish Maritime Research No. 1(63) 2010, Vol. 17

11. Chipuk C., Clark M, Hoffman C., Peavy J., Sabet R., Wilson B.: *Design of Floating Production Storage Offloading Vessel for the Gulf of Mexico.* Ocean Engineering Program, Texas 2003

12. Det Norske Veritas: *Classification using Performance Criteria determined by Risk Assessment Methodology.* OSS-121 (OFFSHORE SERVICE SPECIFICATION), January 2001

13. Det Norske Veritas: *Offshore 2000 Rules for Classification of Floating Production and Storage Units.* OSS -102, January 2001

14. Ersdal G.: *Green water workshop.* Norwegian Petroleum Directorate, Stavanger, Norway, 2000

15. Ersdal G, Kvitrud A.: *Green Water on Norwegian Production Ships.* Proceedings of the Tenth (2000) International Offshore and Polar Engineering Conference, Seattle, USA, 28 May ÷ 2 June, 2000

16. Frank W.: *Oscillation of Cylinders in or below the Free Surface of Deep Fluids.* Technical Report No. 2375, Naval Ship Research and Development Centre, Washington DC, U.S.A., 1967

17. Gorf P., Barltrop N., Okan B., Hodgson T., Rainey R.: *FPSO Bow Damage in Steep Waves.* Rogue Waves 2000, SeaTechWeek 2000, Le Quartz, Brest, France 2000

18. Graff, W. J.: *Introduction to offshore structures – Design, fabrication, installation.* Gulf Publishing Company, Houston 1981

19. HSE (Health and Safety Executive) Report: *Analysis of Green Water Susceptibility of FPSO/FSUs on the UKCS* OTO 2001:005

20. HSE: *Review of HSE Green Water Study.* Research Project 3794, MARIN, completion 2000

21. HSE: *FPSO Response in Long and Short crested Seas.* Research Project 3959, 2002/018, 2002

22. HSE: *Review of API (American Petroleum Institute) RP 2FPS* (Recommended Practice for Planning, Designing and Constructing Floating Production Systems), OTO 2001-006

23. Journée J.M.J.: *Verification and Validation of Ship Motions Program SEAWAY.* Report1213a, Delft University of Technology, The Netherlands, 2001

24. Karppinen T.: *Criteria for Seakeeping Performance Predictions*, Technical Research Centre of Finland, Espoo 1987

25. Lloyds Register of Shipping: *Rules and Regulations for the Classification of a Floating Installation at a Fixed Location.* July 1999

26. Lloyds Register of Shipping: *Ship-Type FPSO Hull Structural Appraisal.* OS/GN/99002, June 1999

27. Luo Y., Baudic S., Poranski P., Wichers J., Stansberg C.T., Ormberg H.: *Deepstar Study on Predicting FPSO Responses - Model Tests VS Numerical Analysis.* Offshore Technology Conference, 3 May-6 May 2004, Houston, Texas, 2004

28. Mazaheri S., Mesbahi E., Downie M.J.: *Seakeeping Analysis of a Turret-Moored FPSO by Using Artificial Neural Networks.* ASME 2003 22nd International Conference on Offshore Mechanics and Arctic Engineering (OMAE2003),, Cancun, Mexico, June 8÷13, 2003

29. NORSOK Standard N-004: *Design of Steel Structures*, 2004

30. PAFA Consulting Engineers: *Review of Green Water Design and Specification Requirements for FPSO/FSUs.* Hofer House, 185 Uxbridge Road, Hampton, Middlesex, 2000

31. Paik J.K., Thayamballi A.K.: *Ship-Shaped Offshore Installations. Design, Building and Operation.* Cambridge 2007

32. Parker, G.: *The FPSO design and construction guidance manual.* Reserve Technology Institute, Houston 1999

33. Shimamura Y.: *FPSO/FSO: State of the art.* Journal of Marine Science and Technology, No. 7, 2002

34. R M Offshore Ltd., Project Reviews Ltd: *UKOOA FPSO design guidance notes for UKCS service*, 2002

35. Wang G., Tang S., Shin Y.: *A Direct Calculation Approach for Designing a Ship-shaped FPSO's Bow Against Wave Slamming Load.* Proceedings of The Twelfth (2002) International Offshore and Polar Engineering Conference, Kitakyushu, Japan, May 26÷31, 2002

36. Watson D.G.M: *Practical Ship Design.* Gulf Professional Publishing, 2002

37. Xu, L.,Barltrop: *Wave slap loading on FPSO bows.* Research Report No. 324, Health and Safety Executive, UK, 2005

38. Xu, L.,Barltrop, N.,Okan, B.: *Bow impact loading on FPSOs. Part 1 - Experimental investigation*, Elsevier, 2008

39. Xu, L.,Barltrop: *Bow impact loading on FPSOs. Part 2. Theoretical investigation,* Ocean Engineering, 35 (2008), 2008.

CONTACT WITH THE AUTHOR
Tomasz Cepowski, Assoc. Prof.
Institute of Marine Navigation,
Maritime University of Szczecin
Wały Chrobrego 1/2
70-500 Szczecin, POLAND
e-mail: cepowski@am.szczecin.pl

Numerical analysis of effect of asymmetric stern of ship on its screw propeller efficiency

Tomasz Abramowski, Ph. D.
Katarzyna Żelazny, D.Sc., Eng.
Tadeusz Szelangiewicz, Prof.
West Pomeranian University of Technology, Szczecin

ABSTRACT

During designing the ship its designer tends to achieve as-high-as possible efficiency of ship's propulsion system. The greatest impact on the efficiency is introduced by ship's screw propeller whose efficiency depends not only on its geometry but also distribution of wake current velocity. To change wake current distribution and improve propeller efficiency an asymmetric form is usually applied to stern part of ship hull. This paper presents results of numerical analysis of wake current velocity distribution, performed by using a CFD method for a B 573 ship of symmetric stern and the same ship of an asymmetric stern. Next, the mean values of screw propeller efficiency in non-homogenous water velocity field were calculated for both the hull versions of B 573 ship.

Keywords: asymmetric ship's stern; computational fluid dynamics (CFD); screw propeller efficiency

INTRODUCTION

During designing the ship one of the most important tasks is to so design its propulsion system as to ensure reaching an assumed service speed at as-high-as-possible propulsion efficiency. Screw propeller constitutes the crucial element of the propulsion system, whose efficiency decides on the overall propulsive efficiency of the ship. Screw propeller efficiency depends mainly on its geometry and loading as well as water velocity distribution in wake current. To improve the wake velocity distribution various additional devices such as: nozzles, half-nozzles or suitably profiled fins attached to underwater part of ship's hull before screw propeller, are applied [13] (sometimes they are intended for the mitigating of hull plating vibration resulting from operation of screw propeller). Another solution intended for the changing of wake velocity distribution and improving of propeller efficiency is to apply an asymmetric form to ship's hull stern in its underwater part.

Since 1982 have appeared ships of an asymmetric stern, designed and built in accordance with the patents [8, 9, 10, 12]. Model tests and measurements performed on existing ships showed a decrease in propulsion power in the range from 5 to 10 % [4, 6, 7, 11]. Also, B 183 container carriers built by Szczecin Shipyard, were fitted with an asymmetric stern.

Within the frame of the R&D project [9] comparative wake current investigations for the B 573 ship of symmetric stern, whose model test results were available [5], and for the ship's hull of a modified form – introduction of an asymmetric stern, were made. The modification of underwater part of hull was introduced in a very limited range so as to keep the ship's main design parameters, unchanged. For both the obtained wake currents, the calculations of mean value of screw propeller efficiency in non-homogenous water velocity field, were performed.

NUMERICAL CALCULATIONS OF WAKE CURRENT

The numerical calculations of wake current for the B 573 ship's hull of modified stern part, were conducted with the use of Fluent system; the hull stern body lines are presented in Fig. 1.

In advance of the actual calculations a comparative test was performed for the symmetric version of the ship's hull (Fig. 1a), results of which compared with those of the model tests are presented in [2]. Next, wake current calculations for the asymmetric ship hull (Fig. 1b) were made (details concerning its computational model and numerical mesh are contained in [1]). Example axial velocity profiles and velocity vectors in propeller disc area are given in Fig. 2 and 3. Distribution of circumferential and axial velocity components for the asymmetric stern, is shown in Fig. 4. The effect of the asymmetric stern on wake fraction distribution as compared with that for the symmetric stern, is presented in Fig. 5.
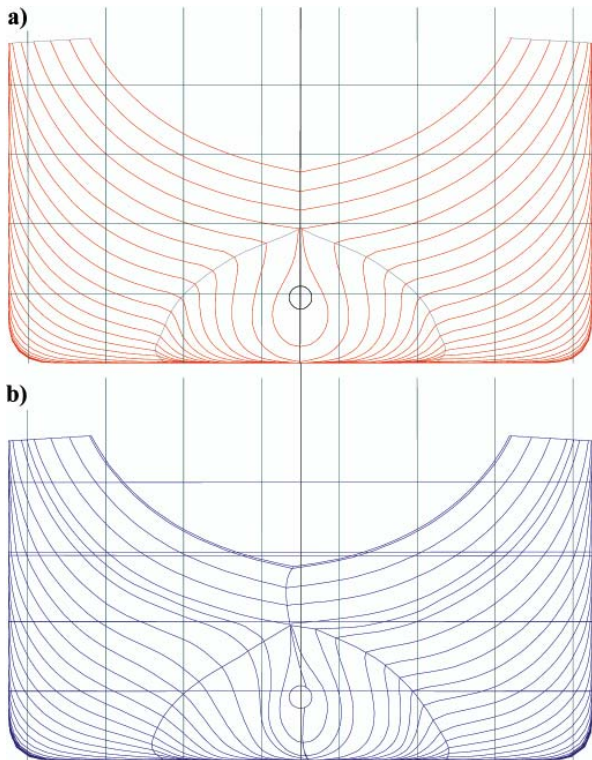
Fig. 1. *Body lines of stern part of B 573 ship hull:* **a)** *before modification (symmetric stern),* **b)** *after modification (asymmetric stern)*
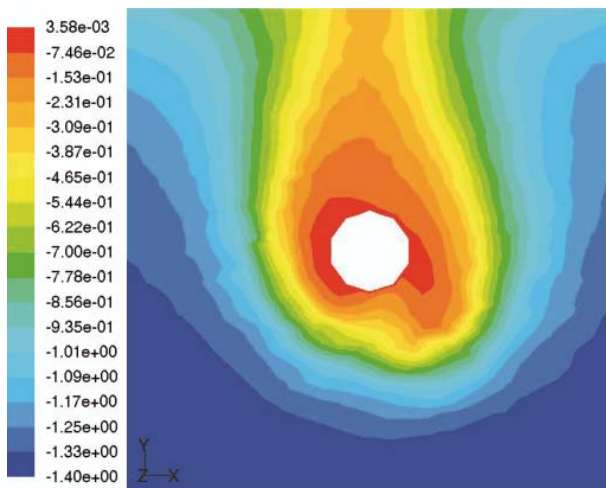
Fig. 2. *Axial velocity profiles – asymmetric stern*
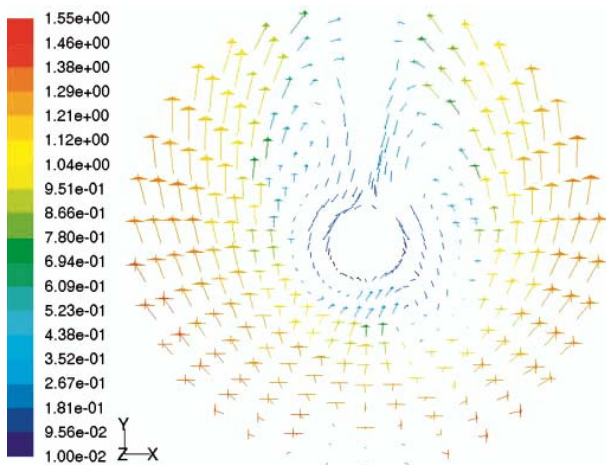
Fig. 3. *Velocity vectors – asymmetric stern*
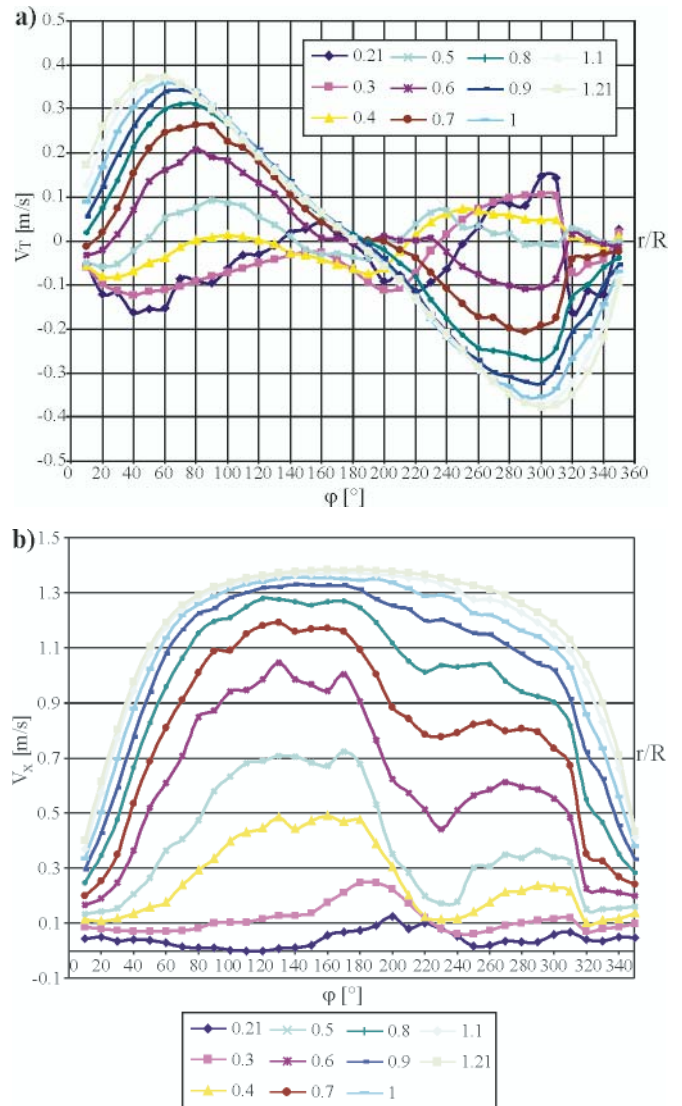
Fig. 4. *Distribution of velocity components:* **a)** *circumferential,* **b)** *axial – for the asymmetric stern, given at different values of the relative radius(r/R)*

MEAN EFFICIENCY OF SCREW PROPELLER IN NON-HOMOGENOUS WATER VELOCITY FIELD FOR ASYMMETRIC STERN FORM

The modification of stern part of B 573 ship hull (consisting in making stern form asymmetric) was aimed at checking which way the modification would affect the mean efficiency of screw propeller in non-homogenous water velocity field. The authors of the following publications or patents [4, 6, 7, 8, 9, 10, 11, 12] have argued that for an asymmetric stern to obtain a propulsion power decrease is possible at the same ship's speed relative to the ship fitted with symmetric stern. Calculations of the mean efficiency of the final screw propeller of B 573 ship, operating in non-homogenous water velocity field, were performed for both the ship's versions: with symmetric and asymmetric stern. The way of conducting the calculations and relevant tests are described in [3]. The results of numerical calculations of the mean efficiency of screw propeller are given in Fig. 6 where the results for all the remaining hull form modifications analyzed in [3], are also shown.
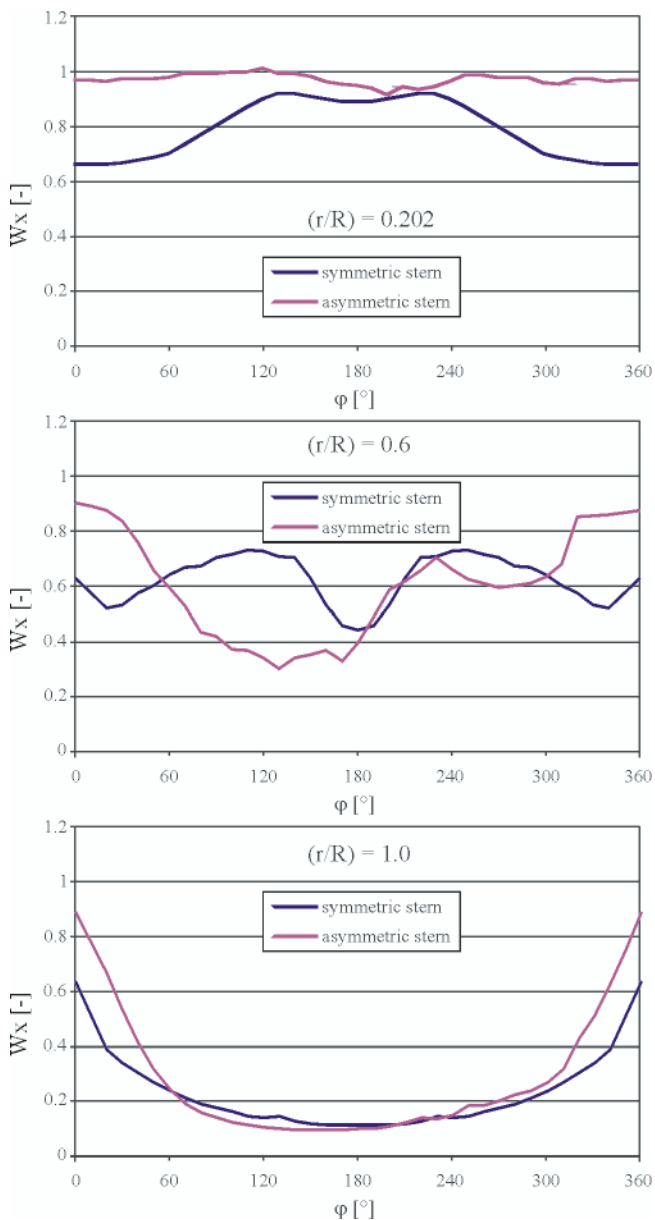
Fig. 5. *Distribution of the axial wake fraction W$_x$ for both the symmetric and asymmetric stern, given at the values of the relative radius (r/R) = 0.202; 0.6; 1.0*
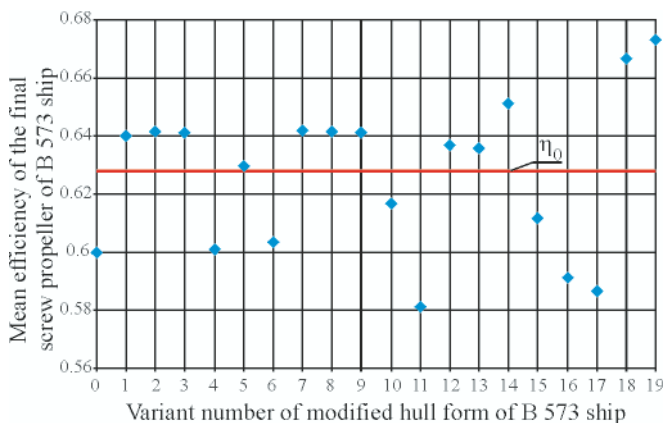
Fig. 6. *Mean efficiency of the final screw propeller of B 573 ship, operating in non-homogenous wake current field. **Notation**: η_0 – maximum efficiency of the final screw propeller in homogenous water velocity field (free propeller); **Variant No.0** – the initial hull form of B 573 ship (without modification), wake current field - as measured during model tests; **Variant No.18** – the manually modified stern part of ship's hull – symmetric hull form; **Variant No.19** – the manually modified stern part of ship's hull – asymmetric hull form*

CONCLUSIONS

1. The results obtained from the numerical analyses in question indicate that an asymmetric stern of underwater part of ship's hull introduces a very favourable effect to the mean efficiency of screw propeller operating in non-homogenous water velocity field. The results should be deemed preliminary but quantitive for both the variants of ship's hull stern, i.e. symmetric and asymmetric; in both the cases the same investigation method was used and the results were achieved with the same accuracy.

2. To be able to state how much screw propeller efficiency for the ship of asymmetric stern can be really increased, numerical investigations should be performed for a ship of known complete hull geometry and available results of model tests or full-scale measurements.

3. Authors of the patents concerning asymmetric ship stern (at least 4 patents are valid: 2 German and 2 Polish) defined a given form of stern part of ship's hull in relevant patent specifications. In each of them is defined a strictly determined form being simultaneously different from those given in the remaining patents. Every author states that his hull form is the best regarding increased propeller efficiency and lowered power demand for ship propulsion. The obtained results of numerical analyses confirm that fact, but during the performed investigations it was found out that the assumed form of underwater part of ship's hull stern is not at all one of the forms defined in the patent specifications in question. It was preliminarily concluded that an optimum form of stern part of ship's hull may also depend on many geometrical parameters of the entire hull as well as on ship's operational parameters, e.g. ship's speed or its screw propeller geometry and loading.

4. The preliminary results of the performed numerical analyses are deemed very encouraging therefore research work aimed at the determining of relations between geometrical quantities characterizing asymmetric stern form and screw propeller efficiency, will be continued.

BIBLIOGRAPHY

1. Abramowski T., Szelangiewicz T.: *Numerical analysis of influence of ship hull form modification on ship resistance and propulsion characteristics, Part I: Influence of hull form modification on ship resistance characteristics.* Polish Maritime Research, No 4/2009, Gdańsk 2009
2. Abramowski T., Szelangiewicz T.: *Numerical analysis of influence of ship hull form modification on ship resistance and propulsion characteristics, Part II: Influence of hull form modification on wake current behind the ship.* Polish Maritime Research, No.1/2010, Gdańsk 2010
3. Abramowski T., Szelangiewicz T.: *Numerical analysis of influence of ship hull form modification on ship resistance and propulsion characteristics, Part III: Influence of hull form modification on screw propeller efficiency.* Polish Maritime Research, No. 1/2010, Gdańsk 2010
4. Collatz G., Laudan J.: *Das asymmetrische Hinterschiff.* Jahrbuch Shiffbautechn. Gesellschaft, 1984
5. Jaworski S., Syrocki W.: *Ship B 573: Results of Model Test – Resistance, Wake Measurments.* Technical Report No RH-95/T-041A, Ship Design and Research Centre, Gdańsk 1995

6. Nawrocki S.: *The effect of asymmetric stern on propulsion efficiency from model test of a bulk carrier.* Shiff und Hafen 10, 1987, p. 41

7. N.N.: *Development of the asymmetric stern and service results.* Naval Architect, 1989, p. E181

8. Nönnecke E.A.: *Reduzierung des Treibstoffverbrauches und Senkung der Betriebskosten der Seeschiffe durch propulsionverbessernde Maßnahmen.* Hansa, 1978, p. 176

9. Nönnecke E.A.: *Schiffe mit treibstoffsparendem asymmetrischen Heck – Anwendungen und Efrahrungen.* Shiff und Haffen, 9, 1978

10. Nönnecke E.A.: *The asymmetric stern and its development since 1982.* Shipbuilding Technology International, 1987, p. 31

11. Piskorz-Nałęcki J.W.: *The influence of the asymmetric afterbody and the horizontal fins on the rudder blade on the propulsive efficiency, Workshop on Developments in Hull Form Design.* Wageningen, The Netherlands, 22 ÷ 24 October 1985

12. Piskorz-Nałęcki J.W.: *Stern part of ship's hull. Patent specification* (in Polish). Urząd Patentowy PRL (Polish Patent Office) No. 44 213, Warsaw 1988

13. Schneekluth H., Bertram V.: *Ship Design for Efficiency and Economy*. Butterworth Heinemann, Oxford 1998

14. Szelangiewicz T.: *Numerical investigations of rudder/propeller/ship stern interaction aimed at improving transport ship's propulsion and manoeuvrability qualities* (in Polish). Final report of the R&D project No. R 10 008 01, Szczecin 2009.

CONTACT WITH THE AUTHORS
Tomasz Abramowski, Ph. D.
Katarzyna Żelazny, D.Sc., Eng.
Tadeusz Szelangiewicz, Prof.
West Pomeranian University of Technology, Szczecin
Faculty of Marine Technology
Al. Piastów 41
71-065 Szczecin, POLAND
e-mail: tadeusz.szelangiewicz@ps.pl

A complete design of tandem co-rotating propellers using the new computer system

Tadeusz Koronowicz, Prof.
Zbigniew Krzemianowski, Ph. D.
Teresa Tuszkowska, Ph. D.
The Szewalski Institute of Fluid Flow Machinery
of the Polish Academy of Sciences in Gdansk
Jan A. Szantyr, Prof.
Gdansk University of Technology

ABSTRACT

The computer system for the complete design of the tandem co-rotating propellers, presented in this article, has several common blocks and procedures with the computer system for the design of conventional single propellers, presented in detail in Polish Maritime Research No. 1 Vol. 16 (2009). In this article only these blocks and procedures are described, which are different in both systems. The comparative analysis of the designed tandem propeller and a conventional propeller is also included.

Keywords: ship propellers; tandem co-rotating propellers; design methods; computational fluid dynamics

INTRODUCTION

The tandem co-rotating propeller consists in fact of two propellers, usually of the same diameter and the same number of blades, mounted on the same shaft with certain angular shift between them (cf. Fig. 1). Application of such propellers may be advantageous when a very high power must be absorbed by a single shaft propeller having a limited diameter. Design of such propellers requires taking into account the mutual hydrodynamic interaction effects between the forward and aft propeller. The design of tandem co-rotating propellers is based on the same requirements and assumptions which are employed in the design of conventional single propellers [1, 3]. Apart from that, the design of tandem propellers requires the following new requirements:

a) determination of the division of the hydrodynamic loading between the forward and aft propellers,
b) determination of the mutually induced velocity field, i.e. the field induced by the forward propeller at the aft one and vice versa. This field must be taken into account not only in the design, but also in the analysis of the tandem propeller operation in the non-uniform inflow velocity field behind the ship hull.

Similarly as in the design of the conventional single propellers, the computer system for the complete design of the tandem propellers must include three interacting programs (blocks of procedures):
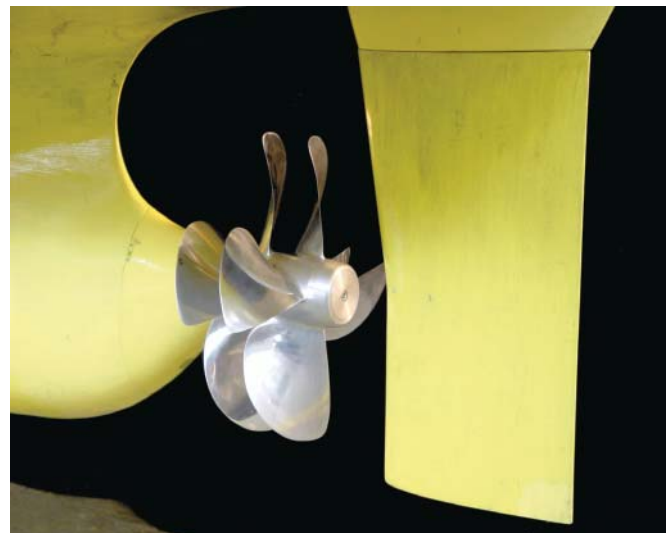
*Fig. 1. A typical tandem co-rotating propeller
(Model tests in the Ship Hydromechanics Division of CTO SA)*

1) the programs for determination of the design velocity field for both propellers,
2) the program for the propeller design,
3) the program for the analysis of the tandem propeller operation in the non-uniform velocity field behind the ship hull, taking into account the mutual hydrodynamic interaction between both propellers.
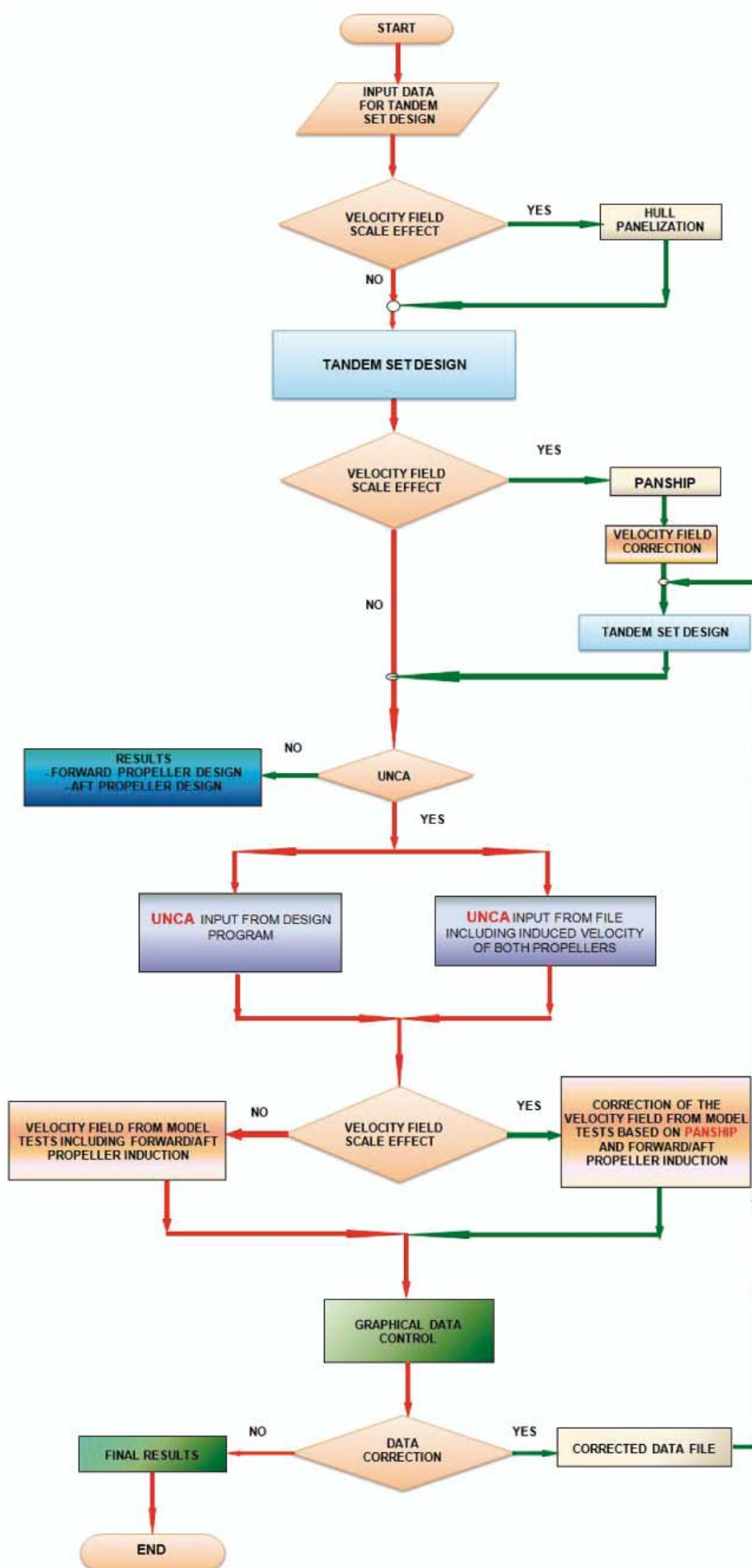
Fig. 2. *The block diagram of the computer system for the complete design of the tandem co-rotating propellers*
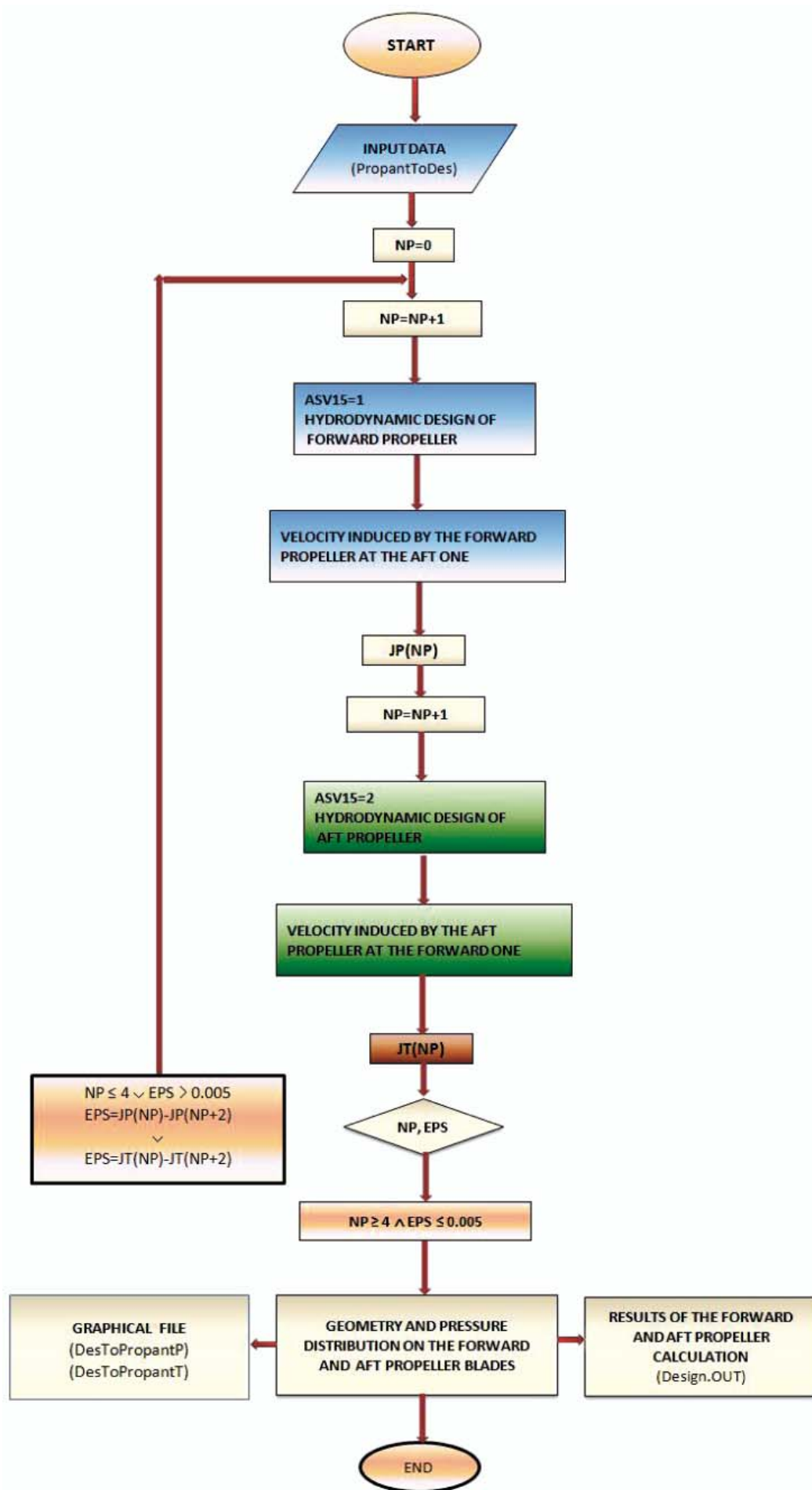
Fig. 3. *The block diagram of the design procedure for the tandem co-rotating propellers*
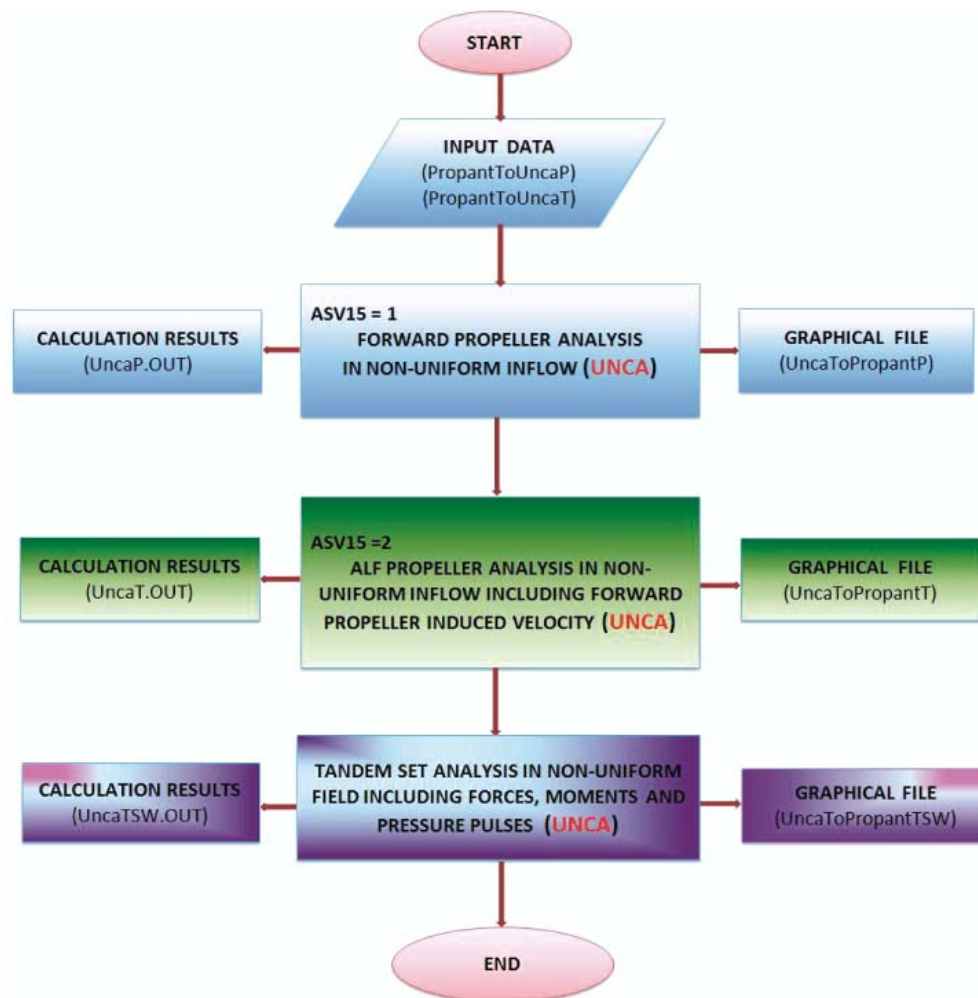
Fig. 4. The block diagram for the program for analysis of the tandem propeller operation

With respect to the design system for conventional single propellers, the system for tandem propellers differs by the following elements:

a) the procedures for the graphical presentation of the geometry of both propellers independently,

b) the procedures for determination of the design velocity field for both propellers, taking into account their mutual interaction,

c) the procedure for modification of the non-uniform velocity field used in the analysis of the propeller operation by the program UNCA,

d) the procedures for determination of the pressure pulses induced by both propellers separately and by the entire tandem propeller set,

e) the procedures for determination of the shaft bearing forces for both propellers separately and for the entire tandem set.

The appropriate interaction between all programs and procedures ensures the correct design of the tandem co-rotating propellers. The computer system integrates all necessary components and the process of tandem propellers design may be controlled directly from the computer screen, without the necessity for preparation of the separate input data files for the respective computer programs. Moreover, the system is equipped with the necessary graphical procedures for the control of input data and of the intermediate results, as well as for the convenient modification of the geometry of the designed propellers in the course of the design calculations. The block diagram of the computer system for design of tandem propellers differs from the block diagram of the system for conventional propeller design [1]. The basic block diagram (cf. Fig. 2) is supplemented with the block diagram of the program for design of the tandem propellers (cf. Fig. 3) and with the block diagram of the program for analysis of the tandem propeller operation (cf. Fig. 4).

PRESENTATION OF THE SELECTED BLOCKS OF THE DESIGN SYSTEM

The computer system for the design of tandem propellers set has many common blocks with the system for the design of conventional single propellers. Below only new elements, specific for the case of tandem propellers, are presented in detail. The elements common for tandem and conventional propellers are only briefly mentioned.

The input data

The input data include all magnitudes necessary for performing optionally four versions of the design calculation, similarly as in the case of the conventional single propellers [1]. The input data may be introduced directly from the computer screen or in the form of the file prepared earlier.

The input parameter characteristic for the tandem co-rotating propellers is the distance between the generator lines of the forward and aft propellers. Another characteristic parameter of the tandem propellers is the angular shift between the forward and aft propeller, which is determined in the course of the design calculation in the program.

The program enables graphical control and, if necessary – easy modification of the input data. For example, the points defining radial distribution of the geometrical parameters of the propeller such as blade outline, blade thickness or blade rake and skew, may be easily moved on the computer screen to their correct positions. An example of such correction in case of the blade skewback is shown in Fig. 5.
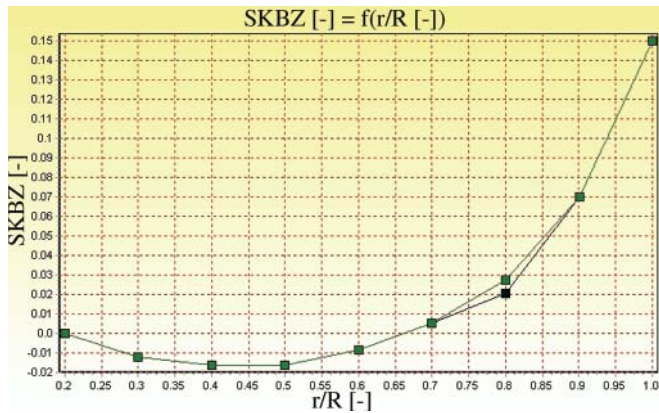
Fig. 5. The control display of the propeller blade skewback, showing the correction of the erroneous data at radius 0.8

The design program

The algorithm of the design program for the tandem co-rotating propellers differs significantly from the algorithm for design of the conventional single propeller presented in [1]. The main differences are:

a) the design calculations is performed only for the given total thrust of the tandem propeller set,
b) the program automatically defines the optimum division of the total thrust between the forward and aft propeller,
c) the velocities induced by each of the propellers at the location of the other one must be computed and taken into account in the design. This is achieved in an iterative process.

The design calculation is performed in the same way for all four possible design tasks (analogically as in the case of conventional single propellers). The design calculation ends with the results which are available in the form of numerical files and they may be also presented graphically on the computer screen. An example of the graphical presentation of the designed tandem propeller set may be seen in Fig. 6. The set of propellers shown on the screen may be rotated and viewed from an arbitrary angle. All graphical presentations may be directly printed out or stored in special files.
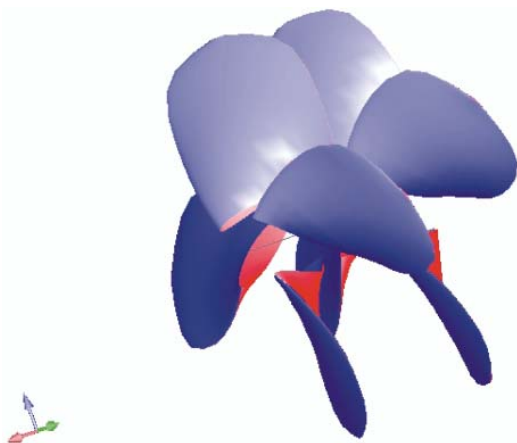
Fig. 6. The rendered view of the designed tandem propeller

As it has been mentioned above, the new and indispensable element of the tandem propellers design procedure is the determination of the velocity induced by the system of bound vortices representing the propeller blades and by the systems of trailing, free vortices shed from these blades. As may be seen in the block diagram shown in Fig. 3, this determination has the form of an iterative process based on calculation of the mutual interaction of both propellers of the tandem set.

The induced velocity field

In the design calculation based on the vortex theory the system of bound and trailing vortices representing the propeller is determined in a simplified way, in which the trailing vortices form the helical surfaces. This approach is sufficiently accurate for calculation of the velocity induced on the propeller blades, leading to the definition of the blade geometry. In the case where the induced velocity in front and behind the blades must be determined, this simplified model is no longer sufficient.

In the physical reality the system of trailing vortices behind the propeller blades undergoes contraction and deformation, in which the processes of vortex concentration and dissipation of vorticity play an important role. As a result, the concentrated tip vortices are formed behind each blade and a concentrated hub vortex is formed along the propeller axis. Such a system of vortices induces a specific velocity field in the near vicinity of the propeller, as shown in Figs 7-11.
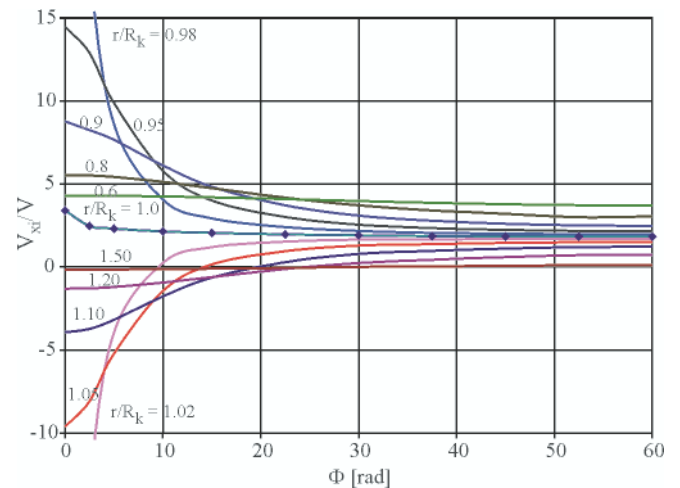
Fig. 7. The axial component of the velocity induced behind the three-bladed propeller as the function of the angular co-ordinate Φ
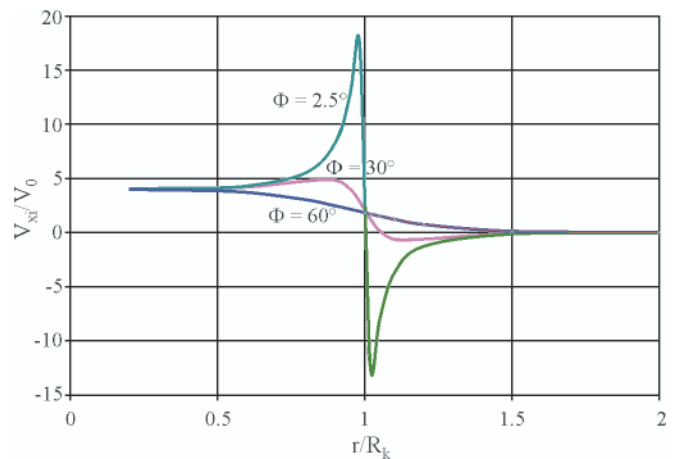
Fig. 8. The axial component of the velocity induced behind the three-bladed propeller for selected sections Φ = const
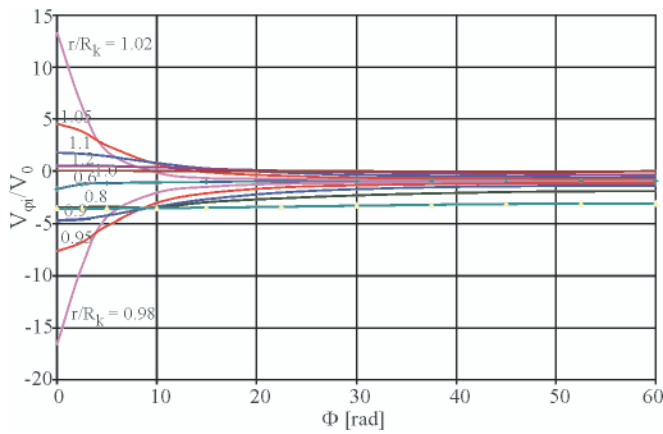
Fig. 9. *The tangential component of the velocity induced behind the three-bladed propeller as the function of the angular co-ordinate Φ*
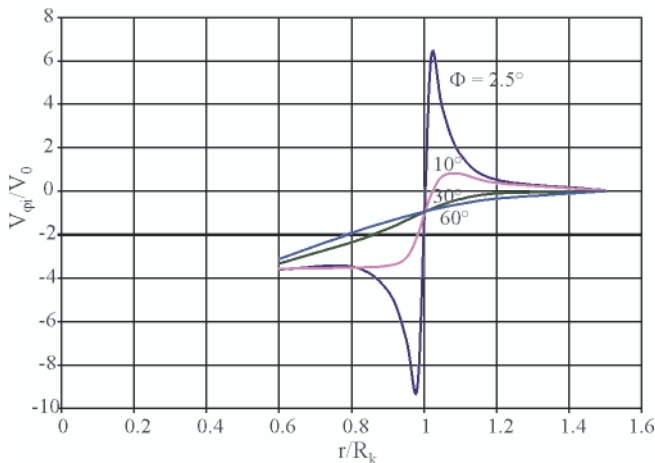
Fig. 10. *The tangential component of the velocity induced behind the three-bladed propeller for selected sections Φ = const*
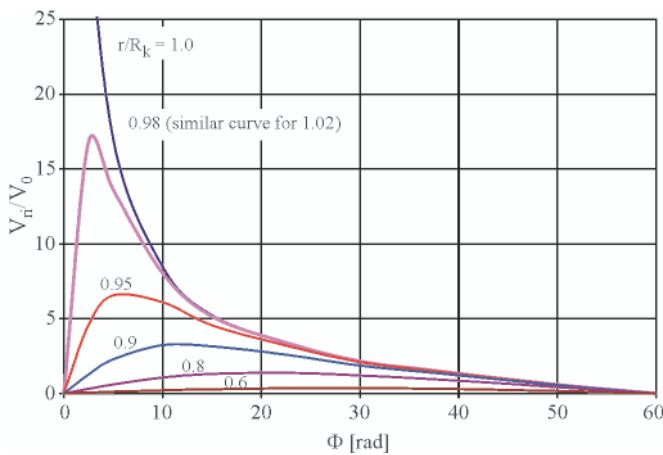
Fig. 11. *The radial component of the velocity induced behind the three-bladed propeller as the function of the angular co-ordinate Φ*

The velocity field shown in these Figures has been determined at the distance of one radius behind the propeller. All dimensions are related to the radius of the location of the tip trailing vortex centre R_k. The computational model of the free vortex system is composed of the strongly concentrated tip vortices and the hub vortex [4,6]. The computations for vortices of different degree of concentration have shown that the induced velocity field in the region between the tip vortices is independent from the degree of concentration of vortices, assuming that the location of their centres is correct. On the contrary, there are large differences in the vicinity of the free vortices (for the values of the angular co-ordinate Φ close to zero). In the case of lower concentration of vorticity the extreme values of velocity are smaller.

The aft propeller achieves the best performance and the lowest risk of cavitation when its blades are located in places, where the velocity induced by the front propeller is the lowest and the radial gradient of this velocity is small (cf. Figs. 7 and 9). This condition is fulfilled exactly in the middle between the free vortices shed from the front propeller blades (in the case of three-bladed propellers, as shown in Figs. 7-11, this corresponds to the angular co-ordinate value Φ = 60 [deg]. Consequently, the determination of the mutual angular position of the forward and aft propellers of the tandem set is very important in the design process.

The velocity induced by the aft propeller at the forward propeller is several times smaller and more uniformly distributed in space. The mutual angular position of the forward and aft propeller is determined in the design program by means of the theoretical-empirical relation, described in detail in [4-9]. The value of the angular shift between the forward and aft propeller is given in the results.

The results for each propeller of the tandem set are presented in the same format as for the conventional single propeller (see [1]). Additionally, the values of total thrust, torque and power for the entire tandem set are included.

The program for the analysis of the tandem propeller operation in the non-uniform velocity field

The computer program UNCA for the analysis of the propeller operation in the non-uniform velocity field is an important component of the propeller design process. The main part of the algorithm of this program is the determination of the extent of different forms of unsteady cavitation on the propeller blades. The original computational model integrates the unsteady vortex lifting surface theory with the time-dependent sheet cavity. This algorithm is described in detail in [10-12].

In the case of the analysis of tandem propellers the mutually induced velocities of the forward and aft propeller should be taken into account. This is achieved by an additional procedure inserted into UNCA, which calculates the propeller induced velocity in the arbitrary points in front and behind the propeller. This induced velocity field is superimposed on the non-uniform velocity field generated by the ship hull. Such a modified velocity field enables the analysis of the forward and aft propeller of the tandem set.

Both newly designed propellers of the tandem set are analyzed by the program UNCA from the point of view of:
a) detection of the different forms of cavitation in a number of selected angular positions of the propeller blades in the non-uniform velocity field,
b) calculation of the pressure pulsations induced by each of the propellers separately and by the entire tandem set on the hull surface or in the surrounding space,
c) calculation of the fluctuating bearing forces and moments on each of the propellers separately and by the entire tandem set.

After analyzing the results from the program UNCA the design calculation may be repeated, introducing modifications of the propeller geometry with purpose of achieving better propeller performance in the non-uniform velocity field. For example, the following parameters may be modified:
a) the values and character of the radial distribution of the blade skewback,
b) the values and character of the radial distribution of the blade profile chord lengths,
c) the values and character of the radial distribution of the blade thickness,

d) the type of chord-wise blade thickness distribution,
e) the type of chord-wise mean line camber distribution,
f) the radial distribution of the hydrodynamic loading,
g) the number of propeller blades,
h) the division of the hydrodynamic loading between the forward and aft propeller of the tandem set.

The analysis of the tandem set operation in the non-uniform inflow velocity field is performed only for the design condition, because any change in the propeller advance velocity or the rate of rotation leads to changes in the induced velocity field of the forward and aft propeller of the tandem set.

An example of the calculation results of the tandem co-rotating propeller set is included in the next section of the article, devoted to the comparative analysis of the conventional propeller and the tandem propeller set, both designed for the same conditions.

COMPARATIVE ANALYSIS OF THE RESULTS

Many years of experience and practice show that in most cases the single fixed and controllable pitch propellers fulfil the most demanding requirements concerning efficiency, cavitation performance, fluctuating bearing forces, pressure pulsations generated on the hull, and hydro-acoustic emission. However, some specific field of application may be found, in which the tandem co-rotating propeller sets are likely to be better.

The tandem co-rotating sets are characterized by a large number of blades. There be $Z = 4 + 4 = 8$, $Z = 5 + 5 = 10$, and even $Z = 6 + 6 = 12$ blades. Placing of such a large number of blades in one propeller disc leads to a significant reduction of efficiency and may cause serious manufacturing problems. The harmonic amplitudes of the fluctuating bearing forces and propeller-generated pressure pulsations are related to the number of propeller blades – lower values are usually obtained for a larger number of blades. Moreover, in the case of tandem co-rotating propellers it is easier to avoid cavitation – the combined expanded blade area ratio of the forward and aft propellers may be well over 1.0

In order to illustrate the above statements, the comparative design calculations of a single propeller and an equivalent tandem co-rotating propeller set are presented below. A large and fast ship has been selected as the test example. The design ship speed is $V = 25.3$ knots, with the required propeller thrust equal to $T = 3750$ kN. The design rate of propeller rotation was $n = 100$ rpm.

For the single propeller the following results were obtained:

The optimum diameter: $D_{opt} = 8.25$ m.
The expanded blade area ratio: $Ae/Ao = 0.92$.
The power delivered to propeller: $P_d = 43989$ kW.
The mass of the blades: $G = 40640$ kg,
The propeller moment of inertia: $GD^2 = 1154566$ kGm².

In the same design condition the following results were obtained for the tandem co-rotating set:

The optimum diameter: $D_{opt} = 7.40$ m
The expanded blade area ratio: $Ae/Ao = (0.65 + 0.65) = 1.3$.
The power delivered to propeller: $P_d = 42880$ kW.
The combined mass of blades: $G = (23630 + 21955)$ kG = = 45585 kg,
The combined propeller moment of inertia: $GD^2 = (506735 + + 465040)$ kGm² = 971775 kGm².

For both propellers operating in the same velocity field behind the hull wake, the harmonic amplitudes of the unsteady bearing forces and of the pressure pulsations generated in the same points on the hull were calculated and they are presented in Figs. 12-15.
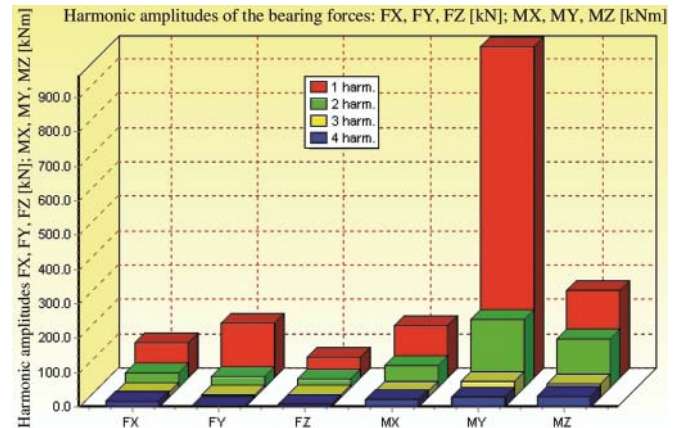
Fig. 12. *Harmonic amplitudes of the bearing forces for the single propeller*
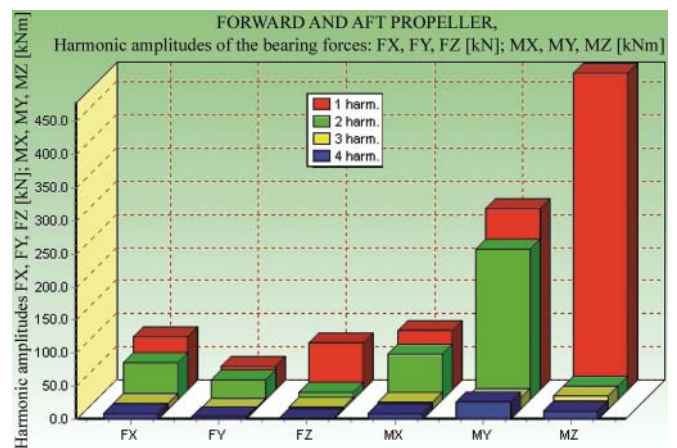
Fig. 13. *Harmonic amplitudes of the bearing forces for the tandem propeller set*
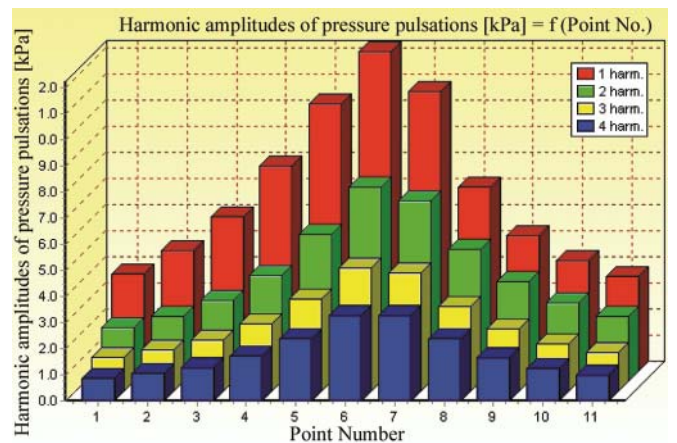
Fig. 14. *Harmonic amplitudes of the pressure pulsations induced on the hull by the single propeller*

The above presented results demonstrate the significant advantage of the tandem propeller set over the conventional single propeller. This is not a general rule, but the presented example has been selected in such a way that this advantage can be demonstrated in certain specific operating conditions. In this example the tandem propeller set can be characterized by the following results:

- the lower delivered power than for the single propeller,
- the lower harmonic amplitudes of the unsteady bearing forces,
- the lower harmonic amplitudes of the pressure pulsations induced on the hull,
- the cavitation phenomena similar to those on the single propeller.
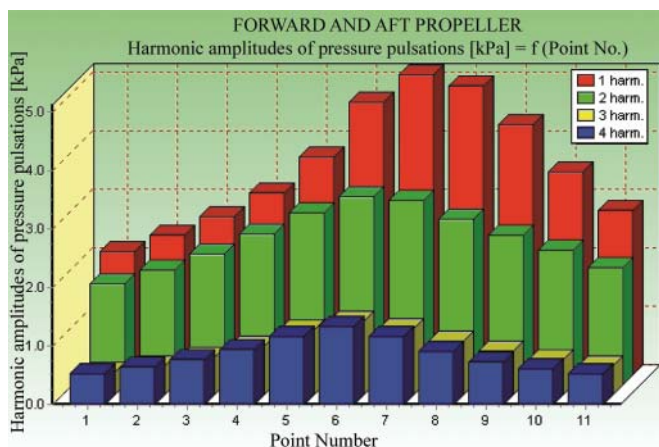
Fig. 15. Harmonic amplitudes of the pressure pulsations generated on the hull by the tandem propeller set
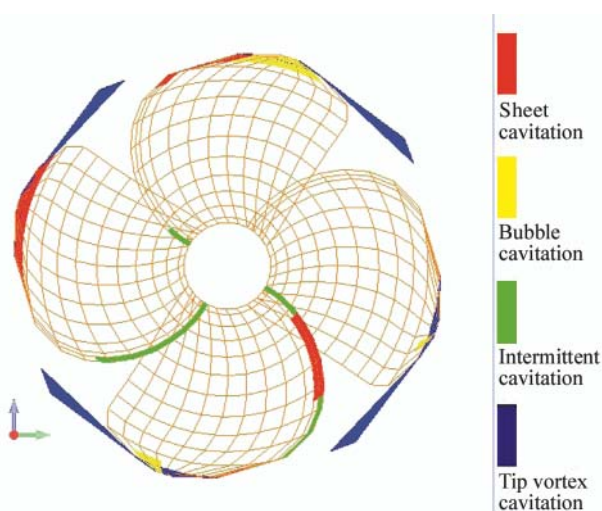
Fig. 16. Cavitation phenomena on the suction side of the single propeller
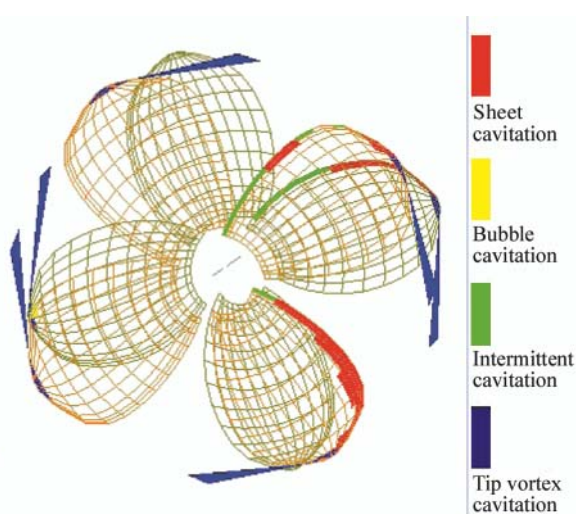
Fig. 17. Cavitation phenomena on the suction side of the tandem propeller set

The most controversial result is the lower delivered power for the tandem propeller set. This is mainly due to the higher value of the hull efficiency for the tandem propeller set. The hull efficiency depends strongly on the diameter of the propeller. In the analyzed example the optimum diameter for the single propeller is D = 8.25 m, while the optimum diameter of the tandem propeller set is equal to D = 7.4 m. In this case the hull efficiency was about 5 per cent higher for the smaller diameter.

The lower values of the harmonic amplitudes of the unsteady bearing forces result from the higher number of blades in the tandem propeller set, while the lower values of the pressure pulsations result both from the higher number of blades and the smaller diameter of this set.

FINAL REMARKS

The above presented computer system facilitates the process of design of the tandem co-rotating propellers. The system integrates all components necessary for the correct design of the tandem propellers. The design and analysis calculations themselves are performed very quickly and the graphical procedures enable an easy interpretation and analysis of the results. The short computation time allows an easy analysis of many variants of the design. For example the following parameters of the designed propeller may be varied without leaving the computer system:
- the number and shape of the propeller blades,
- the ship speed and the rate of propeller rotation,
- the division of thrust between the forward and aft propeller,
- the radial distribution of the hydrodynamic loading,
- the axial distance between the forward and aft propeller.

This enables an effective optimization of the tandem co-rotating propellers from the point of view of propulsive efficiency, cavitation, induced pressure pulsations, acoustic pressures and fluctuating bearing forces. The graphical presentation of all results makes this optimization process even easier.

The above presented example, as well as the results of computations presented in [2] for ducted propellers, demonstrate that propellers other than a conventional single propeller are worth considering in the design process of ships. The three propeller design systems [1, 2], based on the same basic elements of the design calculations, in which the preparation of the input data is almost identical, enable an easy comparative analysis and an appropriate selection of the optimum propeller type for any application.

BIBLIOGRAPHY

1. Koronowicz T., Krzemianowski Z., Tuszkowska T., Szantyr J. A.: *A complete design of ship propellers using the new computer system.* Polish Maritime Research. No. 1/2009, vol.16
2. Koronowicz T., Krzemianowski Z., Tuszkowska T., Szantyr J. A.: *A complete design of ducted propellers using the new computer system.* Polish Maritime Research. No. 2/2009, vol.16
3. Koronowicz T.: *Algorithm of the Design Program Based on the Single Layer Lifting Surface Model Applied to the Arbitrarily Skewed Propellers.* (in Polish) IFFM Report No. 295/86
4. Koronowicz T.; *Analysis of the Velocity Field Induced by the System of Helical Vortices.* (in Polish) IFFM Report No. 643/1969
5. Tuszkowska T.,Koronowicz T.: *Determination of the Geometrical Characteristics of the Aft Propeller of the Tandem Propeller Set.* (in Polish) IFFM Report No. 20/695/1971

6. Koronowicz T.: *Determination of the Velocity Field in the Close Vicinity of a Screw Propeller.* (in Polish) IFFM Report No. 58/729/1973

7. Koronowicz T.: *Determination of the Variation of the Induced Velocities in the Propeller Wake.* (in Polish) IFFM Report No. 83/745/1974

8. Tuszkowska T.: *The Influence of Propeller Location in a Tandem Co-Rotating Propeller Set on Hydrodynamic Characteristics.*(in Polish) Transactions IFFM No. 65, 1974

9. Tuszkowska T.: *The Influence of Axial Location in a Tandem Co-Rotating Propeller Set on Hydrodynamic Characteristics.*(in Polish) Transactions IMP PAN No. 69, 1975

10. Szantyr J. A.: *A Computer Program for Calculation of Cavitation Extent and Excitation Forces for a Propeller Operating in the Non-uniform Velocity Field*, Int. Shipbuilding Progress, Vol. 26 No. 296, 1979

11. Szantyr J., A.: *A Deformable Lifting Surface Method for Determination of Unsteady Cavitation on the Propeller Blade and Its Hydrodynamic Consequences* (in Polish), Bulletin of IFFM No. 183/1110/84, 1984

12. Szantyr J. A. A Method for Analysis of Cavitating Marine Propellers in non-uniform Flow, Intern. Shipbuilding Progress Vol. 41, No. 427, 1994

CONTACT WITH THE AUTHORS

Tadeusz Koronowicz, Prof.
Zbigniew Krzemianowski, Ph. D.
Teresa Tuszkowska, Ph. D.
Institute of Fluid-Flow Machinery,
Polish Academy of Sciences
Fiszera 14
80-952 Gdansk, POLAND
e-mail: ttk@interecho.com

Jan A. Szantyr, Prof.
Department of Turbomachinery
and Fluid Mechanics,
Gdańsk University of Technology
Narutowicza 11/12
80-233 Gdansk, POLAND
e-mail: jas@pg.gda.pl

Analysis of hazard to operator during design process of safe ship power plant

T. Kowalewski, M. Sc.
A. Podsiadło, Ph. D.
W. Tarełko, Assoc. Prof.
Gdynia Maritime University

ABSTRACT

This paper presents comparison of two methods for assessment of hazards to ship power plant operator, used in the preliminary stage of ship power plant design process: the matrix method and that based on fuzzy logic. And, it reports this way results of realization of the research projects [1, 2] financed by Polish Ministry of Science and Higher Education.The assessment of hazard to ship power plant operator, carried out at preliminary design stages meets certain difficulties resulting from that information connected with his safety are scarce or associated with high uncertainty. Therefore fuzzy logic was decided to be used to safety assesment. It was found out that at preliminary design stages application of the fuzzy-logic-based assessment yielded better results as compared with the classic matrix method.

Keywords: safety; design process; ship power plant; hazard; fuzzy inference

INTRODUCTION

Hazard analysis makes it possible to effectively rationalize activities aimed at safety assurance, carried out in the design phase of technical systems. Qualiatitve methods of hazard analysis are commonly used as they are more easily applicable and require much less detailed data than the quantitative ones.

In practice the following occupational hazard assessment methods are usually applied:
- matrix methods in which hazard (risk) value is read from special weighing tables (matrices), e.g. preliminary hazard analysis (PHA), risk matrix acc. the Polish Standard PN 18002,
- index methods in which final hazard (risk) value is a more or less complex product of assumed estimating weights, e.g. the Risk Score, Five Steps Method,
- risk graphs where risk value is calculated from an appropriately designed graph, e.g. the Risk Graph,
- other methods with the use of which reviews of control lists are carried out according to elaborated procedures, or detail analyses of production processes and systems, e.g. the Method of Control Lists (CL), „What- If?" Method.

In the subject-matter literature on occupational hazard assessment, methods based on fuzzy logic are lacking. In this paper are presented results of realization of the research projects [1, 2] financed by Polish Ministry of Science and Higher Education. During the research various assessment methods of occupational hazard to ship power plant operator were considered. It was assumed that the subjective risk will be the basis for assessing the occupational hazard. It means that occurrence probability of hazards and quantity of possible consequences resulting from the hazards is assessed with help of experts in the considered area. To achieve such subjective information a special questionnaire was prepared. The information gained from it was used for occupational hazard assessment by using two methods: the matrix method and that based on fuzzy logic.

RESEARCH QUESTIONNAIRE FOR SUBJECTIVE RISK ASSESSING

To determine subjective information on hazards to ship power plant operator performing operational tasks it was decided to use the output from realization of the first research project of these authors [1]. In its frame were revealed the hazards which greatly impact safety of ship power plant operators. The research questionnaire was aimed at gaining information which makes it possible to estimate operator's hazard level for particular symptoms of the hazards.

For purposes of gaining subjective information from experts and its further assessing the following kinds of hazards to operator were assumed:
- functional ones (connected with function of a device):
  - chemical hazard - resulting from factors whose chemical features may endanger health of operator (presonal injury accident or illness),

- thermal hazard - resulting from possible contact of ship power plant operator with media or/and surfaces of structural elements of various temperature values,
- pressure hazard – resulting from possible contact of ship power plant operator with media or/and surfaces of structural elements being under pressure,
- hazard due to work environment factors– in ship power plant its operator may be exposed to action of factors associated with ship's operation state (noise, vibrations, air parameters and composition, etc).
- mechanical energy hazard – resulting from possible exposure of operator to action of factors generated by an element in its working motion or releasing its elastic deformation,
- electric energy hazard– resulting from possible contact of ship power plant operator with electrically fed machines and devices,
- operational hazards (connected with a kind of realized task):
  - hazards resulting from realization of plant operation procedures,
  - hazards resulting from the range of the plant operation maintaining,
  - hazards resulting from the range of supply procedures,
  - hazards resulting from safety state control.

Each of the specified hazards to operator is assessed with respect to the following factors:
- possibility of contact of operator with a given kind of hazard, specified in the questionnaire,
- degree of hazard to operator in the case of direct contact with a given, specified in the questionnaire, kind of hazard.

On the basis of the elaborated questionnaire weighing coefficients for particular kinds of hazard were determined. Owing to that during assessment of operator's safety to account for a different impact of particular kinds of hazards, was possible.

On the basis of the assessment results is gained the information necessary for planning corrective and preventing actions directed to discrepances identified in the process. On the basis of the analysis performed in [1] design phases in which such analysis can be done, were determined. It was found out that the information being at designer's disposal already in the preliminary design stage is sufficient for identification of hazardous areas in ship power plant. Therefore was undertaken an attempt at elaborating, on the basis of preliminary design of ship power plant, such assessment procedure of operator's safety state, on which the following actions could be based:
- choice of the most effective ways for improving safety of operators,
- assessment of degree of improvement of safety of operators.

In order to limit a number of considered areas potentially hazardous to operator the notion of *Elementary Hazardous Situation (EHS)* was introduced. By using the *EHS* were defined the situations in which a *Service Operation* on a given *Structural Unit* in a given *Operating Zone* would be realized. The *Structural Unit* was defined to be a broad-understood technical object, namely, an arbitrary element, part, device, machine and its equipment, installation, which can be considered separately. And, the *Service Operation* constitutes a set of elementary actions of operator, aimed at realization of a given operating task, e.g. shutting the valve, disconnecting the coupling, dismounting the cover etc. The *Operating Zones* determine spatial location of a place in which operations are performed on given structural units. The *EHSs* are analyzed with regard to procedures realized in ship power plant being in given operational states.

RISK ASSESSMENT BY USING RISK MATRIX

In view of specificity of ship power plant in principle any its place can be more or less hazardous to operators, depending on a kind of realized operating tasks. Therefore it was assumed that scenarios of hazards to operator consist of operational procedures which indicate successively realized operations dealing with given structural units located in given zones of ship power plant. For each distinguished *Elementary Hazardous Situation* operator's risk is assessed by attributing noxious and dangerous factors, i.e. determined values, to considered hazards. Level of risk to operator realizing a operation within *n-th* procedure, on *m-th* unit located in *k-th* zone of ship power plant, is expressed by means of three indices which account for risk associated with:
- kind of the procedure: $I_{OF, m}^{(n)}$,
- function realized by the unit: $I_{FF, m}^{(n)}$,
- functions realized by a set of units located in the neighbourhood of the operator: $I_{RF, k}^{(n)}$.

A high risk associated with hazards due to dangerous and noxious factors induced from the outside is not always connected with high risk resulting from unit's operation and/or a kind of action realized by operator. Therefore risk level of a given elementary hazardous situation is assessed according to the three-point scale (Tab. 1) for each hazard source separately, depending on its relation to respective average value:

$$(\overline{I_{OF, m}^{(n)}}, \overline{I_{FF, m}^{(n)}}, \overline{I_{RF, k}^{(n)}})$$

calculated for all elementary hazardous situations distinguished in the set of considered procedures.

A result of risk level assessment of elementary hazardous situations as well as relevant procedure is not a sum of estimates but the highest estimate attributed to a given scenario (Tab. 1).

Tab. 1. Assessment of operator's risk level during realization of service operations

Operating procedure		Risk level of action			Assessment of risk level of operation	Assessment of risk level of procedure
		Procedure	Unit	Zone		
		$I_{OF, m}^{(n)}$	$I_{FF, m}^{(n)}$	$I_{RF, k}^{(n)}$		
$P_1 = \langle a_{1,1}, ..., a_{1,i}, ..., a_{1,p1} \rangle$	$a_{1,1}$	1	1	1	1	**3**
	...	...	...	...	...	
	$a_{1,i}$	1	3	1	3	
	...	...	...	...	...	
	$a_{1,p1}$	1	1	2	2	

Procedure	Load by operations $I_A^{(n)}$	Load by units $I_U^{(n)}$	Load by zones $I_R^{(n)}$	Final result of assessment
P_1	2	3	1	**6**
…	…	…	…	**…**
P_p	3	3	2	**8**

A large value of estimate of potential risk to operator during realization of *n-th* procedure may result from a different number of realized operations which may deal with one or a greater number of units located in one or many zones of ship power plant. Therefore to assess range of operator's risk it is proposed to determine, for each procedure, values of the indices of loading by operations, $I_A^{(n)}$, procedures, $I_U^{(n)}$, and zones, $I_R^{(n)}$.

A high level of hazard due to dangerous and noxious factors resulting from number of realized operations is not always connected with a high level of hazard associated with number of units and zones of ship power plant. Therefore risk range of a given operating procedure is proposed to be assessed according to the three-point scale (Tab. 1) for each kind of hazard separately, depending on its relation to respective average value calculated for a set of considered procedures.

Final result of assessment for a given procedure is a sum of estimates for loading by operations, units and zones (Tab. 2).

Results of assessment of level and range of operator's risk constitute the basis for making decisions about which hazard scenarios (operating procedures) should be subjected to moderating strategies (Tab. 3).

Tab. 3. Summary of results of assessment of operator's risk during realization of operating procedure

Risk level of operating procedure	Risk range of operating procedure		
	3	4-6	7-9
3	**R**	**Z**	**Z**
2	**U**	**R**	**Z**
1	**U**	**U**	**R**

The result **Z** – 'moderate' – stands for necessity of undertaking corrective actions to lower the risk to a permissible level (average or lower one).

The result **R** – 'consider' – stands for that to plan actions aimed at lowering the risk is advisable.

The result **U** – 'substantiate' – stands for that it is advisable to consider if further lowering the risk level is possible or to ensure that the risk would maintain on the same level at least.

As already mentioned, for each distinguished *Elementary Hazardous Situation* operator's risk is assessed by attributing noxious and endangering factors, i.e.definite values to input variables. On the basis of the questionnaire tests performed with a group of ship engineers, to every distinguished input variables a constant weighing coefficient was attributed. Moreover, for every distinguished state (symptom) of every variable, assessment coefficients of risk level and of frequency of its occurence, were determined.

The product of occurrence frequency of a given hazard - inducing event and its consequences is assumed to be a risk measure. A risk estimate category (risk levels) is read from a risk matrix. Such matrix makes it possible to perform, for every distinguished factor (either functional or operational), the following:
− to attribute risk estimate due to action of a distinguished factor, expressed by the integer numbers: 5, 4, 3, 2 and 1, as well as verbally: very high risk, high risk, medium risk, low risk, very low risk,
− to apply the estimations to risk assessment of:
  - an Elementary Hazardous Situation (EHS),
  - a set of EHSs considered from a given point of view, e.g. risk assessment for a given structural unit (which service operations are performed by a given operator and which technical objects are in his surroundings).
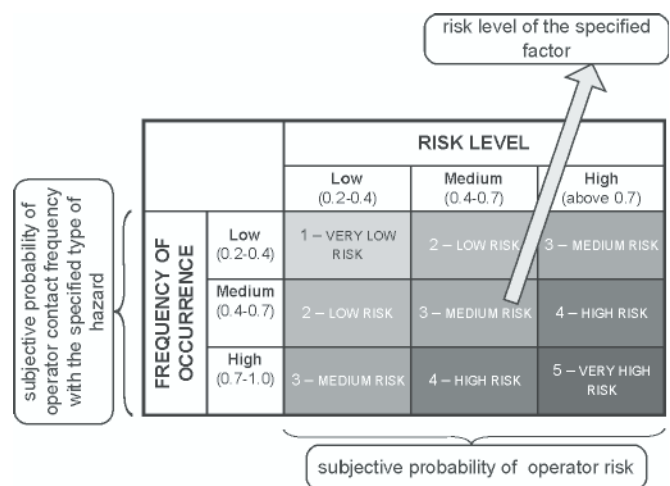
Fig. 1. The hazard-induced risk assessment matrix

In general, risk is defined as the product of occurrence frequency of a given hazard – and probable losses resulting from an incurred damage. On this basis and the preformed questionnaire tests the hazard-induced risk assessment matrix was elaborated (Fig. 1).

RISK ASSESSMENT OF ELEMENTARY HAZARDOUS SITUATION BY USING FUZZY LOGIC

The first attempt to making use of fuzzy logic to risk assessment for ship power plant operator was described in [3]. Since the time the method has been subjected to certain modifications. The assessing of operator's risk has been so far based only on determining hazards to safety of operator during realization of given operations. In order to more reliably determine possible hazards, information associated with frequency of operator's contact with selected kinds of hazards, has been taken into account. Additionally, forms of memebership functions of particular fuzzy sets have been modified.

Data achieved from the questionnaires were applied to building fuzzy sets both in discrete and continuous domain. Sets in the continuous domain were used to hazards due to temperature and pressure. Values obtained from the questionnaires for the hazards were linearly approximated and normalized to achieve sets of a triangular or trapezoidal form. For the remaining hazards the sets were expressed in the discrete form because of a limited number of elements in the space of consideration, X. The example discrete memebership functions of degree of hazard to operator in case of his direct contact with a given kind of hazard, are presented in Fig. 2. The continuous memebership functions
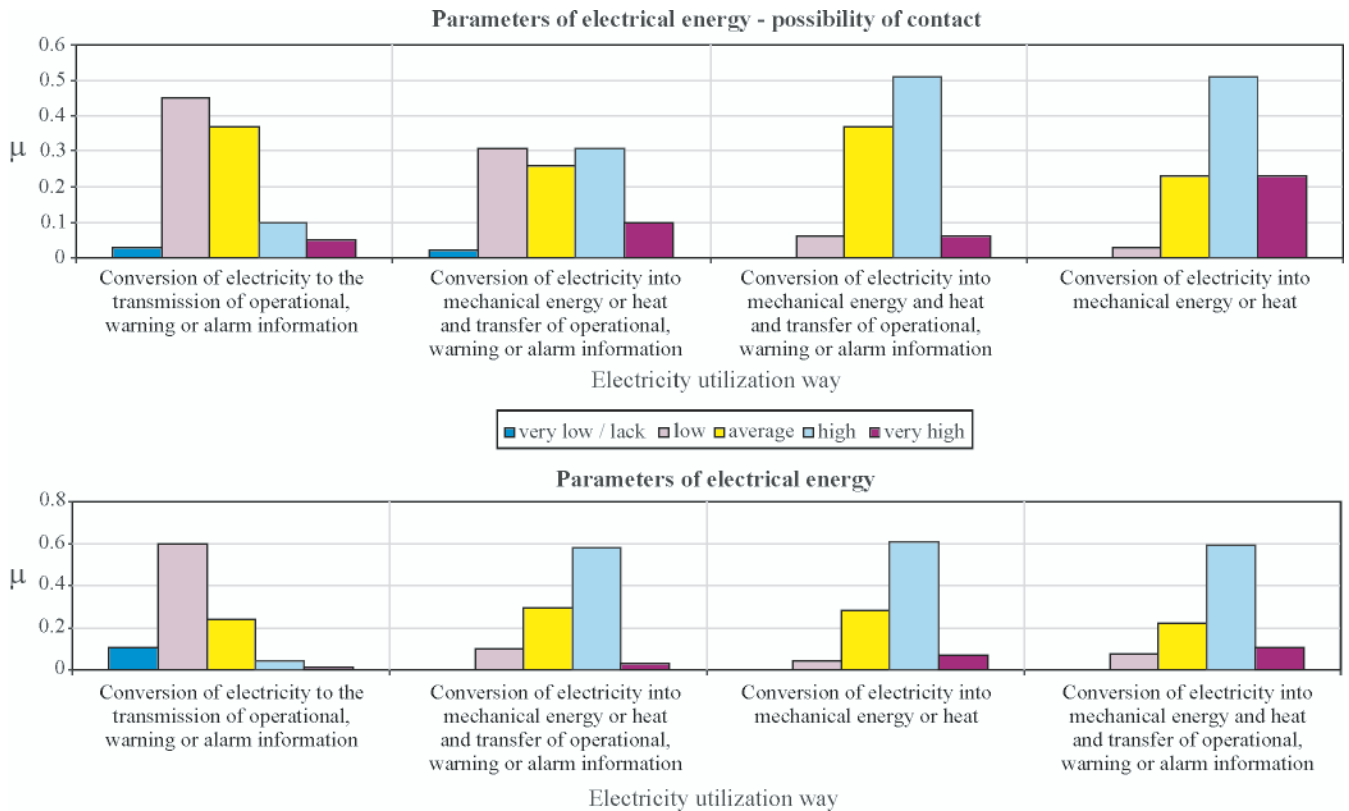
Fig. 2. *Discrete memebership functions of degree of electrical hazard to operator*

for fuzzy sets are shown in Fig. 3. To ensure comparability of risk assessments for every *Elementary Hazardous Situation* with the use of fuzzy logic, the linearly ordered range, from 0 to 5.0, of resulting hazard to operator, was assumed (Fig. 4).

The assessing of risk resulting from *Elementary Hazardous Situation* is made by using fuzzy inference.

It consists in:
− determination of:
  - degree of hazard to operator in case of his direct contact with particular kinds of hazard,
  - possibility of contact of operator with particular kinds of hazard,
− calculation of an aggregated assessment index of hazard level induced by an *Elementary Hazardous Situation (EHS)*,
− the carrying-out of defuzzification to make it possible to assess risk of the *EHS*.

Assessments of degree of hazard to operator as well as possibility of his contact with particular kinds of hazard are obtained from memebership functions on the basis of a set of rules. The rules are of a fuzzy matrix form. The example matrix of rules, which makes it possible to determine level of pressure hazard to operator is shown in Fig. 5.

```
fuzzy_matrix(pressure_rules):-
pressure * pres_cont ->risk_level;

very_low * very_low -> very_low;
very_low * low -> very_low;
very_low * average -> very_low;
very_low * high -> low;
very_low * very_high->low;
…
```

Fig. 5. *Matrix of rules for pressure hazard*
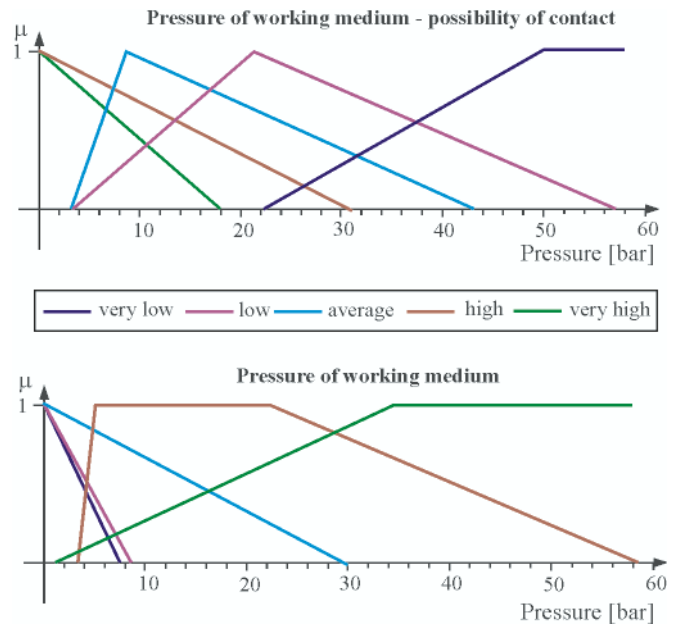
Fig. 3. *Memebership functions which determine pressure hazard to operator*
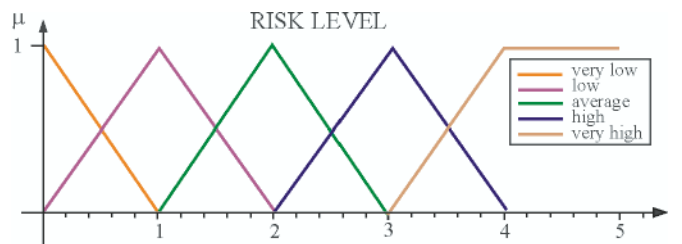
Fig. 4. *Resulting fuzzy sets which determine degree of hazard (risk level) to operator*

The rules contained in it can be iterpreted as follows: "If pressure hazard level (in case of direct contact) is very low and possibility of contact (with the symptom) is very low then the level of the hazard to operator is very low".

The resulting values which determine level of hazard to operator are achieved as a result of fuzzy inference according to Mamdani model. During the process the matrix of rules is searched in order to determine degree of their activation. Only the rules concerning fuzzy sets dealing with the assumed input quantities, are taken into account. Each of the rules generates a resulting fuzzy set of a definite height. In the next phase the sets are summed-up. The so - obtained fuzzy set makes it possible to determine finally a level of hazard to operator.

To form such a matrix at twelve input variables is very difficult. Therefore the variables were grouped into six pairs composed of hazard levels (in case of direct contact) and possibility of contact with a given kind of hazard. For each of the pairs separate resulting fuzzy sets are determined in the fuzzy inference process. In the final phase of the inference a 'sharp' resulting value is determined in the defuzzification process on the basis of sum of the sets.

To exemplify the fuzzy inference an example assessment of hazard during replacement of heavy oil transporting pump is considered. The task is realized by using a fuzzy inference mechanism available in the programming language PROLOG LPA.

E.g. if the following symptoms are assumed initial values:

- *hazard due to work environment factors:* manoeuvres,
- *chemical hazard:* fuel (heavy oil),
- *pressure hazard:*12.5 bar
- *thermal hazard:* 150°C
- *mechanical energy hazard:* rotating element in permanent or periodical motion,
- *electrical energy hazard* - electrical energy is converted to mechanical or thermal one, then the resulting risk level amounts to 2.2.
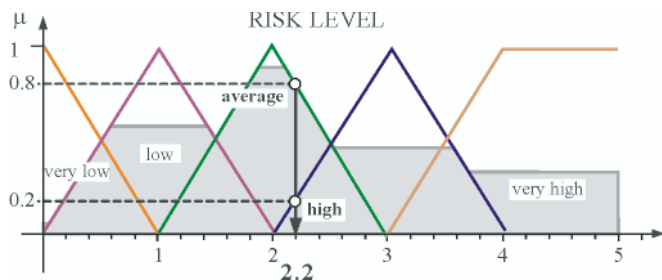
Fig. 6. Final value of risk assessment of Elementary Hazardous Situation after defuzzification

The obtained value is equivalent to the average risk level of μ = 0.8 and the high risk level of μ = 0.2 (Fig. 6).

CONCLUSIONS

On the basis of the results obtained in the course of the performed investigations it can be stated that the risk assessment of elementary hazardous situation with the use of the risk matrix shows certain disadvantages among which the following, a.o., can be numbered:

- the additive method for determining assessment index of degree of hazard to operator, that causes the linear ordering of potential impact of particular symptoms of particular variables, and not quite adequately reflects real impact of

particular symptoms of distinguished factors on inducing hazard to operator,
- the necessity of performing assessment of all *Hazardous Zones* covered by realized operating procedure, even in the case when the zones can not in reality produce any potential hazard.

In the case of the assessment method of risk resulting from *Elementary Hazardous Situation,* based on fuzzy logic, it is possible to fulfil a very important postulate, namely to ensure comparability of operator's hazard level in case of all *Elementary Hazardous Situations.*

Moreover, there is not necessary to determine weighing coefficients for particular functional factors, as this is the case when assessing risk from *Elementary Hazardous Situation* by using the risk matrix. It results from that the assessment is performed by user of the system (ship power plant designer responsible for accounting for operator's safety during design process), but not its designer. It means that assessment of level of a hazard to operator, resulting from possible action of functional factors, is performed during the design process from the point of view of harmfulness of possible effects to operator. The user of the system, considering a set of states of a given functional factor, assesses harmfulness of effects to operator not comparing them with gravity of effects resulting from other functional factors.

It can be stated that fuzzy logic offers wide possibilities in analyzing safety of ship power plant operator, especially in the initial design stages where information associated with his safety are very scarce or uncertain.

In contrast to the classical solutions, the method of operator's risk level assessment with the use of fuzzy rules, reflects qualitative aspects of human knowledge in a more realistic way, and the inference process itself does not require making any quantitative analyzes.

BIBLIOGRAPHY

1. Tarełko W. *et al.*: *Antropotechnical assumptions for the designing of safe technical objects - the content-related report* (in Polish). Report on realization of the research project No. 8T07C 011 20 financed by Polish Scientific Resarch Commitee (KBN). Bulletin No. 1. KPT. Gdynia Maritime University, Gdynia 2004
2. Tarełko W. *et al.*: *A method of designing safety of operators of complex technical objects - the content-related report* (in Polish). Report on realization of the research project No. 4T07B02529 financed by Polish Scientific Resarch Commitee (KBN). Bulletin No. 1. KPT. Gdynia Maritime University, Gdynia 2009
3. Kowalewski T., Podsiadło A., Tarełko W.: *Application of fuzzy inference to assessment of degree of hazard to ship power plant operator*. Polish Maritime Research, No. 3(53), vol. 14, Gdańsk 2007

T. Kowalewski, M. Sc.
A.Podsiadło, Ph. D.
W.Tarełko, Assoc. Prof.
Faculty of Marine Engineering,
Gdynia Maritime University
Morska 83
81-225 Gdynia, POLAND
e-mail: tar@am.gdynia.pl

A method for evaluating the performance of a marine piston internal combustion engine used as the main engine on a ship during its voyage in different sailing conditions

Jerzy Girtler, Prof.
Gdańsk University of Technology

ABSTRACT

A method is presented for evaluating the performance of piston internal combustion engines used as the main engines on sea-going ships and acting in typical operating conditions. These conditions are described taking into account the performance area of engines of this type. The presented method provides opportunities for calculating the numerical effect of the action using the integral calculus. The above effect is presented as a physical quantity expressed by a number with the metric unit called the joule-second. Proposed is the use of types of integrands (which are functional dependences of the energy converted in these engines on time) which make it possible to use the second fundamental theorem of calculus justifying the use of the Newton-Leibniz formula. The object of the analysis is the process of changes of the energy converted in the internal combustion engines during their operation, described with the aid of a deterministic model of the real process taking into account its sample realisation.

Keywords: engine operation; combustion engine performance evaluation;
interpretation of energy conversion; Newton-Leibniz formula; model of engine operation

INTRODUCTION

In the references [2, 3, 4, 5, 8, 9, 10] their authors propose to interpret the operation of an internal combustion engine as the machine energy state which allows the delivered energy to be converted and transmitted to the receivers, such as, for instance, propellers, pumps, compressors, etc. For the operation understood in the above way, a method was proposed for evaluating the operation of piston Diesel engines used in marine industry, which would take into account engine wear [2, 3, 6]. The method based of a well founded assumption that the increasing wear (of both the surface and volumetric nature) of the piston internal combustion engines, like in case of other energy conversion machines, is accompanied by decreasing efficiency of conversion and transmission of the delivered energy [7, 11].

The presently proposed method for evaluating the performance of the piston internal combustion engines used as the main engines on the ships (the engines used in the main propulsion system of the ship) takes into account the fact that correct operation of these engines requires securing the delivery of relevant portion of energy to the energy receiver, which is the screw propeller. Securing the energy transmission to the propeller requires from the main engine to operate in such a way that that the ship is able to move at required speed in certain sailing conditions, which are most of all determined by the height and length of the waves, the speed and direction of the wind, the speed and direction of the sea currents, and the depth and width of the water region on

which the ship sails. The above operation requires converting relevant portions of energy in working spaces (cylinders) of the main engine, depending on current sailing conditions. This energy is delivered in the fuel and air to the engine combustion chambers during engine operation. The operation of the main engine consists in converting this energy into heat and work and its further transmission to the ship's screw propeller as the energy receiver. In the case of piston internal combustion engines, the chemical energy contained in the fuel-air mixture is firstly converted in the combustion chambers into the thermal energy (heat) of the exhaust gas, and than – into the mechanical energy of the moving piston from the upper top centre (TDC) to the bottom dead centre (BDC). This interpretation of the energy conversion takes into account that the heat is the form of energy conversion from the chemical energy of the fuel-air mixture into the thermal energy, while the work is the form of energy conversion from the thermal energy into the mechanical energy [3, 7]. Obviously, the energy conversion in the engine is accompanied by changes of the converted energy.

During the engine operation, the energy (E) can be converted at different rates, to respond to the requirements connected with the current task to be done by the engine [7, 11]. The energy conversion rate is meant here as the amount of energy related to the time unit (energy flux) and denoted as $\dot{E} = a$. Generally, the above task can be understood as delivering the energy needed for executing the task in certain operating conditions and certain time. The engine operation, understood as energy delivery in certain time, will take larger and larger values with the increasing time of operation. Therefore the

engine usability for executing the given task can be evaluated by comparing its possible operation with the required operation, necessary for the execution of the given task. The possible operation is the operation which can be executed by the engine at its current technical state, while the required operation is the operation of the engine which secures the execution of the task in the existing operating conditions. Therefore evaluating the operation of the main engine and its usability for executing the given task requires first formulating the conditions of engine operation and then working out the model (deterministic or stochastic) of the operation of the engine which will take into account the sailing conditions.

CONDITIONS OF THE MAIN ENGINE OPERATION

The conditions of the main engine operation depend on the conditions in which they work, the latter being defined by the external conditions of ship sailing and tasks undertaken by ship users (the crew). The abovementioned conditions and tasks are the reasons why different portions of energy are converted in different times in the engine working spaces. However, in each case the operation of the main engine is determined by its performance area defined by engine speed characteristics, such as: external characteristics and control characteristics [7, 11]. If the main engine propeller characteristics, which also belong to the group of speed characteristics, are mapped on the engine speed characteristics, then the operating ranges are determined for the given engine.

Figure 1 shows the theoretical characteristics, while the real characteristics are presented in Fig. 2. The real characteristics differ from their theoretical counterparts, as the average torque (M_o) of the piston internal combustion engine is the function of the average effective pressure (p_e), the values of which depend not only on the dose of the delivered fuel (the fuel charge) but also on the engine rotational speed (n).

The torque (M_o) as the function of the average effective pressure (p_e) is given by the following formula [6, 7, 11]:

$$M_o = c_s p_e \qquad (1)$$

where:

$$p_e = f(G_p, W_d, p_d, R_\mu, T_d, L_o, \lambda, \eta_v, \eta_i, \eta_m) \qquad (2)$$

and:

c_s – coefficient describing constructional characteristics of the engine
G_p – fuel charge
W_d – net caloric value of the fuel
p_d – pressure of the air delivered to engine working spaces
R_μ – universal (absolute) gas constant (R·M)
T_d – temperature of the air delivered to the engine working spaces
L_o – theoretical amount of air required for burning 1 kg of fuel
λ – excess air number
η_v – efficiency of engine working space (cylinder) filling
η_i – indicated efficiency
η_m – mechanical efficiency of the engine.

The operation of the main engine is limited in time in the overload area, especially in the case of the torque overload area represented by the area 2-3-4-9-2 on the theoretical characteristic (Fig. 1) and by the area 9*-3*-4-9-9*on the real characteristic (Fig. 2). Moreover, the engine cannot also operate long when it is only overloaded with high rotational speed, see the area 6-7-8-9-6 on the theoretical characteristic and the area

6-7*-10*-9-6 on the real characteristic. Obviously, the operation of the engine is even more limited in time when it is overloaded with both the load and the rotational speed, which is represented by the area 4-5-6-9-4 on both the theoretical characteristic (Fig. 1) and the real characteristic (Fig. 2).
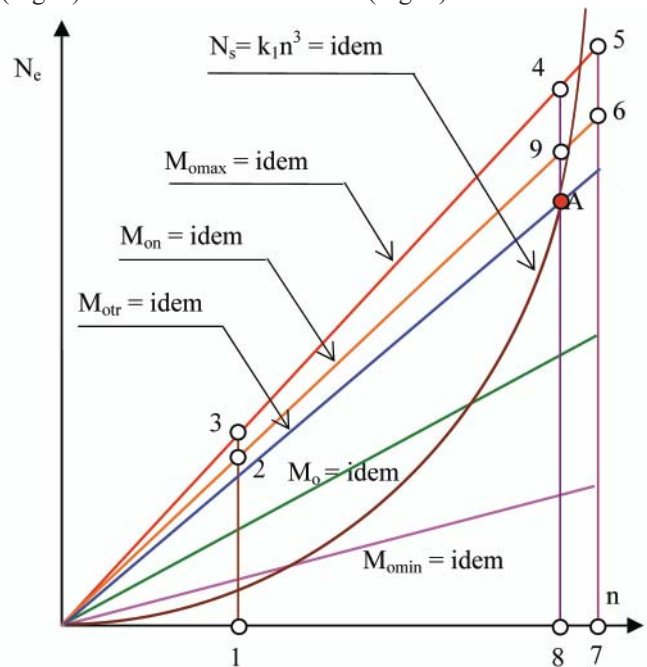
Fig. 1. Theoretical speed characteristics of the piston engine used as the main propulsion (main engine) on a sea-going ship:
• engine performance area (the area of permissible engine loads, the area of so-called stable operation of the engine) → 1-2-9-8-1,
• engine overload area → 2-3-4-5-6-7-8-9-2

The theoretical characteristics $N_e = f(n)$ result from the relation [6, 7, 11]:

$$N_e = \omega M_o \qquad (3)$$

where:
N_e – effective power of the engine
ω – rotational speed of the engine crankshaft
M_o – average torque (turning moment) of the engine.

The real characteristics of the engine (Fig. 2) differ from their theoretical counterparts (Fig. 1) because the torque M_o is the function of the average effective pressure (p_e), the value of which depends on physical quantities being the functions of the engine rotational speed (n). In general, the relation between the pressure p_e and the abovementioned quantities is given by the formula (2).

The physical quantities λ, η_v, η_i, η_m in formula (2) are the functions of the engine rotational speed (n). Therefore assuming that W_d = idem, p_d = idem, R_μ = idem, T_d = idem, L_o = idem, we can write:

$$p_e = c_p n \qquad (4)$$

where [6, 7]:

$$c_p = f(G_p, W_d, p_d, T_d, R_\mu, L_o) \qquad (5)$$

and:
$G_p, W_d, p_d, T_d, R_\mu, L_o$ – physical quantities having the same interpretation as in the description of formula (2).

Since the remaining physical quantities in formula (2) are functions of the engine rotational speed (n), i.e.

$$\lambda = f(n), \eta_v = f(n), \eta_i = f(n), \eta_m = f(n)$$
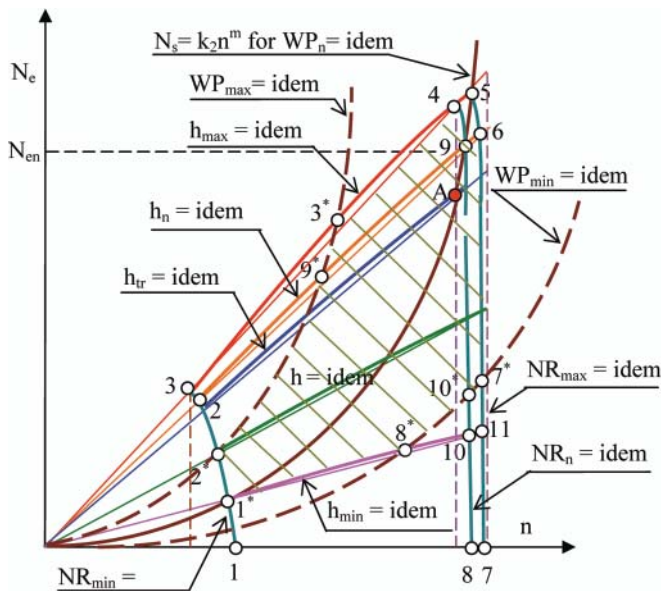
Fig. 2. *Speed characteristics of the real piston engine used as the main propulsion (main engine) on a sea-going ship:*
• engine performance area (the area of permissible engine loads, the area of so-called stable operation of the engine) → 1*-2*-9*-9-10*-10-8*-1*;
• engine overload area → 2-3-3*-4-5-6-7*-10*-9-2;
• area illustrating the range of engine operation (Fig. 2):
1*-2*-9*-3*-4-5-6-7*-10*-8*-1*.
Here: N_e - *effective power of the engine,* N_{en} - *nominal (rated) effective power,* **n** - *rotational speed,* M_o - *average torque (turning moment),* M_{omax} - *maximal torque,* M_{on} - *nominal (rated) torque,* M_{otr} - *continuous torque,* M_{omin} - *minimal torque,* h_{max} - *maximal setting of the injection pump,* h_n – *nominal (rated) setting of the injection pump,* h_{tr} - *continuous setting of the injection pump,* h_{min} - *minimal setting of the injection pump,* NR_{max} - *maximal setting of the controller,* NR_n - *nominal (rated) setting of the controller,* NR_{min} - *minimal setting of the controller,* WP_{max} - *most difficult conditions for ship sailing (largest resistance of motion),* WP_n – *nominal conditions for ship sailing,* WP_{min} – *easiest conditions for ship sailing (smallest resistance of motion),* $N_s = k_1 n^3$ – *theoretical propeller characteristic illustrating the dependence of the power needed by the propeller on the rotational speed (n),* $N_s = k_2 n^m$ – *real propeller characteristic illustrating the dependence of the power needed by the propeller on the rotational speed (n),* k_1 – *theoretical power factor,* k_2 – *real power factor,* **m** – *coefficient depending on the shape of the ship hull (for the displacement hulls m ≈ 3,0)*

then the real performance area (working area) of the engine will be limited by the curves: h_{max} = idem, NR_{max} = idem, h_{min} = idem and NR_{min} = idem. However, the engine operation range will be determined by the area smaller than the performance area, as the main engine can only operate in such a way that it secures delivering to the ship propeller the energy which is needed for current task execution. The amount of this energy needed by the screw propeller in certain operating conditions depends on the real propeller characteristic $N_s = f(k_2, n)$, which is different for different sailing conditions WP_n = idem. In general we can write [11]:

$$N_s = k_2 n^m \qquad (6)$$

where:
k_2, n, m – physical quantities having the same interpretation as in the description of Fig. 2.

The factor k_2 in formula (6) mainly depends on WP (ambient conditions, sailing conditions), which are affected by:
• state of the sea (height, speed and direction of waves),
• speed and direction of sea currents,
• speed and direction of the wind,
• depth and width of the water region on which the ship sails,
• condition of the underwater part of the hull,
• ship's heel and trim.

Moreover this factor depends on the type of ship motion (free motion, towing another ship, etc.), its loading condition, hull dimensions and shape, and the speed of ship motion.

The WP conditions can change within the range from most favourable (WP_{min} = idem) down to least favourable (WP_{max} = idem), which was illustrated in Fig. 2. These conditions determine the operating area for the main engine, which is illustrated by the area: 1*-2*-9*-3*-4-5-6-7*-10*-8*-1*.

When analysing the operating range of this type of engines, we can consider it obvious [11] that the engine loading conditions change (Fig. 2) from point:
• 1* to 2* along the control characteristic NR_{min} = idem,
• 2* to 3* along the propeller characteristic WP_{max} = idem,
• 3* to 4 and 5 along the characteristic of engine external power for the maximal injection pump setting h_{max} = idem,
• 5 to 6 and 7* along the control characteristic NR_{max} = idem,
• 7* to 10* and 8* along the propeller characteristic WP_{min} = idem,
• 8* to 1* along the characteristic of engine external power for the minimal injection pump setting h_{min} = idem.

The described range of the main engine operation is shown in Fig. 2 as the hatched area. Within this range the main engine can be loaded with different power (N_e) depending on current sailing conditions (WP) and the resultant propeller characteristics changing between WP_{min} and WP_{max}. The power generated by the main engine is always determined by the engine/propeller cooperation point localised at the crossing of the characteristic of engine external power with the propeller characteristic. A sample selection of points of engine/propeller cooperation is shown in Fig. 2, including:
• point A created by crossing of the characteristics h_{tr} = idem and WP_n = idem,
• point 9 created by crossing of the characteristics h_n = idem and WP_n = idem,
• point 5 created by crossing of the characteristics h_{max} = idem and WP_n = idem

The above cooperation points are created depending on the selected injection pump setting (h = idem) for one given propeller characteristic (WP = idem). Therefore it may happen that for the given propeller characteristic the main engine can be loaded with power according to the following external power characteristics [7, 11]:
• external characteristic of partial power N_{ec} (h_c = idem, c = 1, 2, …, $N_{ec} < N_{etr}$),
• external characteristic of continuous operating power N_{etr} (h_{tr} = idem),
• external characteristic of nominal power N_{en} (h_n = idem),
• external characteristic of maximal power N_{emax} (h_{max} = idem).

Sample realisation of changing the main engine power during engine operation is shown in Fig. 3.

The effective power N_e generated by the main engine (Fig. 2 and Fig. 3) contains the information how fast the effective work L_e will be done in certain time t [7, 11]. That means that the power characterises the engine operation in the aspect of converting the energy into work in the engine working spaces, taking into account different losses, especially thermal losses. However, the engine operation consisting only in energy conversion into work is not possible if earlier the energy has not been converted into heat in the engine working spaces [2, 3, 7, 11]. Therefore, when analysing the operation of the main engine we should take into account the energy contained in the air/fuel mixture which, delivered to the engine, is first
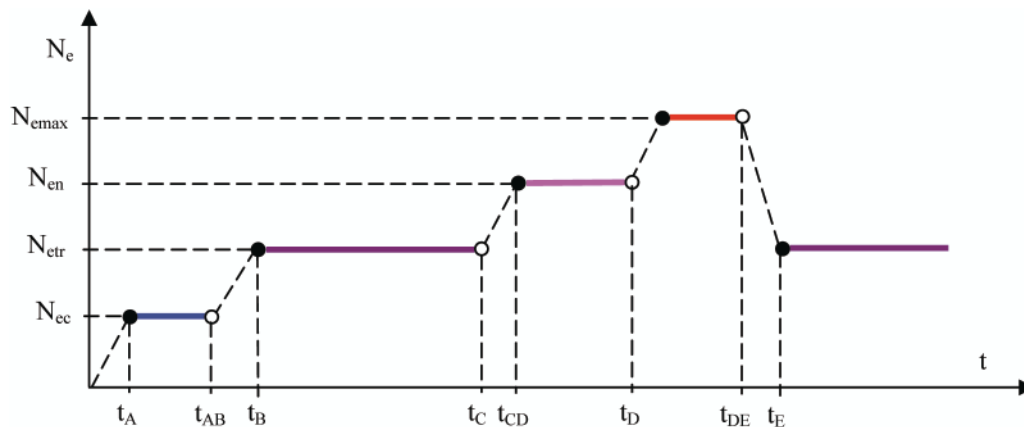
Fig. 3. *Sample realisation of the process of main engine load changes during engine operation: N_e – effective power, t – time of operation*
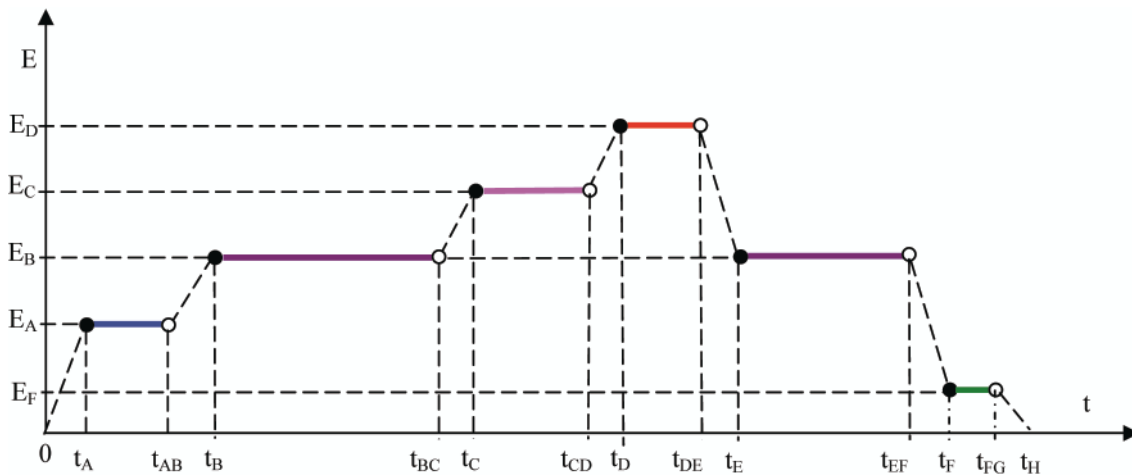
Fig. 4. *Realisation of the process of main engine energy changes during engine operation: E – converted energy, t – time of operation*

converted to heat (Q) and then to work (L), rather than the engine power output. The analysis should take into account the process of conversion of the energy delivered to the engine. In this process, its particular states are to be the energy states which release the energy $E_i (i = A, B, C, D, F, …, I)$, to provide opportunities (Fig. 3) for generation particular powers N_{ej} ($j = c$, tr, n, max), necessary for correct engine operation and securing the realisation of the operating task.

The above analysis requires working out a deterministic, or stochastic model of the process which secures power changes, like the case shown in Fig. 3, for instance. The discussion presented further in the article bases on the deterministic model of the main engine operation at given time.

DETERMINISTIC MODEL OF MAIN ENGINE OPERATION AND ITS APPLICATION TO PERFORMANCE EVALUATION

After adopting the deterministic model of the process of main engine operation at given time it is easily to evaluate the engine operation using the integral calculus. Obviously, this evaluation depends on an individual realisation of the above process. Its sample realisation which secures power changes like in the case shown in Fig. 3 is shown in Fig. 4. The model provides opportunities for evaluating the performance of the analysed engine using the integral calculus.

The interpretation of the symbols used in Fig. 4 is the following:

- t_A, t_B, t_C, t_D, t_F – operation times, at which the engine energy states appear which make it possible to convert successively the energy E_A, E_B, E_C, E_D, E_F,

- t_E, - operation time, at which the engine energy state appears again which makes it possible to convert the energy E_B,
- E_A, E_B, E_C, E_D, E_F – energies, which make it possible for the engine to reach the effective powers $N_{ec}, N_{etr}, N_{en} N_{emax}$, N_{ecmin} (minimal partial power), respectively
- $t_{AB}, t_{BC}, t_{CD}, t_{DE}, t_{FG}$ – operation times, at which the energy states decay (stop existing) which make it possible to convert successively the energy E_A, E_B, E_C, E_D, E_F,
- t_{EF} – operation time, at which the energy state decays again which makes it possible to convert the energy E_B created at time t_E,
- $\langle 0, t_A \rangle$ – time interval (time) after which the energy E_A is reached,
- $\langle t_A, t_{AB} \rangle$ – time interval (time) during which the energy E_A is converted,
- $\langle t_{AB}, t_B \rangle$ – time after which the energy E_B is reached,
- $\langle t_B, t_{BC} \rangle$ – time during which the energy E_B is converted,
- $\langle t_{BC}, t_C \rangle$ – time after which the energy E_C is reached,
- $\langle t_C, t_{CD} \rangle$ – time during which the energy E_C is converted,
- $\langle t_{CD}, t_D \rangle$ – time after which the energy E_D is reached,
- $\langle t_D, t_{DE} \rangle$ – time during which the energy E_D is converted,
- $\langle t_{DE}, t_E \rangle$ – time after which the energy E_B is reached again,
- $\langle t_E, t_{EF} \rangle$ – time during which the energy E_B is converted,
- $\langle t_{EF}, t_F \rangle$ – time after which the energy E_F is reached,
- $\langle t_F, t_{FG} \rangle$ – time during which the energy E_F is converted,
- $\langle t_{FG}, t_H \rangle$ – time after which the engine is stopped and the energy is not converted any longer (at time t_H the energy is $E_H = 0$).

Evaluating the performance of the main engine in the form of a number and the metric unit called the joule-second, and presenting this operation in the form of a relevant area in the E-t

coordinate system, require integrating the energy in particular time intervals and summing up the obtained integrals.

It results from the realisation of the process of main engine energy changes during engine operation, see Fig. 4, that during the time t_A after starting the engine the energy E_A is converted. The increase of this energy can be linear (like the case shown in the figure), but can also take a course of the second or third order parabola, depending on the operating strategy of increasing the main engine load.

Evaluating the main engine performance in the time interval between $\langle 0, t_A \rangle$ with the aid of the integral calculus requires finding the antiderivative of the energy $E(t)$, which is a function of the time of engine operation in this time interval. Therefore we should not only calculate the integrals of the function $E(t)$, but also decide upon their existence. We can state that the energy functions, both linear and parabolic, have their antiderivatives because they are continuous in the examined time interval $\langle 0, t_A \rangle$. The theorem about the existence of these antiderivatives results from the theorem of the existence of the antiderivative, which for the purpose of the engine operation investigations can be formulated in the following way [1]: if the function $E(t)$ is continuous in the integration interval T, than this function has the antiderivative in this interval. Therefore we can make use of the second fundamental theorem of calculus (the Newton-Leibnitz theorem) and write that the engine performance in the time interval $\langle 0, t_A \rangle$ is:

$$D(0, t_A) = D(t_A) = \int_0^{t_A} E(t)dt = D(t)\Big|_0^{t_A} = D(t_A) - D(0) \quad (7)$$

The engine performance in the interval $\langle 0, t_A \rangle$ can be calculated from formula (7) assuming one of three earlier mentioned functional relations between the energy and the time, i.e. when:

a) $E(t) = at$, and then:

$$D(0, t_A) = \int_0^{t_A} atdt = a\frac{t^2}{2}\Big|_0^{t_A} = \frac{1}{2}at_A^2 = \frac{1}{2}E_A t_A \quad (8)$$

b) $E(t) = \dot{a}t^2$, and then:

$$D(0, t_A) = \int_0^{t_A} \dot{a}t^2 dt = \dot{a}\frac{t^3}{3}\Big|_0^{t_A} = \frac{1}{3}\dot{a}t_A^3 = \frac{1}{3}E_A t_A \quad (9)$$

c) $E(t) = \ddot{a}t^3$, and then:

$$D(0, t_A) = \int_0^{t_A} \ddot{a}t^3 dt = \ddot{a}\frac{t^4}{4}\Big|_0^{t_A} = \frac{1}{4}\ddot{a}t_A^4 = \frac{1}{4}E_A t_A \quad (10)$$

where:
a   –   engine operation rate, meant as the rate of conversion of the energy E,
$\dot{a}$ –   engine operation rate related to the time unit,
$\ddot{a}$ –   derivative of the engine operation rate with respect to time, engine operation acceleration.

In case when the object of concern of the main engine user is such engine operation which is characterised by sole energy conversion into work, the engine operation rate (a) can be interpreted as the power, i.e. the work related to the time at which it was done. This is obvious as the power contains the information how fast the work is, or can be, done. Therefore the power can be interpreted as the rate of work realisation.

In the time interval $\langle t_A, t_{AB} \rangle$ the energy conversion E_A = idem takes place. Therefore in this time interval the engine performance can be evaluated in the following way:

$$D(t_A, t_{AB}) = \int_{t_A}^{t_{AB}} E_A dt = E_A t\Big|_{t_A}^{t_{AB}} = E_A(t_{AB} - t_A) \quad (11)$$

In the time interval $\langle t_{AB}, t_B \rangle$ the energy converted in the engine working spaces increases from E_A to E_B. We can assume that the energy increase converted in this interval can be described using similar integrands as for the time interval $\langle 0, t_A \rangle$. But we limit here the engine performance evaluation only to the case of linear energy increase. The area of engine operation in this interval is limited by the following inequalities:

$$\left.\begin{array}{l} t_{AB} \leq t \leq t_B \\ E_A \leq E(t) \leq E_A + at \end{array}\right\} \quad (12)$$

To make the result of integration more clear, we should change the integration limits taking into account an obvious fact that the energy change takes place in the engine operation time interval $\langle 0, t_B - t_{AB} \rangle$, which is equal to the interval $\langle t_{AB}, t_B \rangle$. Then the engine operation area is:

$$D(t_{AB}, t_B) = \int_0^{t_B - t_{AB}} (E_A + at)dt = E_A t\Big|_0^{t_B - t_{AB}} + a\frac{1}{2}t^2\Big|_0^{t_B - t_{AB}} =$$
$$= E_A(t_B - t_{AB}) + \frac{1}{2}a(t_B - t_{AB})^2 \quad (13)$$

Since:

$$a = \frac{E_B - E_{AB}}{t_B - t_{AB}}$$

where:
$E_{AB} = E_A$

then:

$$D(t_{AB}, t_B) = E_A(t_B - t_{AB}) + \frac{1}{2}(E_B - E_A)(t_B - t_{AB}) \quad (14)$$

where:
a   –   physical quantity having similar interpretation as in formulas (8-10)

In the similar way we can evaluate the engine performance in the remaining time intervals, see (Fig. 4), i.e.:
• in the time interval $\langle t_B, t_{BC} \rangle$ in which the energy E_B = idem is converted,

$$D(t_B, t_{BC}) = \int_{t_B}^{t_{BC}} E_B dt = E_B t\Big|_{t_B}^{t_{BC}} = E_B(t_{BC} - t_B) \quad (15)$$

• in the time interval $\langle t_{BC}, t_C \rangle$ in which:

$$a = \frac{E_C - E_{BC}}{t_C - t_{BC}}, \quad E_{BC} = E_B$$

$$D(t_{BC}, t_C) = \int_0^{t_C - t_{BC}} (E_B + at)dt = E_B t\Big|_0^{t_C - t_{BC}} + a\frac{1}{2}t^2\Big|_0^{t_C - t_{BC}} =$$
$$= E_B(t_C - t_{BC}) + \frac{1}{2}(E_C - E_B)(t_C - t_{BC}) \quad (16)$$

• in the time interval $\langle t_C, t_{CD} \rangle$ in which the energy E_C = idem is converted,

$$D(t_C, t_{CD}) = \int_{t_C}^{t_{CD}} E_C dt = E_C t\Big|_{t_C}^{t_{CD}} = E_C(t_{CD} - t_C) \quad (17)$$

- in the time interval $\langle t_{CD}, t_D \rangle$ in which:

$$a = \frac{E_D - E_{CD}}{t_D - t_{CD}}, \quad E_{CD} = E_C$$

$$D(t_{CD}, t_D) = \int_0^{t_D - t_{CD}} (E_C + at)dt = E_C \Big|_0^{t_D - t_{CD}} + a\frac{1}{2}t^2 \Big|_0^{t_D - t_{CD}} =$$

$$= E_C(t_D - t_{CD}) + \frac{1}{2}(E_D - E_C)(t_D - t_{CD}) \tag{18}$$

- in the time interval $\langle t_D, t_{DE} \rangle$ in which the energy $E_D = idem$ is converted,

$$D(t_D, t_{DE}) = \int_{t_D}^{t_{DE}} E_D dt = E_D t \Big|_{t_D}^{t_{DE}} = E_D(t_{DE} - t_D) \tag{19}$$

- in the time interval $\langle t_{DE}, t_E \rangle$ in which:

$$a = \frac{E_B - E_{DE}}{t_E - t_{DE}}, \quad E_{DE} = E_D$$

$$D(t_{DE}, t_E) = \int_0^{t_E - t_{DE}} (E_D - at)dt = E_D \Big|_0^{t_E - t_{DE}} - a\frac{1}{2}t^2 \Big|_0^{t_E - t_{DE}} =$$

$$= E_D(t_E - t_{DE}) - \frac{1}{2}(E_D - E_B)(t_E - t_{DE}) \tag{20}$$

since $a < 0$, as $E_D > E_B$

- in the time interval $\langle t_E, t_{EF} \rangle$ – i.e. the time in which the energy $E_B = idem$ is converted,

$$D(t_E, t_{EF}) = \int_{t_E}^{t_{EF}} E_B dt = E_B t \Big|_{t_E}^{t_{EF}} = E_B(t_{EF} - t_E) \tag{21}$$

- in the time interval $\langle t_{EF}, t_F \rangle$ in which:

$$a = \frac{E_F - E_{EF}}{t_F - t_{EF}}, \quad E_{EF} = E_B$$

$$D(t_{EF}, t_F) = \int_0^{t_F - t_{EF}} (E_B - at)dt = E_B \Big|_0^{t_F - t_{EF}} - a\frac{1}{2}t^2 \Big|_0^{t_F - t_{EF}} =$$

$$= E_B(t_F - t_{EF}) - \frac{1}{2}(E_B - E_F)(t_F - t_{EF}) \tag{22}$$

since $a < 0$, as $E_B > E_F$

- in the time interval $\langle t_F, t_{FG} \rangle$ – i.e. the time in which the energy $E_F = idem$ is converted,

$$D(t_F, t_{FG}) = \int_{t_F}^{t_{FG}} E_F dt = E_F t \Big|_{t_F}^{t_{FG}} = E_F(t_{FG} - t_F) \tag{23}$$

- in the time interval $\langle t_{FG}, t_H \rangle$ in which:

$$a = -\frac{E_F}{t_H - t_{FG}}$$

$$D(t_{FG}, t_H) = \int_0^{t_H - t_{FG}} (E_F - at)dt = E_F \Big|_0^{t_H - t_{FG}} - a\frac{1}{2}t^2 \Big|_0^{t_H - t_{FG}} =$$

$$= E_F(t_H - t_{FG}) - \frac{1}{2}E_F(t_H - t_{FG}) \tag{24}$$

The physical quantity a in equations (8), (13), (16), (18), (20), (22) and (24), meant as the engine operation rate (rate of conversion of the energy E), should be identified both with the rate of energy conversion into work (a_L) and into heat (a_Q). This results from the fact that in the internal combustion engines the energy conversion into work, done to obtain the required power output, is always accompanied by energy conversion into heat. Therefore evaluating the operation of the engine of this type should not be solely limited to taking into account the power output N_e as the physical quantity characterising the rate of energy conversion into work. But it does not mean that we cannot, in justified cases, evaluate the performance of internal combustion engines only based on the analysis of the energy conversion into work. In those cases in the above equations the physical quantity a will be the effective power (N_e) of an engine of this type [6, 7].

The above analysis leads to the conclusion that the main engine performance in the time interval $\langle 0, t_H \rangle$, realised in accordance with the energy conversion process whose realisation was shown in Fig. 3 and Fig. 4, can be described in the following way:

$$D(0, t_H) = \int_0^{t_A} at\, dt + \int_{t_A}^{t_{AB}} E_A dt + \int_0^{t_B - t_{AB}} (E_A + at)dt + \int_{t_B}^{t_{BC}} E_B dt +$$

$$+ \int_0^{t_C - t_{BC}} (E_B + at)dt + \int_{t_C}^{t_{CD}} E_C dt + \int_0^{t_D - t_{CD}} (E_C + at)dt + \int_{t_D}^{t_{DE}} E_D dt +$$

$$+ \int_0^{t_E - t_{DE}} (E_D - at)dt + \int_{t_E}^{t_{EF}} E_B dt + \int_0^{t_F - t_{EF}} (E_B - at)dt + \int_{t_F}^{t_{FG}} E_F dt +$$

$$+ \int_0^{t_H - t_{FG}} (E_F - at)dt = \frac{1}{2}E_A t_A + E_A(t_B - t_{AB}) +$$

$$+ \frac{1}{2}(E_B - E_A)(t_B - t_{AB}) + E_B(t_{BC} - t_B) + E_B(t_C - t_{BC}) +$$

$$+ \frac{1}{2}(E_C - E_B)(t_C - t_{BC}) + E_C(t_{CD} - t_C) + E_C(t_D - t_{CD}) +$$

$$+ \frac{1}{2}(E_D - E_C)(t_D - t_{CD}) + E_D(t_{DE} - t_D) + E_D(t_E - t_{DE}) +$$

$$- \frac{1}{2}(E_D - E_B)(t_E - t_{DE}) + E_B(t_{EF} - t_E) + E_B(t_F - t_{EF}) +$$

$$- \frac{1}{2}(E_B - E_F)(t_F - t_{EF}) + E_F(t_{FG} - t_F) +$$

$$+ E_F(t_H - t_{FG}) - \frac{1}{2}E_F(t_H - t_{FG}) \tag{25}$$

The presented model of the process of energy changes during the time of operation of an arbitrary main engine, and the method for evaluating its performance with the aid of the integral calculus refers to one of numerous possible realisations of the process of load changes in engines of this type. Obviously, during the time of operation of a sea-going ship in various conditions, individual realisations of the energy change process can differ both in the order of appearance of successive engine loads, and their time durations. These loads are the results of changes of the energy $E_i (i = A, B, C, D, F, ..., I)$, Fig. 4. The engine states corresponding to these energies, analysed in the engine operation time, can be interpreted as the processes of changes of the abovementioned energies. The times of appearance of particular states of this process and the

times of their duration are random variables. Each realisation of the power change process (Fig.3) and its origin – the energy change process (Fig. 4) provides opportunities for analysing the performance of an arbitrary main engine. Moreover, the formulas presented in the article make it possible to express the result of the analysis in the form of a number with the metric unit called the joule-second and in the form of an area bearing the name of the area of operation [2, 3, 6]. The engine operation described in the above way can be called the singular possible operation (D_{MS}). However, for each realisation of this process we can determine the singular required operation (D_{WS}). In general, the required operation (D_W) can be meant as the operation in which the required energy E_W is delivered in the time t_W required for task realisation. In the reference to the analysed realisation of the process of main engine energy changes (Fig. 4), the singular required operation (D_{WS}) can be defined as the engine operation which makes it possible to convert the energy E_D in time not shorter than the time $t_W = t_{DE} - t_D$, required (needed) for task realisation. If the engine can operate in the above way, then we arrive at the following inequality relation:

$$D_{MS} \geq D_{WS} \qquad (26)$$

In this case the engine is capable of doing the task to which it was designed and machined, and therefore can be considered as capable of doing this task, i.e. as the engine at capability state [3, 6]. In the opposite case, comparing the engine operations D_{MS} and D_{WS} leads to the inequality:

$$D_{MS} < D_{WS} \qquad (27)$$

and the engine is to be considered as incapable of doing the given task, i.e. as the engine at incapability state.

In general we can conclude: if the realisation of a task is only possible when the main engine can be loaded within the entire performance area (Fig. 2), then this engine is capable of doing this task. In that case we can say that the engine is at capability state. The engine at this state can be loaded even according to the external maximal power characteristic (h_{max} = idem). Obviously, when the engine cannot be loaded according to the external characteristic h_{max} = idem due to wear of its elements, but according to the characteristics obtained for smaller injection pump setting, for instance the external nominal power characteristic (h_{nom} = idem), its operational applicability is smaller. Even smaller applicability will characterise the engine which can be only loaded according to the external continuous power characteristic (h_{tr} = idem), etc.

REMARKS AND CONCLUSIONS

The article presents the deterministic method for evaluating the performance of a marine piston internal combustion engine used as the main propulsion (main engine) on a ship. The presented method is not limited to the above types of engines, and can also be use for performance evaluation of an arbitrary piston internal combustion engine of both compression-ignition and spark-ignition type.

A separate task is working out a method for evaluating the performance of internal combustion engines in stochastic approach. In this case it should be taken into account that the processes of energy changes realised in time in engine working spaces are stochastic processes. Investigating those processes requires working out their model in the form of a stochastic process which is discrete in states and continuous in time. The discussion presented in the article suggests that the model to be applied here can be the Semi-Markov process, which has the properties of being discrete in states and continuous in time.

The operation of the internal combustion engine is interpreted in the article as delivering the required energy in given time, which can be expressed in the form a physical quantity with the metric unit called the joule-second.

When discussing good and bad points of the energy conversion in internal combustion engines, all aspects of their operation are to be taken in to account and not only their work. The analysis of engine work takes only into account the energy conversion into work, while the energy conversion into heat, which always accompanies the engine work, is neglected.

The proposed method assumes that the energy change can be described by a linear function ($y = at$), but it was mentioned that for this purpose also the second or third order parabola can be used (formulas 9 and 10).

It results from the presented discussion that evaluating the engine performance using the integral calculus is possible if the energy, as the integrand, can be expressed in the form of elementary functions. This is because there are no general principles which would make it possible to calculate integrals of arbitrary functions, unlike the situation which takes place in the differential calculus. Therefore the problem here is not only to calculate the integrals to evaluate the engine performance, but also the more general problem of the existence of these integrals.

In practice, sometimes evaluating the engine performance using the Newton-Leibniz formula (7) cannot be done. It refers to the cases when:
- the performance, as the antiderivative of the energy being the integrand, cannot be described using elementary functions,
- the antiderivative expressing the performance cannot be obtained, due to extremely complicated algebraic transformations required and the resultant high expected probability of error appearance,
- the energy changes can only be presented in tabular form, and not as the function of time.

In cases when the Newton-Leibniz formula (7) is not applicable, approximate methods of integration should be used, among which the best known are the trapezoidal rule and the Simpson's rule.

BIBLIOGRAPHY

1. Delventhal K. M., Kissner A., Kulick M.: *Mathematic. Compendium* (in Polish) Świat Książki, Bertelsmann Media, 2005. Original title: Groses Buch der Mathematik. Compact Verlag Media, 2001.
2. Girtler J.: *Possibility of valuation of operation of marine diesel engines*. Journal of POLISH CIMAC, Vol 4, No 1, 2009.
3. Girtler J.: *Energy-based aspect of operation of diesel engine*. COMBUSTION ENGINES No 2/2009 (137).
4. Girtler J.: *Conception of valuation of combustion engine operation*. Journal of KONES. Powertrain and Transport. Editorial Office Institute of Aeronautics BK, Warsaw 2008.
5. Girtler J.: *Energy-based aspect of machine diagnostics*. (in Polish) Diagnostyka Nr 1(45)/2008. Wyd. Polskie Towarzystwo Diagnostyki Technicznej, Warsaw 2008.
6. Girtler J.: *Work of a compression-ignition engine as the index of its reliability and safety*. II International Scientifically-Technical Conference EXPLO-DIESEL & GAS TURBINE"01. Conference Procedings. Gdansk-Miedzyzdroje-Copenhagen, 2001.
7. Piotrowski I., Witkowski K.: *Operation of marine internal combustion engines*. (in Polish) AM, Gdynia 2002.
8. Rosłanowski J.: *Identification of ships propulsion engine operation by means of dimensional analysis*. Journal of POLISH CIMAC, Vol 4, No 1, 2009.

9. Rudnicki J.: *Loads of ship main diesel . engine in the aspect of practical assessment of its operation*. Journal of POLISH CIMAC, Vol. 3, No 1, 2008.

10. Rudnicki J.: *On making into account value of operational applied to ship main propulsion engine as an example*. Journal of POLISH CIMAC, Vol 4, No 1, 2009.

11. Wojnowski W.: *Marine internal combustion engine plants*. (in Polish), Part I., Wyd. AMW, Gdynia 1998.

CONTACT WITH THE AUTHOR
Jerzy Girtler, Prof.
Faculty of Ocean Engineering
and Ship Technology
Gdansk University of Technology
Narutowicza 11/12
80-233 Gdansk, POLAND
e-mail: jgirtl@pg.gda.pl

Influence of main design parameters of ship propeller shaft water-lubricated bearings on their properties

Wojciech Litwin, Ph. D.
Gdansk University of Technology

ABSTRACT

In recent years more and more frequently can be met ships in which propeller shaft water-lubricated polymer bearings have been applied. It results from their simplicity and associated relatively low initial and operational cost as compared with the complex classical sealed system based on oil-lubricated bearings. It is worth mentioning that the water-lubricated bearings are also environmentally friendly as no risk of pollution with lubricating oil used in classical systems, is involved. Design procedure of bearings in question based on materials made available by producers is relatively simple. However it turns out that choice of an appropriate sliding material, clearance value and optimum arrangement of lubricating grooves may greatly influence bearing's properties. As results from the performed research investigations, bearing of the kind is a highly sensitive unit. Problems of choosing a suitable bearing clearance, designing an optimum bush geometry, selecting a proper bush material are crucial for life time of the bearing. In particular the problem is in forming hydrodynamical properties of bearing as owing to its operation in the fluid friction regime durability of bearings, the very responsible units of propulsion transmission system, can be greatly extended.

Keywords: water lubrictaed bearings; stern tube bearings; sliding bearings

INTRODUCTION

Increasing ecological awareness, more and more stringent requirements for environmental protection, comprehensive control and strict attitude of institutions responsible for monitoring environmental state of waters, and finally cost calculations have made that increasing attention is paid to clean, environmentally safe design solutions.

In recent years many novel materials have been elaborated which are more and more willingly applied to building modern ocean engineering units. Also, novel water-lubricated sliding polymers have been created. Some of them have been approved by ship classification societies for shipbuilding application.

One of the main advantages of water-lubricated bearings of ship propeller shafts is their design simplicity and resulting relatively lower cost as compared with the classical system based on expensive oil-lubricated bearings and complex sealing units. The next obvious advantage of water-lubricated bearings is lack of risk of environmental pollution by lubricating medium.

However the water-lubricated bearings fitted with polymer bushes have also some limitations. The problem is to obtain stable hydrodynamic lubrication because of low viscosity of water. As results from the investigations have been performed so far it is possible though values of lubricating film thickness rarely exceed 10μm. Hence such bearings are very sensitive

to errors in bush shape and shaft position. The greatest hazard results from shaft misalignment also called as skewness of shaft axis [1].

DESCRIPTION OF THE PROBLEM

Sliding bearings lubricated with low-viscosity liquids, e.g. water, are usually very sensitive units. The reason is that if such bearing operates in the fluid friction regime its hydrodynamical load-carrying capacity will be much lower than that of a comparable classical oil-lubricated bearing. It results from low viscosity of the lubricating medium. As already mentioned, such bearings operate at minimum values of lubricating film thickness of the order of only a few micrometers, usually not acceptable for classical bearings even in view of height of unevenness in journal and bush. It should be remembered that at such low lubricating film thicknesses operational conditions of the bearing are influenced by many factors such as errors in shaft position and bush shape. Additionally, is important state of surface of sliding elements and operational conditions such as sliding velocity and pressure which decide on whether the bearing would operate under fluid friction or not. Results of the performed experimental tests have proved that the running-in process of the water-lubricated bearings fitted with polymer bush develops relatively fast. It means that as quickly as after

a few hours of operation the bearing operational characteristics becomes distinctly changed (Fig. 1). Measurement results of shaft axis trajectory and pressure distribution in lubricating film confirm that in the typical marine sliding bearings fluid friction really occurs [1].

Designing a sliding bearing operating under fluid friction one tries to obtain a demanded value of hydrodynamical load-carrying capacity at maintaining certain margin so as to keep - in a failure situation when the load increases and film thickness decreases - the bearing operating still under fluid friction. This is very important because of safety reasons as well as of necessity to increase life time of the bearing, significantly. The described effect of the maintaining of certain margin of load-carrying capacity may be difficult to achieve in slide bearings lubricated with low-viscosity liquids. It results from the much lower maximum load-carrying capacity of the value estimated to be within the range of $0.3 \div 0.5$ MPa, depending on a kind of material.

Therefore in designing a sliding bearing lubricated with a low-viscosity liquid and intended for long and reliable operation one should design it for operation in the fluid friction regime and with a possibly large margin of load-carrying capacity. The design parameters of the bearing such as its size, clearance value, kind of bush material should be taken into account and lubricating grooves arranged appropriately.
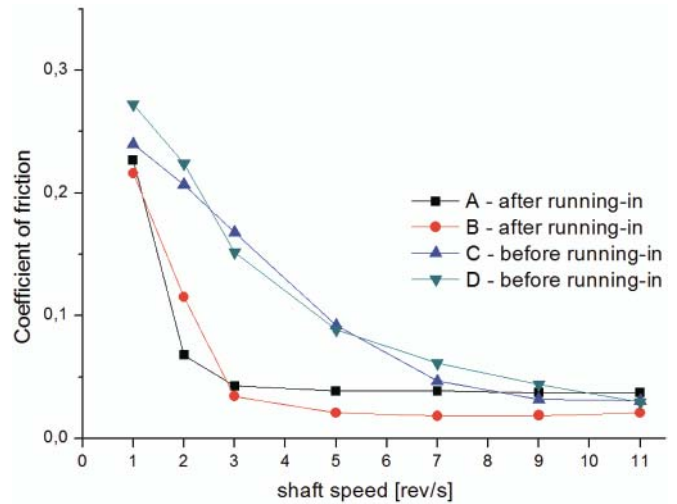
Fig. 1. *Experimentally obtained operational characteristics of sliding bearing in function of shaft rotational speed for the bearings before, (A, B); and after, (B, C); running-in process*
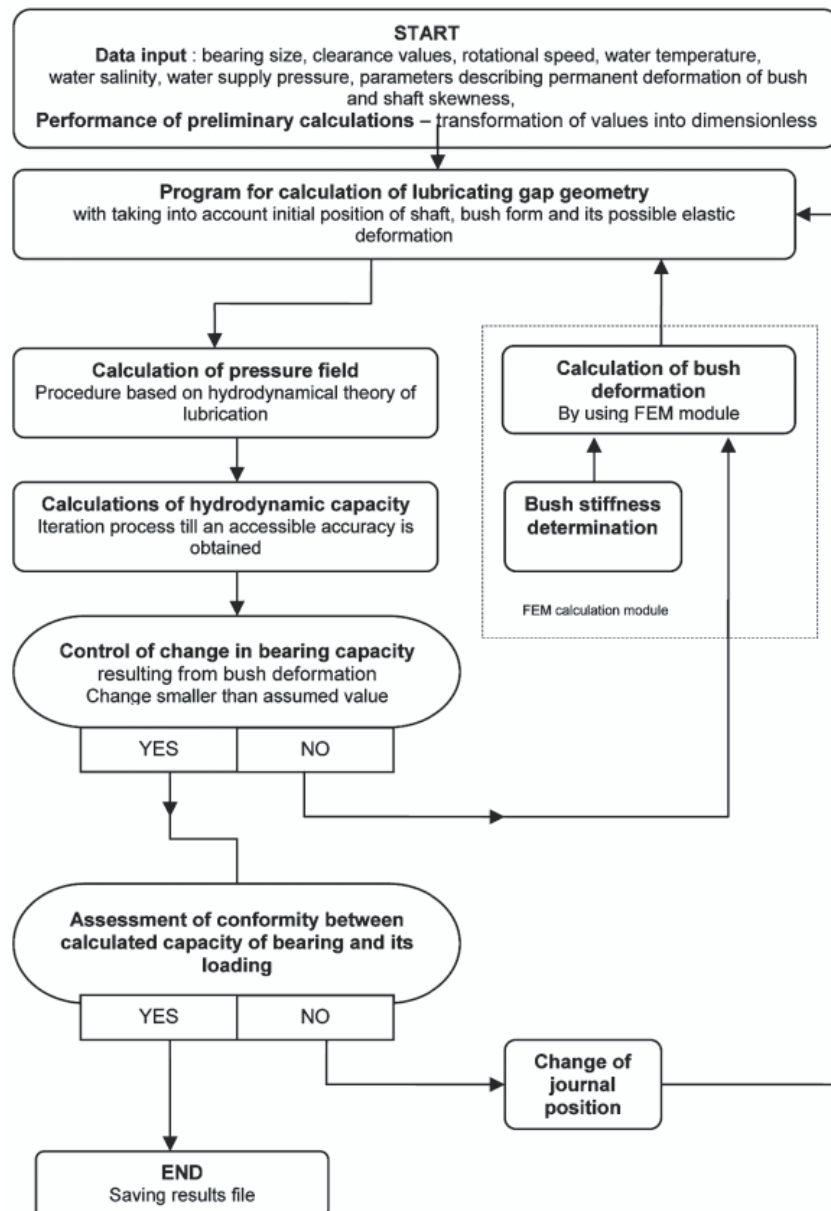
Fig . 2. Schematic diagram of the computation program

CALCULATIONS

For calculations the elasto-hydrodynamic model (EHL) was used. The applied software was composed of two modules. The first of them was intended for the calculating of pressure distribution in lubricating film and based on hydrodynamical theory of lubrication and Reynolds equation. The other made it possible to calculate bush elastic deformation with the use of the finite element method (FEM).

The computational model was verified experimentally. The example calculated pressure distributions set against those from measurements are presented in Fig. 3 and 4. There are at least two reasons as to why certain differences between the results of the calculations and measurements occur. Probably both the measurements and calculations are loaded with an error. The measurement errors may result from an imperfect shape of the bush. The calculation results may be loaded with an error resulting from the assumed constant value of the material elasticity modulus amounting to only 800 MPa in the case in question.
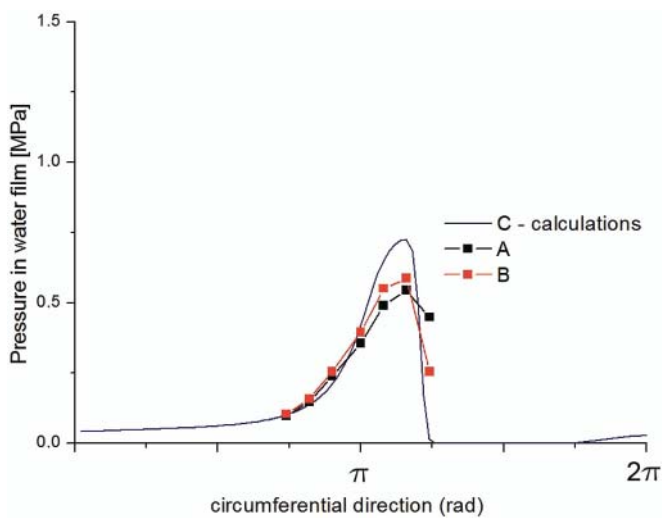
Fig. 3. Pressure distribution in circumferential direction at bearing centerline; calculation results (C) set against measurement results obtained on the test rig for the bearing with elastic bush(A,B); for shaft diameter of 100 [mm], rotational speed of 11 [rps], load of 0.1 [MPa]
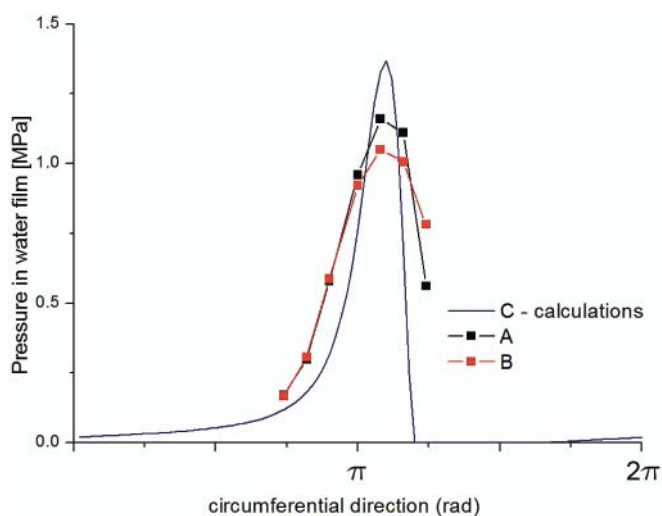
Fig. 4. Pressure distribution in circumferential direction at bearing centerline; calculation results (C) set against measurement results obtained on the test rig for the bearing with elastic bush(A,B); for shaft diameter of 100 [mm], rotational speed of 11 [rps], load of 0.2 [MPa]

All the below showed calculation results were obtained for the bearings similar to those experimentally tested. The

shaft diameter was equal to 100 mm, outer diameter of the bush – 124 mm, length of the bush – 400 mm in compliance with the length/diameter ratio L/D = 4, typical for ship shaft lines. The calculations were conducted for two values of shaft rotational speed: 3 and 11 rps.

IMPACT OF VALUE OF BEARING CLEARANCE AND KIND OF BUSH MATERIAL ON BEARING OPERATIONAL CONDITIONS

One of the crucial design parameters of sliding bearing is its diameter clearance. Authors of subject-matter publications usually make use of the so-called relative clearance whose value for water-lubricated polymer bearings generally ranges from 0.3 to 0.4 % of shaft diameter and depends a.o. on shaft rotational speed. The usually suggested value of the clearance results from the general phenomenon of water absorbing by polymer, which leads to a reduction of internal diameter of bush, that is capable of full blocking the shaft in the extreme case. As results from catalogue data of various polymers the water absorption process may last from a few hours to even a few dozen weeks. This can be very dangerous as shaft seizing can theoretically happen just after ship's docking and even a dozen or so days after ship's departing from shipyard. The propeller shaft seizing and thus making the ship disabled may lead even to a catastrophe of fatal consequences. The water absorbing process of bush has been several times observed during the tests. Polymer is theoretically capable of absorbing a significant amount of water, and its volume increase may reach 6%, but in practice even 0.1% value may be dangerous in view of reducing bush diameter even by a few tenth part of millimeter. Typical polymers applicable to shipbuilding increase their volume in the range from 0.1 to 0.5%. In the past, when on the single bearing test stand a polyamide bush happened to be seized, it took almost three months to be able to dry it and then dismount the shaft.
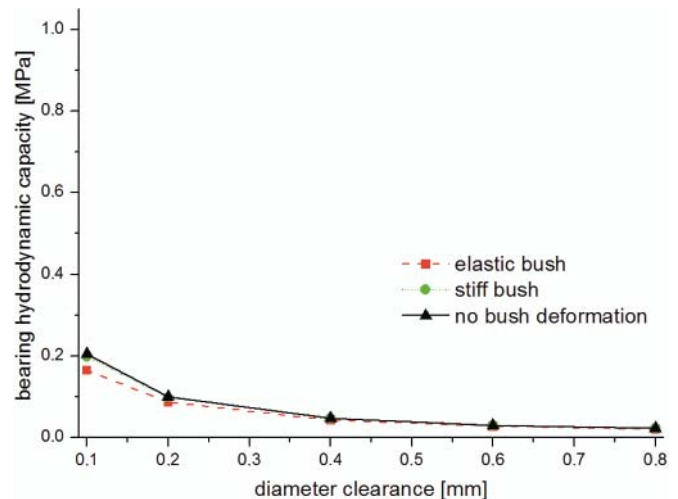
Fig. 5. The maximum theoretical hydrodynamical load-carrying capacity of the bearing fitted with the full bush of 100 mm shaft diameter, calculated for 3 rps shaft rotational speed

To determine impact of bearing clearance value on minimum theoretical hydrodynamical load-carrying capacity of bearing, calculations were performed under the assumption that the minimum acceptable value of lubricating film thickness amounts to 5 µm (Fig. 5 and 6). The value may seem small as compared with that for classical oil-lubricated bearings but as experimental tests demonstrated polymer bearings are capable of stable operating at much thinner lubricating films.

Measurements of drag to motion show bearing work in the fluid friction regime when to estimate value of lubricating film thickness on the basis of shaft axis trajectory and measured clearance circle is already not possible.
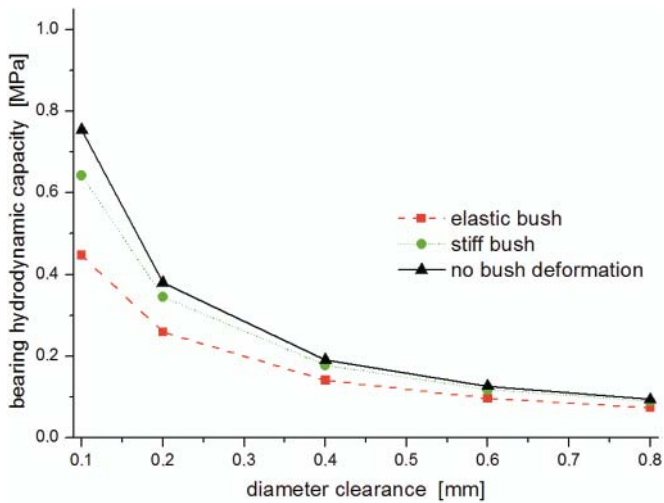
Fig. 6. The maximum theoretical hydrodynamical load-carrying capacity of the bearing fitted with the full bush of 100 mm shaft diameter, calculated for 11 rps shaft rotational speed.

The performed calculations show detrimental impact of increasing the bearing clearance, that greatly reduces potential, theoretical maximum hydrodynamical load-carrying capacity. Analyzing the diagrams one can conclude that for the shaft of the analyzed diameter the recommended clearance value which ranges from 0.3 to 0.4 mm, is too large. Having at one's disposal a polymer of high form stability one is able to design a bearing of much better properties, for operating at relatively greater values of lubricating film thickness in the same conditions.

It is interesting that maximum load-carrying capacity of bearing decreases along with decreasing bush material elasticity (lower modulus of elasticity). However the opposite opinion can be often met. Accordingly, sometimes is stated that an elastic polymer material would operate better under fluid friction than highly stiff one, e.g. ceramics. To disqualify the thesis one should examine the hydrodynamical pressure distribution in a sliding bearing and its impact on elastic bush surface, presented in Fig. 7 ÷ 10.
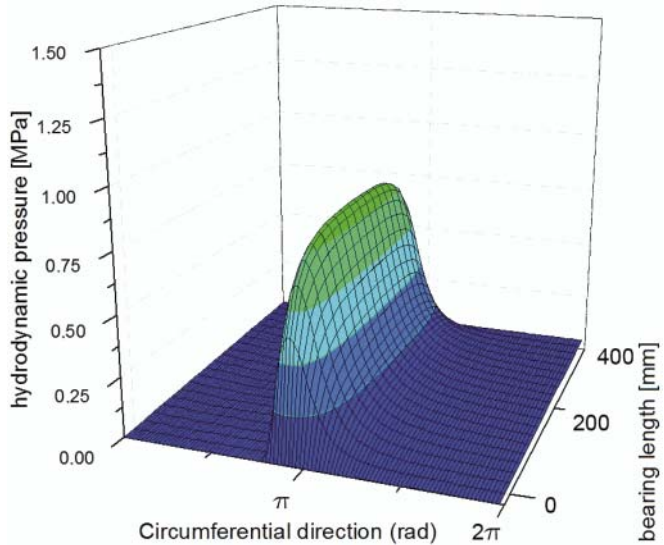
Fig. 7. The calculated pressure distribution in a highly loaded sliding bearing with elastic bush; for shaft diameter of 100 [mm], diameter clearance of 0.4 [mm], lubricating film thickness of 5 [µm]
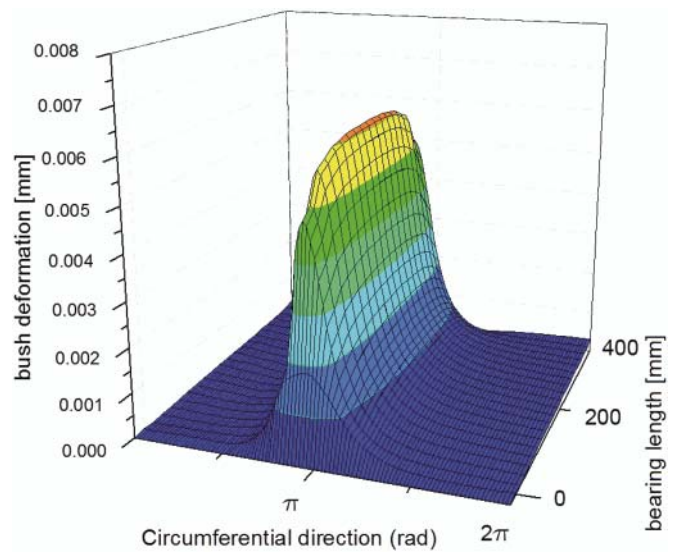
Fig. 8. The calculated bush surface deformation in a highly loaded sliding bearing with elastic bush; for shaft diameter of 100 [mm], diameter clearance of 0.4 [mm], lubricating film thickness of 5 [µm]
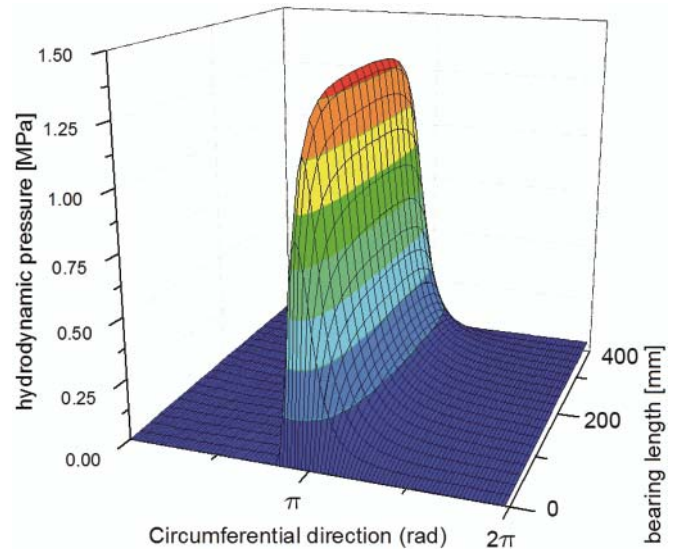
Fig. 9. The calculated pressure distribution in a highly loaded sliding bearing with stiff composite bush; for shaft diameter of 100 [mm], diameter clearance of 0.4 [mm], lubricating film thickness of 5 [µm]
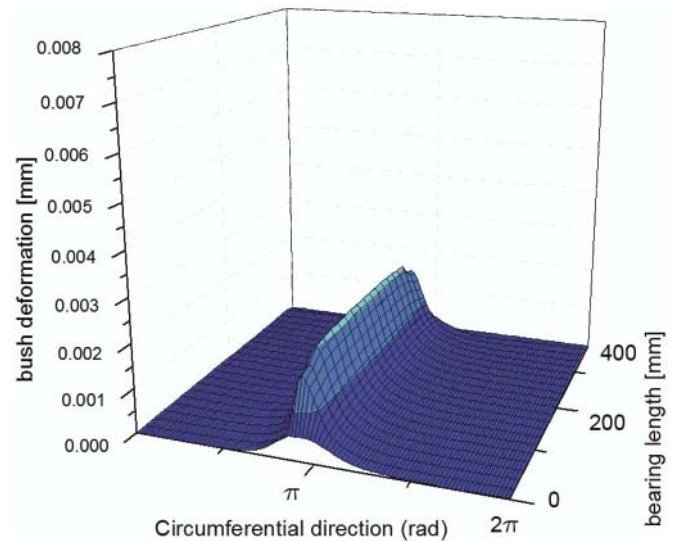
Fig. 10. The calculated bush surface deformation in a highly loaded sliding bearing with stiff composite bush; for shaft diameter of 100 [mm], diameter clearance of 0.4 [mm], lubricating film thickness of 5 [µm]

Calculating hydrodynamical sliding bearing one assumes lack of contact between its journal and bush. In order to calculate the maximum theoretical load-carrying capacity of the bearing one assumes a given minimum, but still acceptable, value of lubricating film thickness. Hence it turns out that assuming a more elastic bush material one makes that area of bush deformation is extended and reaches 7 [μm] in the case in question (Fig. 8), i.e. more than the assumed value of lubricating film thickness. That is why in reality the minimum gap height in the middle of the elastic polymer bush amounts to about 12 [μm] . It led to lowering pressure in the film as compared with the more stiff composite material in which the deformation amounted to a little more than 2μm and the maximum pressure in the film reached about 1.5 MPa (Fig. 9 and 10). Basing on the calculations one can state that gradually increasing loading of the bearings fitted with elastic bush would result in gradual transition from operation under full hydrodynamical lubrication to that under partial fluid friction. A contact zone will appear in the area close to both edges of bush where hydrodynamical pressure is negligible and in consequence deformation is small. Along with gradual load increasing the fluid friction zone will be smaller and smaller and finally disappear when the bearing starts operating entirely in the mixed friction regime. The thesis is confirmed by experimental tests which show the bearings to operate under fluid friction. Analysis of the tested bushes revealed also a significant wear in the contact zone close to outer edges of the investigated bearings.

The next important factor of a great impact on operation of hydrodynamical sliding bearing is kind and temperature of water flowing through the bearing. It is particularly important for open lubricating systems where outboard water is used as a lubricating medium. The case can be assumed when a ship passes from warm fresh waters of Mississippi river to cold waters of North Canada . Then water temperature drop may reach about 20°C and water viscosity may be additionally increased by salt contained in sea water. Hence the dynamical viscosity increase from about 890.2 to 1604.6 [Pa·s] may be expected [2]. To assess viscosity change influence on maximum theoretical load-carrying capacity of bearing appropriate calculations were conducted whose results have been presented below (Fig. 11).
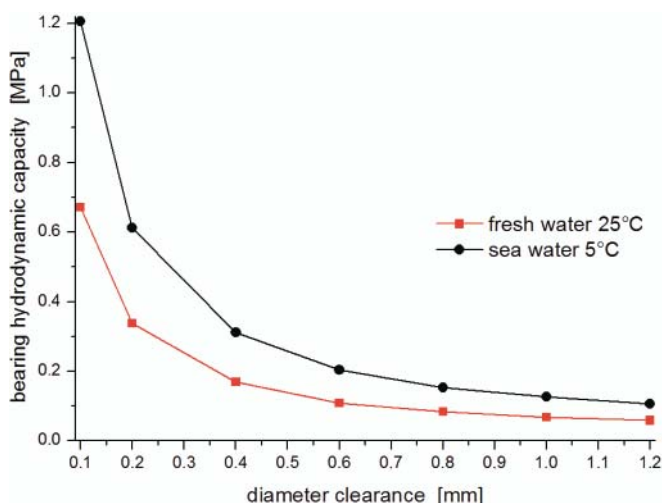
Fig. 11. The calculated maximum theoretical load-carrying capacity of the bearing with full bush; for 100mm shaft diameter, shaft rotational speed of 11 [rps] and two different values of water viscosity:890,2 and 1604,6 [Pa·s]

The results showed that especially in the range of small values of diameter clearance theoretical capacity values could differ almost twofold. During sailing on the analyzed route, if only the bearing operates under fluid friction, film thickness values will be increasing along with temperature dropping and growing salinity of the waters. Also, the possible cooling of water used for lubrication of bearings operating in closed system, may be considered. In this case operational conditions of bearings could be much improved at the expense of a greater energy demand. That is why the solution proposed by some producers to use water from engine's cooling system for lubrication of bearings seems very unfavourable.

IMPACT OF LUBRICATING GROOVES ON BEARING PROPERTIES

Water-lubricated sliding bearings fitted with polymer bush in which longitudinal, passing-through lubricating grooves are made, are the typical solution used not only in shipbuilding but also in water power plants and pumps. As already mentioned, it results first of all from the necessity of effective absorbing heat from friction zone as polymer bush does not transfer heat to casing and is additionally sensitive to elevated temperature [3]. Arrangement of the grooves round bush circumference makes it possible to increase rate of water flow through bearing and allows this way to improve cooling conditions. In practice it turns out that the grooves fulfil one very important function more as wear products and various contaminations sediment in them. It is of particular importance for the simplest propeller shaft bearing systems, the open ones where during ship sailing e.g. in silt-up, shallow inland waterways a large quantity of various contaminations may fall into bearing's interior. The cases are known when even small crustaceans set down inside lubricating grooves.

Studying the subject-matter literature, in particular guidelines for application of various sliding materials, published by worldwide producers, one can conclude that they are very similar to each other. Producers selling prefabricates usually in the form of pipes, make their guidelines first of all directed to designers, in which are included many necessary data such as: recommended values of bearing clearance and thermal shrinkage as well as number, size and arrangement of lubricating grooves. From the publications it can be concluded that two concepts dominate. According to the first of them it is proposed to arrange grooves round entire bush circumference (Fig. 12. variant A). The other concept follows the hydrodynamical lubrication theory. Therefore its authors came to the conclusion that it is not recommended to place grooves in the lower part of bearing as it could limit its potential capabilities (Fig. 12. variant C).
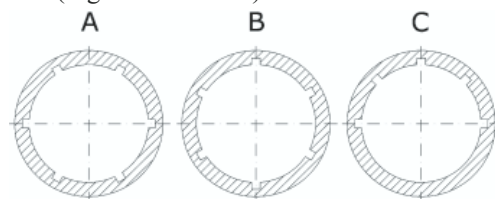
*Fig. 12. Various practically used arrangements of lubricating grooves within bush; **A** - recommended arrangement of many grooves round entire bush circumference, **B** - erroneous position of bush, **C** - bush with grooves located only round the upper half of bush.*

The performed calculations of water-lubricated hydrodynamical sliding bearing fitted with longitudinal open lubricating grooves have demonstrated that their arrangement greatly impacts properties of the bearing. Moreover the calculation results have proved that the proper arrangement of grooves is not of a detrimental effect to the bearing properties (Fig. 13). This results from the influence of grooves on the forming of lubricating film in the bearing. As far as the bearing

fitted with full bush is concerned a gradual hydrodynamic pressure increase takes place within the film (Fig. 15).
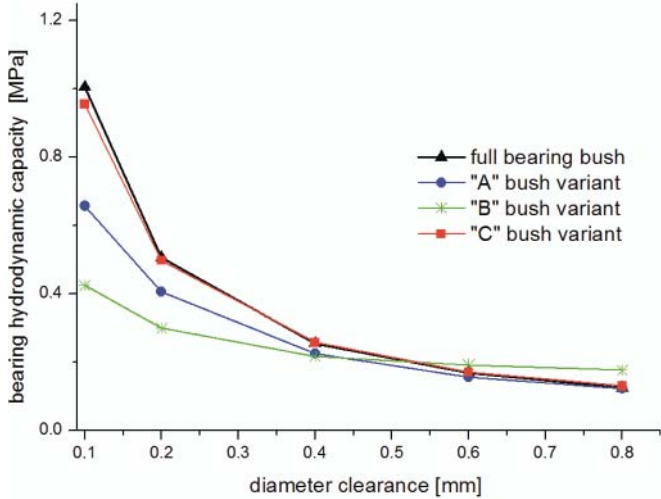
Fig. 13. *The calculated maximum load-carrying capacity of bush in function of bearing clearance; for shaft diameter of 100mm, shaft rotational speed of 11 [rps], fresh water of 7°C temperature, η = 1.43 [kPa·s]*
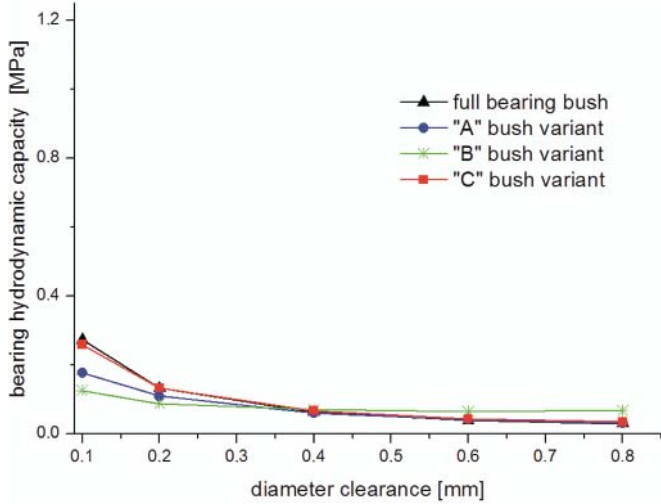
Fig. 14. *The calculated maximum load-carrying capacity of bush in function of bearing clearance; for shaft diameter of 100mm, shaft rotational speed of 3 [rps], fresh water of 7°C temperature, η = 1.43 [kPa·s]*
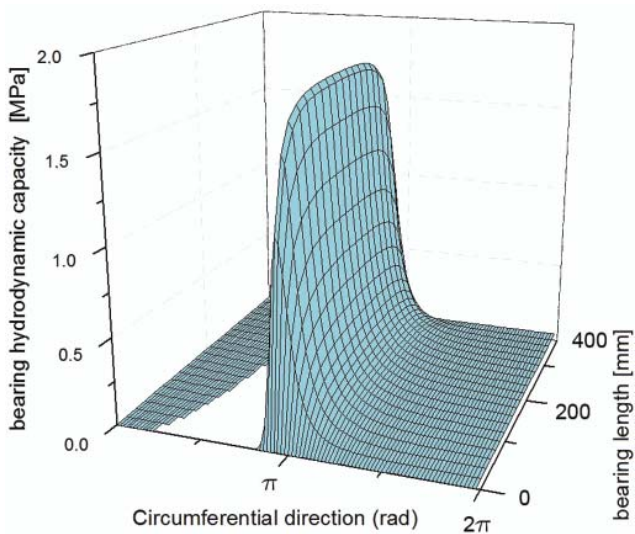
Fig. 15. *The calculated pressure distribution in lubricating film of sliding bearing of full bush; for shaft diameter of 100 [mm], rotational speed of 11 [rps], load-carrying capacity of 15.2 [kN], fresh water at 7 [°C], η = 1,43 [kPa·s]*
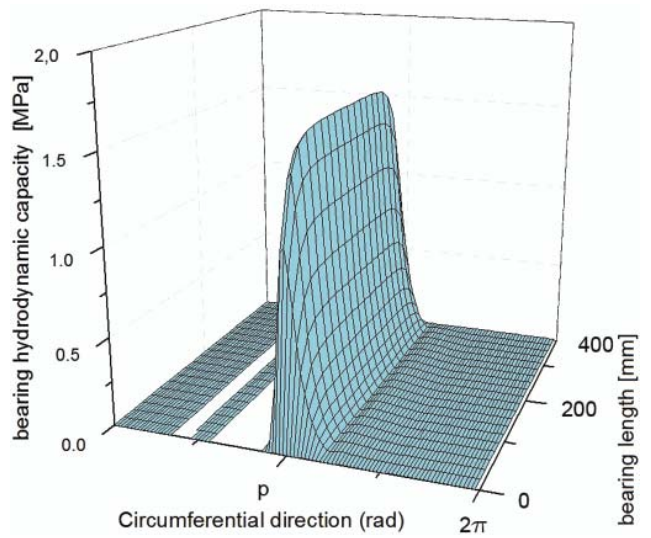
Fig. 16. *The calculated pressure distribution in lubricating film of sliding bearing having six grooves of A variant; for shaft diameter of 100 [mm], rotational speed of 11 [rps], load-carrying capacity of 12.2 [kN], fresh water at 7 [°C], η = 1.43 [kPa·s]*
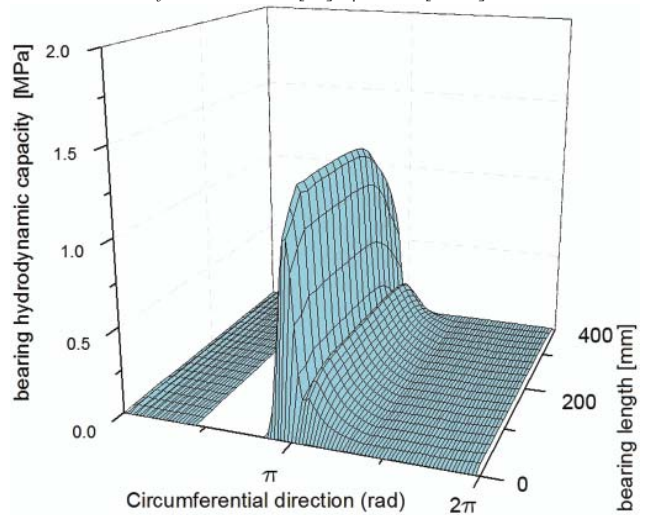
Fig. 17. *The calculated pressure distribution in lubricating film of sliding bearing having six grooves of B variant; for shaft diameter of 100 [mm], rotational speed of 11 [rps], load-carrying capacity of 9 [kN], fresh water at 7 [°C], η = 1.43 [kPa·s]*
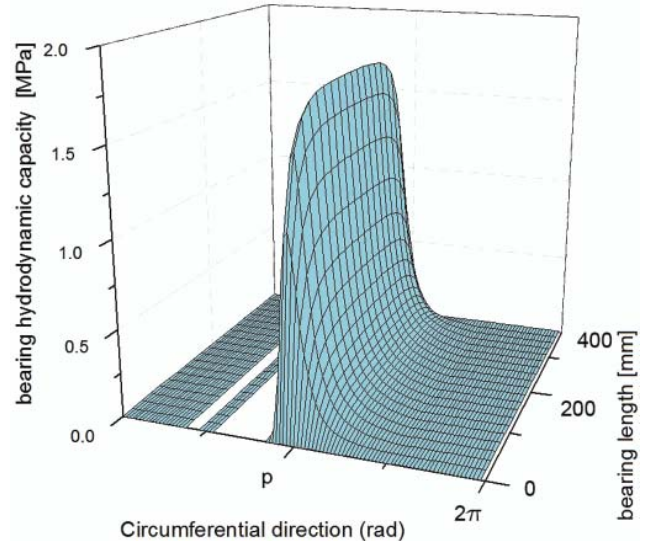
Fig. 18. *The calculated pressure distribution in lubricating film of sliding bearing having six grooves of C variant; for shaft diameter of 100 [mm], rotational speed of 11 [rps], load-carrying capacity of 15 [kN], fresh water at 7 [°C], η = 1.43 [kPa·s]*

The phenomenon is disturbed by lubricating grooves in which the so called solution of lubricating film continuity occurs. Therefore behind the groove the pressure starts to grow again but its increase is usually more violent (Fig. 16). In the worst situation when the grooves are especially unfavourable located a definite reduction of bearing capacity may happen and the pressure increase zone within lubricating film may be split into two parts (Fig. 17). Therefore the optimum solution for ship propeller shafts in which the load generated by rotating mass of the shaft-propeller unit exerts mainly the lower part of bush, consists in leaving the lower part of bush free of lubricating grooves (Fig. 18).

RECAPITULATION

- The ship propeller - shaft water-lubricated bearings fitted with polymer bushes are very sensitive elements. However, if properly designed and assembled, they are able to operate reliably for a long time. They are capable of working under fluid friction in spite of that they are lubricated with low-viscosity liquid. However they show much lower load-carrying capacity as compared with oil-lubricated bearings. In water-lubricated bearings value of lubricating film thickness is usually small and reaches no more than a few micrometers. Hence in typical cases such bearings do not have too large margin of hydrodynamical load-carrying capacity, moreover possible errors in their shape and shaft alignment, especially skewness, make that the bearings would operate in the mixed friction regime.
- As the performed investigations demonstrated the effective method for improving bearing capacity is to limit its clearance value. However is should be remembered that polymers generally absorb water and in consequence enlarge their volume, that may cause power shaft seizing.
- An effective method to increase potential load - carrying capacity of bearing is to apply a stiff composite material to its bush. However it should be taken into account that the bearing will become then greatly sensitive to errors in bush shape and shaft alignment.

- Mechanism of delamination failures in composite bushes is not fully recognized. During many experimental tests have been performed so far it was not possible to generate such failure. To cause it are deemed the local superheating of bearing or propulsion shaft vibrations. Hence in designing a propulsion system of the kind appropriate heat exchange conditions should be ensured. It is especially important for the bearings with polymer bush as heat exchange through casing does not occur in them. A prevailing amount of heat generated in friction zone is to be absorbed by lubricating medium. Therefore in most cases grooves are made in bushes, owing to that it is possible to increase rate of water flow through the bearing. In the typical case, as results from the performed tests, the grooves should be placed only in the upper part of bush in consequence they do not have practically any detrimental effect to hydrodynamical properties of bearing. It should be added that the grooves play also another important function as within them bearing wear products and contaminations can be sedimented.

BIBLIOGRAPHY

1. Litwin W.: *Marine water lubricated main shaft bearings, problems, theoretical and experimental research*; Polish Maritime Research no 4/2009,Vol. 16
2. Litwin W.: *Water – An Extraordinary, Ordinary Lubrication Liquid. Influence Of Water Salinity, Pressure And Temperature On Water Lubricated Bearings Properties*; ASME/STLE International Joint Tribology Conference, October 17-20, 2010, San Francisco, California, USA
3. Rymuza Z.: *Tribology of sliding polymers* (in Polish). WNT (Scientific Technical Publishing House)Warsaw 1986.

CONTACT WITH THE AUTHOR

Wojciech Litwin, Ph. D.
Faculty of Ocean Engineering
and Ship Technology
Gdansk University of Technology
Narutowicza 11/12
80-233 Gdansk, POLAND
e-mail: wlitwin@pg.gda.pl

Evaluation of losses in a hydraulic motor based on the SWSB - 63 motor tests

Agnieszka Maczyszyn, M. Sc.
Gdańsk University of Technology

ABSTRACT

In this paper are compared two models of energy losses: that suggested by Prof. Paszota, Z. in monograph "Energy losses in the hydraulic displacement motors – definitions and relations serving the evaluation of the efficiency of hydrostatic drive" [18] and that of Prof. Balawender, A. in "Energy analysis and methodology of testing of low-speed hydraulic motors" [1]. By using the data obtained from the tests of SWSB-63 hydraulic motors [2] the graphs which illustrate mechanical, volumetric and pressure losses in function of the parameters on which the losses directly depend [18], have been elaborated and showed in comparison with the description of such losses in function of the parameters assumed in [1].
The below presented text has been complemented in relation to that published in the monograph [4] and read during the scientific technical conference „Cylinder 2010" organized by the Mining Engineering Centre „Komag", Gliwice, and held on 20÷22 September 2010 in Rytro, Poland.

Keywords: hydrostatic drive and control; energy efficiency; power of energy losses

INTRODUCTION

Nowadays both client and producer are oriented towards quality, i.e. client to obtain high-quality products and producer to offer products of better and better quality by searching for ways to increase quality of products. Quality of a product can be increased for instance by searching for novel design solutions, manufacturing techniques or research methods. This paper is aimed at highlighting two approaches to losses generated in hydraulic displacement machines, precisely speaking - hydraulic displacement motors.

The models of losses proposed by different authors and in different ways, show results of mechanical, volumetric and pressure losses obtained from tests of the same hydraulic motor.

One of the approaches is the „anti-Sankey's" developed by Prof. Z. Paszota, who systematized the state of knowledge on losses and efficiencies appearing in hydraulic displacement motors [18]. The other approach is that of Prof. Balawender, A., which can be found in [1, 3].

The paper [18] made it possible to order and present, by this author, mechanical, volumetric and pressure losses in function of the parameters which directly influence their magnitude, and in consequence allowed to determine their real values. During determining the losses this author made use of the test results [2] dealing with SWSB-63 medium- pressure high- moment slow-speed motor whose design and description of tests have been contained also in [5].

DESCRIPTION OF LOSSES OCCURRING IN HYDRAULIC MOTOR

Mathematical description of losses occurring in hydraulic displacement machines has been considered since the instant of their invention. The elaborated formulae have been extended by adding new elements and terms associated with growing knowledge on the theme. The way has led a.o. through the achievements of such foreign researchers as: Wilson, Thoma, Prokofiev, Schlösser i Hilbrands, and Polish ones: Stryczek, Balawender and Paszota. Putting focus on the two last authors one is able to present and compare their points of view on losses occurring in hydraulic motors.

Prof. Balawender, A., [1, 3] splits the losses occurring in hydraulic motors into the following:

− moment losses represented by the following model:

$$M_s = C_{Tk}D_t^3p_0 + C_\mu\mu_0\omega D_t^3 + C_{H\rho}\rho\omega^2D_t^3 +$$
$$+ C_{Tp}[1 + k_{om}exp(-\omega\mu_0\Omega_0^{-1})]D_t^3p_1 + C_{Tr}D_t^3p_1$$

where:

C_{Tk} - proportionality coefficient associated with mechanical friction,
D_t - characteristic dimension of hydraulic motor,
p_0 - atmospheric pressure,
C_μ - proportionality coefficient associated with dynamic viscosity of working liquid,

μ_0 - dynamic viscosity coefficient of oil at the parameters (p_o, T_1),

ω - motor shaft angular velocity,

$C_{H\rho}$ - proportionality coefficient associated with pressure losses in passages;

ρ - specific mass of working liquid at the pressure p_o,

C_{Tp} - proportionality coefficient associated with mechanical friction,

k_{om} - the coeffcient expressed as follows: $k_{om} = \Delta M_{oTm} \cdot M_{Tp}^{-1}$,

Ω_0 - power exponent constant,

C_{Tr} - proportionality coefficient associated with friction variability during starting-up,

p_1 - pressure at inlet to hydraulic motor.

− volumetric losses represented by the following models:
  • for hydraulic motor without compensation of gaps:

$$Q_s = C_s V_t \Delta p \omega (2\pi)^{-1} + C_{ol} V_t \Delta p (2\pi \mu_0)^{-1} +$$

$$+ C_{ot}(2\Delta p \rho^{-1})^{-0,5}[(0,5 V_t \pi^{-1})^2]^{1/3} + C_{oz} V_t p_2 (2\pi \mu_0)^{-1}$$

where:

C_s - proportionality coefficient depending on pressure and angular velocity,

V_t - theoretical working volume of motor per unit shaft rotation,

Δp - pressure drop in motor,

C_{ol}, C_{ot} - proportionality coefficient of laminar and turbular component of leakages,

C_{oz} - proportionality coefficient depending on external leakages,

p_2 - pressure at outlet from hydraulic motor.

It can observed that the volumetric losses are the sum of four components: the first term expresses the component depending on pressure and angular velocity ($\omega = 2\pi n$), the second and third – the components due to internal leakages for laminar and turbulent flow, respectively, and the fourth is the component depending on external leakages.
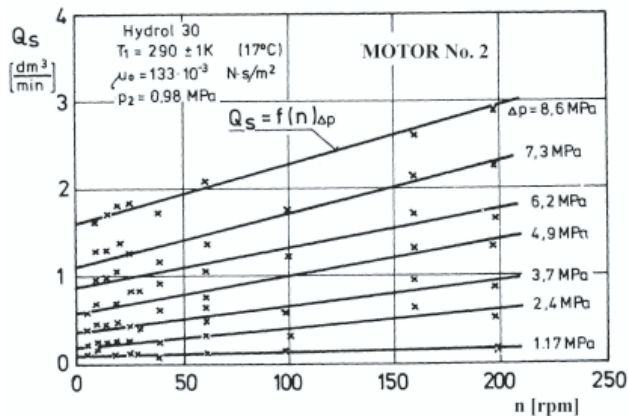
Fig. 1. *Characteristics of total volumetric losses in the SWSB-63 motor, $Q_s = f(n)$, at $\Delta p = const$, acc. [1]*

  • for hydraulic motor with compensation of gaps:

$$Q_s = C_s \frac{V_t}{2\pi} \Delta p \omega + \frac{C'_{ol}}{\mu_0} \frac{V_t}{2\pi} \Delta p (1 + B_h \Delta p)^3 +$$

$$+ C_{ot} \sqrt{\frac{2\Delta p}{\rho}} \sqrt[3]{\left(\frac{V_t}{2\pi}\right)^2} + \frac{C_{oz}}{\mu_0} \frac{V_t}{2\pi} p_2$$

where:

C'_{ol} – proportionality coefficient,

B_h – coefficient which characterizes operation of gaps compensation unit.

In the above given equation the element $(1 + B_h \Delta p)^3$ accounting for gaps compensation unit in motor is added to the component associated with internal leakages for laminar flow.

In Fig. 1 and 2 are presented the diagrams elaborated in [1], which illustrate the above mentioned relationships based on the tests of SWSB-63 motor [2].

In the Prof. Paszota's publications [5 ÷ 19] attention has been paid to the fact that losses occurring in hydraulic motors and pumps are presented either in function of the parameters which simultaneously depend on the losses or in function of the parameters which do not influence the losses directly. The relationships of losses in hydraulic motor, which have been published so far by Prof. Paszota, Z. [18, 19], are presented below:

− the moment $M_{Mm} = f(M_M, n_M, \nu)$ of mechanical losses in the unit „shaft-working chambers" is a function of the moment M_M exerted to motor shaft, demanded shaft rotational speed n_M, and working liquid viscosity ν [18]. In [19] is presented mathematical description of the moment of losses, M_{Mm}, in the unit „shaft-working chambers", as follows:

  • for motor of the theoretical (constant) absorbing capacity q_{Mt} per unit rotation of shaft:

$$M_{Mm|M_M, n_M, b_M=1,,\nu} = \left(k_{7.1.1} + k_{7.1.2} \frac{n_M}{n_{Mt}}\right) \cdot$$

$$\cdot M_{Mt} \left(\frac{\nu}{\nu_n}\right)^{a_{vm}} + k_{7.2} M_M =$$

$$= \left(k_{7.1.1} + k_{7.1.2} \frac{n_M}{n_{Mt}}\right) \frac{q_{Mt} p_n}{2\pi} \left(\frac{\nu}{\nu_n}\right)^{a_{vm}} + k_{7.2} M_M$$

where:

n_{Mt} - theoretical speed of motor shaft,

M_{Mt} - theoretical moment of motor,

ν/ν_n - ratio of the viscosity ν and working liquid reference viscosity $\nu_n = 35$ mm²s⁻¹,

a_{vm} - exponent which describes impact of ν/ν_n on magnitude of moment of mechanical losses in piston displacement motor of liquid -filled casing,

p_n - nominal pressure of system,

k_i - coefficients of losses given by the following expressions:

$$k_{7.1.1} = \frac{M_{Mm|M_M=0, n_M=0, b_M=1, \nu_n}}{M_{Mt}}$$

$$k_{7.1.2} = \frac{M_{Mm|M_M=0, n_M=n_{Mt}, b_M=1, \nu_n} - M_{Mm|M_M=0, n_M=0, b_M=1, \nu_n}}{M_{Mt}}$$

$$k_{7.2} = \frac{M_{Mm|M_M=M_{Mt}, n_M=n_{Mt}, b_M=1, \nu_n} - M_{Mm|M_M=0, n_M=n_{Mt}, b_M=1, \nu_n}}{M_{Mt}}$$

  • for motor of the geometrical (variable) absorbing capacity q_{Mgv} per unit rotation of shaft:
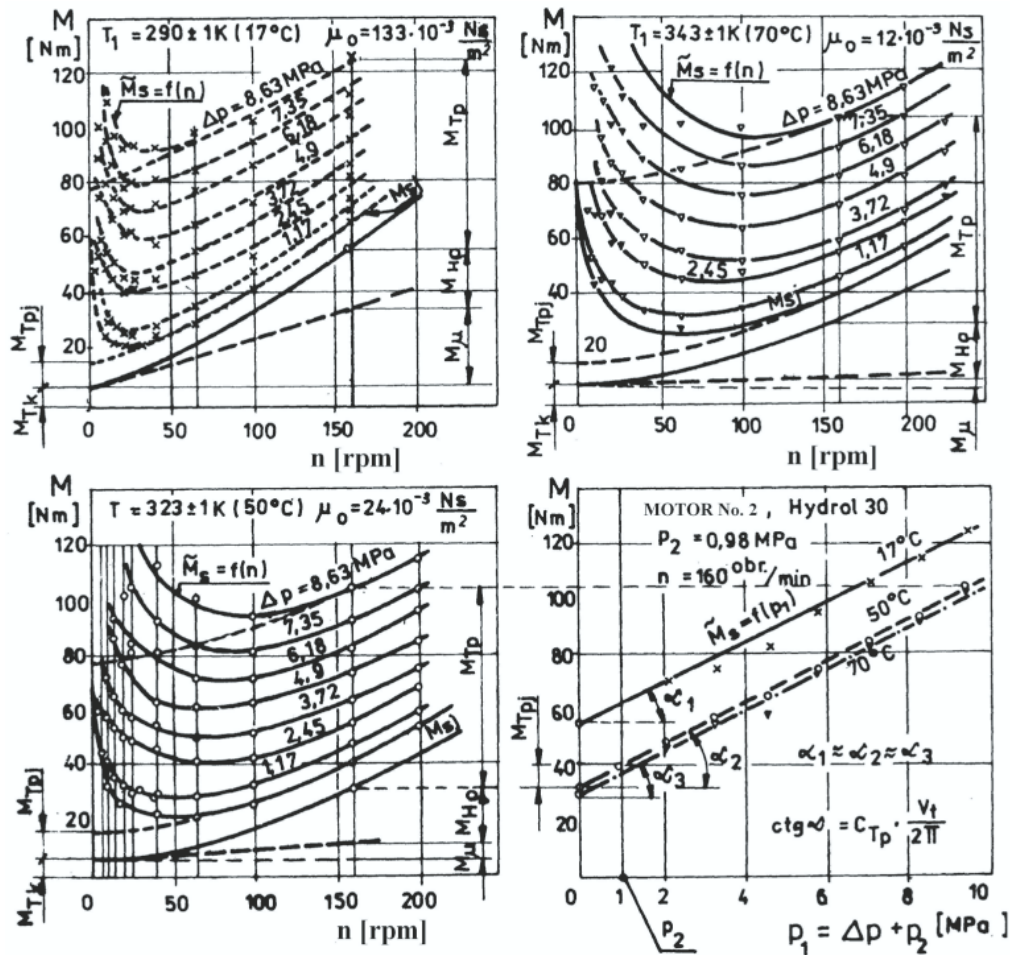
Fig. 2. Components of moment of losses in SWSB-63 motor for different oil temperature values, acc. [1]

$$M_{Mm|M_M, n_M, b_M, v} = \left(k_{7.1.1} + k_{7.1.2} \frac{n_M}{n_{Mt}} b_M \right) \cdot$$

$$\cdot M_{Mt} \left(\frac{v}{v_n} \right)^{a_{vm}} + k_{7.2} M_M =$$

$$= \left(k_{7.1.1} + k_{7.1.2} \frac{n_M}{n_{Mt}} b_M \right) \frac{q_{Mt} p_n}{2\pi} \left(\frac{v}{v_n} \right)^{a_{vm}} + k_{7.2} M_M$$

where:
b_M - coefficient of motor setting.

- the intensity $Q_{Mv} = f(\Delta p_{Mi}, n_M, v)$ of volumetric losses in working chambers is a function of the pressure drop Δp_{Mi} indicated in the chambers and, to some extent, of the motor shaft rotational speed n_M as well as the working liquid viscosity v, [18];
- the working liquid pressure losses $\Delta p_{Mp} = f(Q_M, v)$ within motor passages are a function of the motor absorbing capacity Q_M as well as the working liquid viscosity v, [18].

The test results of energy losses in the SWSB-63 motor, [2], presented in function of the parameters specified in [18], are illustrated in Fig. 3 ÷ 9.
- The characteristics $M_{Mm} = f(M_M)$ at $n_M = const$ and $v = const$ (Fig. 5) were determined on the basis of the data given in [2], by calculating, in addition, the moment M_{Mm} of mechanical

losses in the unit „shaft-working chambers" (defined in [5]) as the difference of the moment M_{Mi} indicated in working chambers (determined from the relation $M_{Mi} = 0.5 \, q_{Mt} \Delta p_{Mi} \pi^{-1}$) and the motor shaft moment M_M.
- By linear approximating the curves given in Fig. 3a÷c, were obtained the data to draw the relation $M_{Mm} = f(n_M)$ at $M_M = const$ and $v = const$, shown in Fig. 4a÷c.
- The characteristics $M_{Mm} = f(v)$ at $M_M = const$ and $n_M = 2.67s^{-1}$ (Fig. 5), were obtained on the basis of Fig. 3a÷c.
- The characteristics $Q_{Mv} = f(\Delta p_{Mi})$ at $n_M = const$ and $v = const$ (Fig. 6a÷c), were obtained by calculating the intensity Q_{Mv} of volumetric losses in motor working chambers as the difference of the motor absorbing capacity Q_M and the product of the theoretical absorbing capacity per unit rotation, q_{Mt}, and the motor shaft rotational speed n_M. The pressure drop Δp_{Mi} indicated in motor working chambers was calculated as the difference of the pressure drop Δp_M in motor and the liquid pressure losses Δp_{Mp} in passages of the motor (acc. [5]).
- The characteristics $Q_{Mv} = f(n_M)$ at $\Delta p_{Mi} = const$ and $v = const$ (Fig. 7 a÷c) were obtained by approximating the curves in Fig. 6 a÷c with the use of trend lines (and trying to get the possible greatest probability; they represent exponential functions).
- The characteristics $\Delta p_{Mp} = f(Q_M)$ at $v = const$ (Fig. 8 a÷c) were drawn on the basis of the data taken from [2].
- The characteristics $\Delta p_{Mp} = f(v)$ at $Q_{Mt} = const$ (Fig. 9) were obtained on the basis of the characteristics $\Delta p_{Mp} = f(Q_M)$ (Fig. 8 a÷c) by accounting for impact of liquid viscosity at the intensity equal to the theoretical absorbing capacity Q_{Mt}.
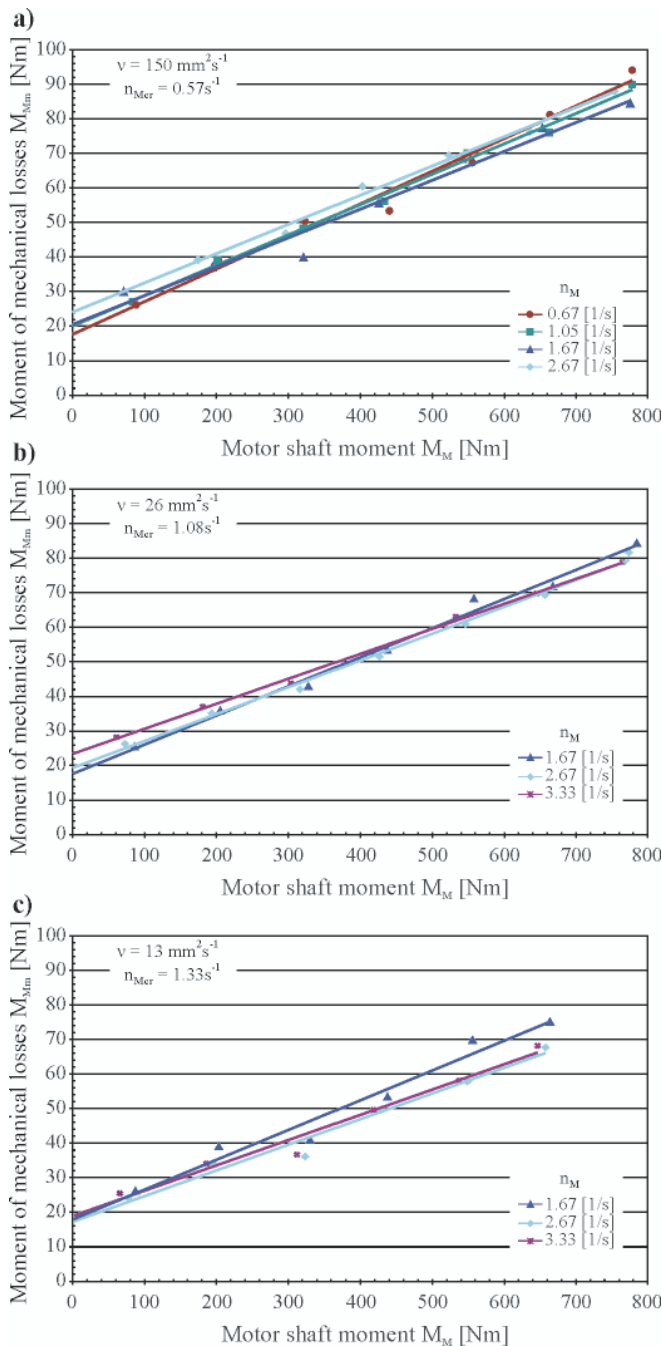
Fig. 3. *The moment of mechanical losses in the unit „ shaft-working chambers", M_{Mm}, of SWSB-63 motor in function of the shaft moment M_M at steady values of the shaft rotational speed n_M: **a)** $v = 150 \ mm^2s^{-1}$; **b)** $v = 26 \ mm^2s^{-1}$; **c)** $v = 13 \ mm^2s^{-1}$. As the critical shaft rotational speed n_{Mcr} was assumed the speed below which the speed irregularity δn_M is greater than 10 %*

Fig. 4. *The moment of mechanical losses in the unit „ shaft-working chambers", M_{Mm}, of SWSB-63 motor in function of the shaft rotational speed n_M at steady values of the shaft moment M_M: **a)** $v = 150 \ mm^2s^{-1}$; **b)** $v = 26 \ mm^2s^{-1}$; **c)** $v = 13 \ mm^2s^{-1}$. As the critical shaft rotational speed n_{Mcr} was assumed the speed below which the speed irregularity δn_M is greater than 10 %*

The critical rotational speed n_{Mcr} was assumed on the level corresponding to the relatively high irregularity of motor rotational speed, $\delta n_M \approx 10 \%$. On the diagrams (Fig. 3÷7), below the assumed value of the critical speed n_{Mcr} such characteristics were not determined.

The theoretical absorbing capacity Q_{Mt} was calculated as the product of the theoretical absorbing capacity per unit rotation, q_{Mt}, and the motor shaft theoretical rotational speed n_{Mt}.

COMPARISON OF TWO ESTIMATIONS OF LOSSES WHICH OCCUR IN MOTOR

1. The separation of mechanical losses (the moment, M_{Mm}, of mechanical losses in the unit „ shaft-working chambers")

from the „hydraulic" ones (the working liquid pressure losses Δp_{Mp} in working passages), proposed in [18], changes the image of the moment- of- losses characteristics (Fig. 2, 3, 4, 5) and their value. This can be observed in Fig. 2 where values of the moment of losses, M_s, at the steady rotational speed $n_M = 2.67s^{-1}$ ($n = 160$ rpm) and three constant values of the working liquid viscosity v, vary within the range of 30 ÷ 60 Nm, whereas values of the moment, M_{Mm}, of mechanical losses in the unit „ shaft – working chambers" (Fig. 5) for the same viscosity values, in which the relationships given in [18] are taken into account, vary within the range of 17 ÷ 24 Nm.

2. The moment of losses, M_s, (Fig. 2) presented in function of the rotational speed n and at steady values of the pressure
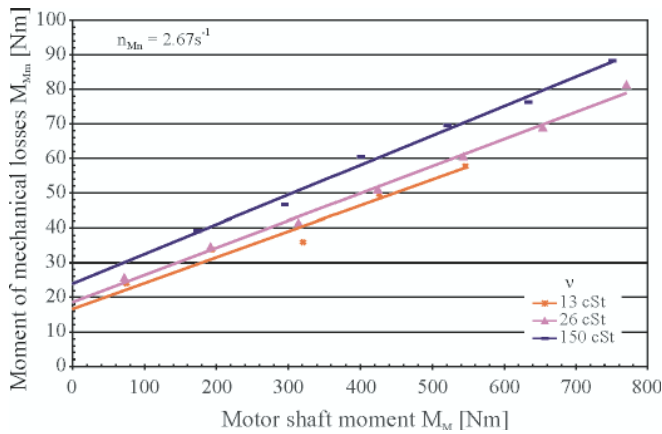
Fig. 5. The moment of mechanical losses in the unit „ shaft-working chambers”, M_{Mm}, of SWSB-63 motor in function of the shaft moment M_M at the theoretical shaft rotational speed $n_{Mt} = 2.67s^{-1}$ and steady values of the working liquid viscosity v

drop Δp in motor, is influenced by mechanical losses in the unit „shaft – working chambers”, volumetric losses in working chambers, as well as pressure losses in motor passages. The moment, M_{Mm}, of mechanical losses in the unit „shaft – working chambers” is presented in Fig. 3, 4 and 5, where it is demonstrated that, according to [18], the moment of mechanical losses, $M_{Mm} = f(M_M, n_M, v)$, is a function of the demanded moment M_M exerted to motor shaft, demanded shaft rotational speed n_M as well as working liquid viscosity v.

3. In the diagrams showing the moment, M_{Mm}, of mechanical losses in the unit „ shaft- working chambers” in function of the motor shaft moment M_M and at steady values of the motor rotational speed n_M (Fig. 3 a÷c), can be observed correct relation between the moment $M_{Mm|M_M = 0}$ of mechanical losses, determined at $M_M = 0$, and the shaft rotational speed n_M. The increasing shaft rotational speed n_M is accompanied by the increasing moment $M_{Mm|M_M = 0}$ associated with increasing inertia forces of structural elements as well as increasing friction forces between motor elements and working liquid. In the mathematical expressions which describe the moment of losses $M_{Mm|M_M = 0}$ it is assumed that the increase is linear [19]. At greater loads it can be observed that rotational speed irregularity made the moment of losses increasing.

4. In order to keep the image readable, in Fig. 3 a÷c were depicted neither measurement points nor straight lines obtained from the measurements done at speed values below the critical speed n_{Mcr} which turned out to be high though the speed was assumed that below which the speed irregularity δn_M is greater than 10 %. The tested SWSB-63 motor was characterized by a great rotational speed irregularity, that resulted in difficulties in proper determining mechanical and volumetric losses.
    The motor rotational speed irregularity is very high (of the order of 100 % or even greater) at small values of the shaft speed n_M, large values of the moment M_M and small values of the working liquid viscosity v. Then, mechanical losses grow and are difficult to be determined.

5. Neglecting the range of excessively great rotational speed irregularity (Fig. 4 a÷c), one can observe that the increasing of the rotational speed n_M leads to the increasing of the moment M_{Mm} of mechanical losses in the unit „shaft-working chambers”; this is specially visible at the large value of the viscosity $v = 150$ mm²s⁻¹, and less - at the smaller values of the viscosity $v = 26$ mm²s⁻¹ and
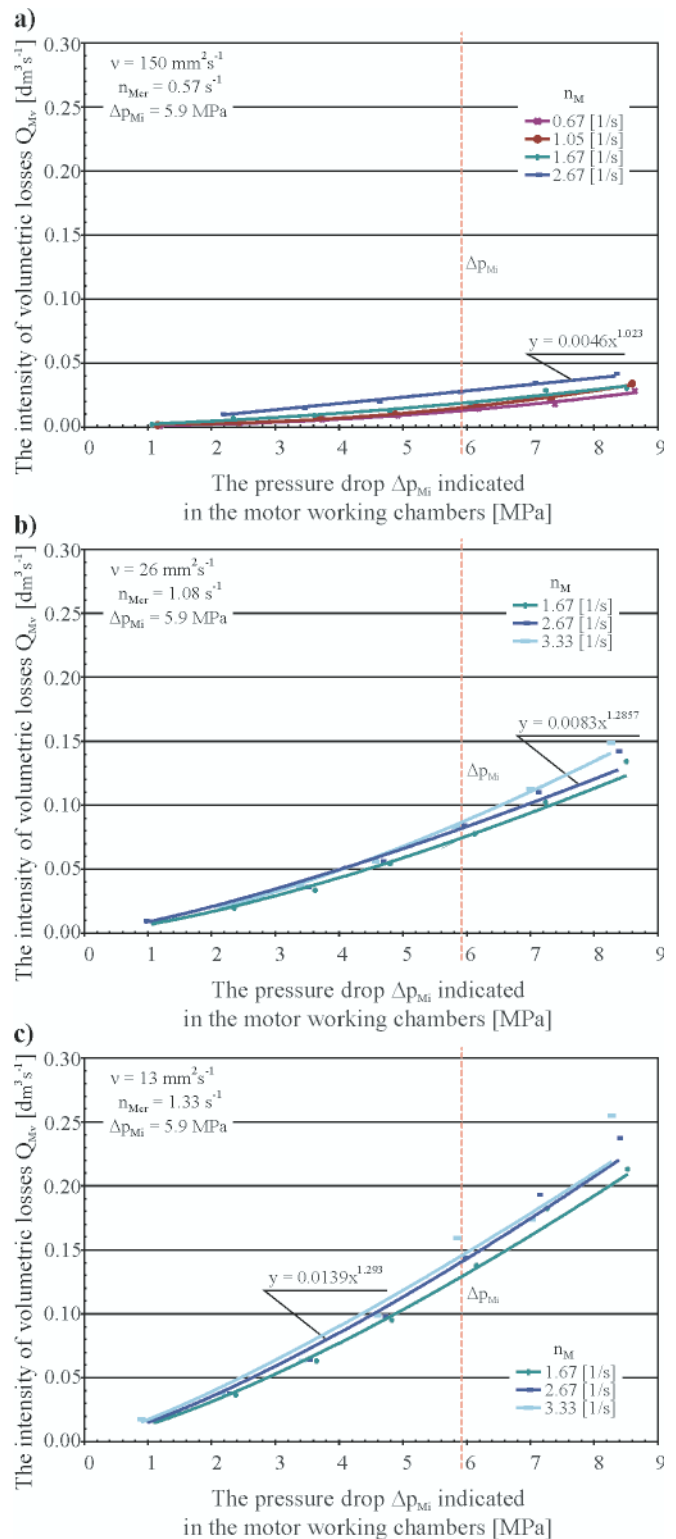
Fig. 6. The intensity, Q_{Mv}, of volumetric losses in working chambers of SWSB-63 motor in function of the pressure drop Δp_{Mi} indicated in the working chambers at steady values of the shaft rotational speed n_M; a) $v = 150$ mm²s⁻¹; b) $v = 26$ mm²s⁻¹; c) $v = 13$ mm²s⁻¹. As the critical shaft rotational speed n_{Mcr} was assumed the speed below which the speed irregularity δn_M is greater than 10 %. The description of the function $y = f(x)$ given in the diagrams reflects only a character of the phenomenon but not its full mathematical description

$v = 13$ mm²s⁻¹. The increasing of the moment of mechanical losses along with the increasing of the shaft speed results from friction forces between elements of the unit „ shaft-working chambers” and working liquid, and inertia forces of the unit's elements as well.

a)

b)

c)
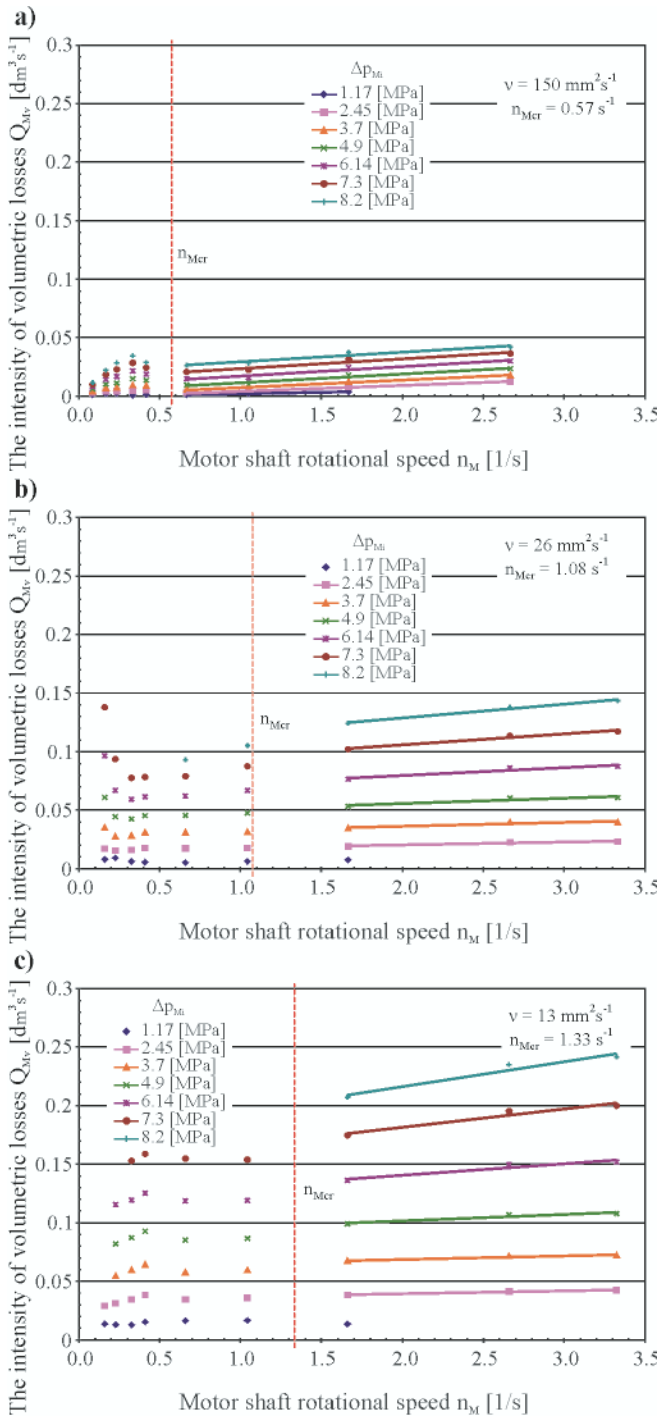
*Fig. 7. The intensity, Q_{Mv}, of volumetric losses in working chambers of SWSB-63 motor in function of the shaft rotational speeed n_M at steady values of the pressure drop Δp_{Mi} indicated in the working chambers; **a)** $v = 150\ mm^2 s^{-1}$; **b)** $v = 26\ mm^2 s^{-1}$; **c)** $v = 13\ mm^2 s^{-1}$. As the critical shaft rotational speed n_{Mcr} was assumed the speed below which the speed irregularity δn_M is greater than 10 %*

6. The images of the relationship of the moment, M_{Mm}, of mechanical losses in the unit „shaft-working chambers" (Fig. 4) and the moment M_s of losses acc. Fig. 2 versus the rotational speed n_M, are entirely different. In Fig. 2 a very distinct increase of the losses moment along with the rotational speed increasing is observed, and in Fig. 4 the lines tend to go rather horizontally. Attention should be paid to the fact that because of irregular operation of the motor a part of measurement points in Fig. 4 was taken out and not accounted for, but in Fig. 2 lines were put through the points and that was accounted for in motor operation analysis.

a)

b)

c)
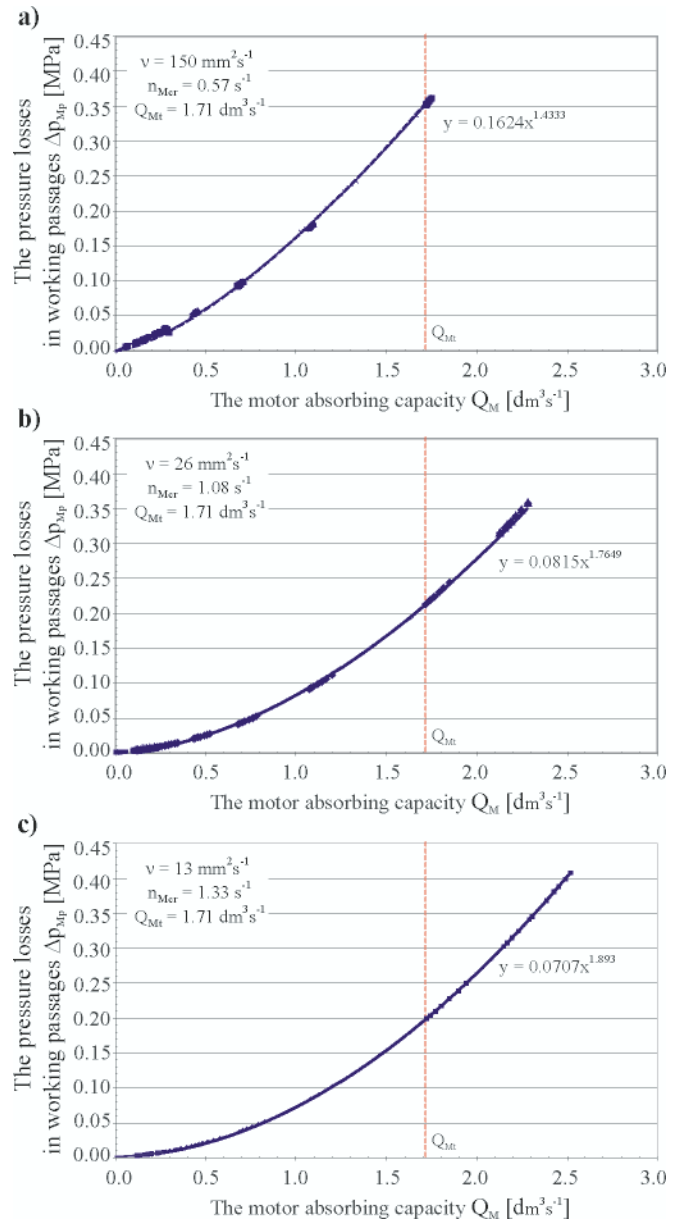
*Fig. 8. The working liquid pressure losses, Δp_{Mp}, in SWSB-63 motor passages in function of the motor absorbing capacity Q_M; **a)** $v = 150\ mm^2 s^{-1}$; **b)** $v = 26\ mm^2 s^{-1}$; **c)** $v = 13\ mm^2 s^{-1}$. The theoretical absorbing capacity $Q_{Mt} = 1.71\ dm^3 s^{-1}$ was determined from the relation: $q_{Mt} \cdot n_{Mt}$. The description of the function $y = f(x)$ given in the diagrams reflects only a character of the phenomenon but not its full mathematical description*

7. The impact of the working liquid viscosity v (mainly in motor casing) on the moment, M_{Mm}, of mechanical losses in the unit „shaft- working chambers" in function of the shaft moment M_M at the steady rotational speed $n_{Mt} = 2.67\ s^{-1}$ (Fig. 5) and determined for the shaft loading moment $M_M = 0$, is described by the power exponent $a_{vm} \approx 0.15$, acc. [19].

8. The images of the relationship between the intensity, Q_{Mv}, of volumetric losses in motor chambers and the pressure drop, Δp_{Mi}, indicated in the chambers (Fig. 6), at steady values of the shaft rotational speed n_M, described by the exponential function $Q_{Mv} \sim \Delta p^c_{Mi}$, make it possible to determine character of the losses associated with working liquid flow and simultaneous influence of changes in throttling gaps of the motor. The power exponent c take the following values: **a)** ($v = 150\ mm^2 s^{-1}$) c = 1,02; **b)** ($v = 26\ mm^2 s^{-1}$) c = 1.29, **c)** ($v = 13\ mm^2 s^{-1}$) c = 1.29. The c- exponent values are greater than c = 1, hence it is possible to conclude that in
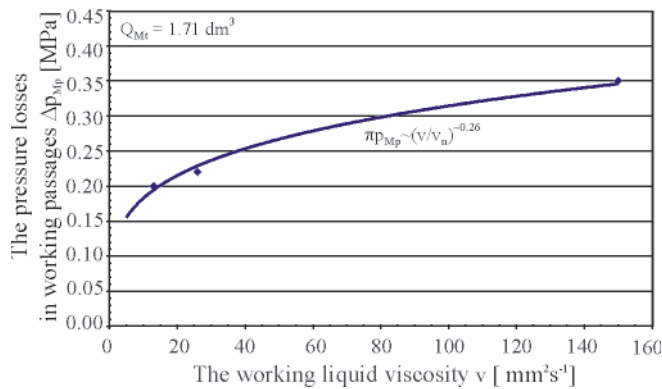
Fig. 9. *The working liquid pressure losses Δp_{Mp} in SWSB-63 motor passages in function of the working liquid viscosity v at the intensity equal to the theoretical absorbing capacity $Q_{Mt} = 1.71\ dm^3s^{-1}$*

the tested motor the intensity, Q_{Mv}, of volumetric losses in working chambers is influenced by the cross-section area of the gaps in chambers, increasing along with Δp_{Mi}.

9. The impact of the working liquid viscosity v on the intensity, Q_{Mv}, of volumetric losses in working chambers (Fig. 6), at $\Delta p_{Mi} = 5.9$ MPa and the rotational speed $n_M = 1.67$ s^{-1}, is determined by the power exponent a_{vv} as follows: $Q_{Mv} \sim (v/v_n)^{avv}$ [7], where $a_{vv} \approx -0.77$. And, at the theoretical rotational speed $n_{Mt} = 2.67$ s^{-1} the exponent value increases up to $a_{vv} \approx -0.62$. The a_{vv} - exponent values make it possible to conclude that flow of volumetric losses through working chambers is of a turbulent character with an increasing degree of disturbance along with the increasing of the shaft rotational speed n_M.

10. The image of the relationship between the liquid pressure loss Δp_{Mp} associated with its flow through working passages and the motor absorbing capacity Q_M makes it possible to determine a character of working liquid flow through the passages by approximating the curves of Fig. 8 a÷c with the use of the exponential function $\Delta p_{Mp} \sim Q_M^{\ d}$ [6]. The determined power exponent d take the following values: **a)** ($v = 150$ mm^{2}s^{-1}) d = 1.43; **b)** ($v = 26$ mm^{2}s^{-1}) d = 1.76; **c)** ($v = 13$ mm^{2}s^{-1}) d = 1.89. The d - exponent values make it possible to conclude that in the passages of the tested motor a not fully developed turbulent flow takes place along with the growing degree of disturbance accompanying the decreasing of the working liquid viscosity v.

11. The impact of the working liquid viscosity v on the working liquid pressure drop Δp_{Mp} in the passages (Fig. 8) was determined by using the power exponent a_{vp} appearing in the relationship $\Delta p_{Mp} \sim (v/v_n)^{avp}$ at the intensity equal to the theoretical motor absorbing capacity $Q_{Mt} = 1.71$ dm^{3}s^{-1}; then, its value was equal to $a_{vp} \approx 0.26$.

CONCLUSIONS

1. This paper is the first attempt to show the differences in assessing mechanical, volumetric and pressure losses occurring in hydraulic motor, resulting from that the assessments were made on the basis of different parameters. Two kinds of models of the losses were compared. The models proposed by Prof. Balawender, A. [1, 3] are very sophisticated, contain the parameters which themselves depend on the losses. The models of Prof. Paszota, Z., [18, 19], which are still under development, constitute the descriptions in which the losses are determined in function of the parameters which directly influence the losses, but are not dependent on them. The approach makes it possible to clearly present difference in assessing magnitude and proportion of the particular losses.

2. Correctness of such presentation of the moment, M_{Mm}, of motor mechanical losses occurring in the unit „ shaft – working chambers" consists not only in elimination of „hydraulic" losses from it, but also in presentation of the moment of mechanical losses in function of the parameters which directly influence its magnitude, i.e. in function of the demanded motor shaft loading moment M_M, demanded rotational speed n_M, as well as in function of the working liquid viscosity v.

3. The presented mechanical losses $M_{Mm} = f(M_M, n_M, v)$ in the unit „ shaft-working chambers", the volumetric losses $Q_{Mv} = f(\Delta p_{Mi}, n_M, v)$ in working chambers and pressure losses $\Delta p_{Mp} = f(Q_M, v)$ in motor passages have different character and are functions of different parameters, though it could at first glance seem that they are connected to each other by one common parameter, i.e the working liquid viscosity v. However its impact on particular losses is different. This was demonstrated with the use of the power exponent a_v offerred by the method, proposed by Prof. Paszota [5 ÷ 19], consisting in assessing particular kinds of losses by means of the loss coeffcients k_i which make it possible - due to their universal description - to assess the losses not only in particular elements but also in the whole system.

BIBLIOGRAPHY

1. Balawender A.: *Energy analysis and set of testing methods of slow-speed hydraulic motors* (in Polish). Wydawnictwo Politechnika Gdańska (Gdańsk University of Technology Publishing House), Gdańsk 1988

2. Balawender A., Osiecki A., Paszota Z., Klimkiewicz W., Ciepielowski J.: *Tests of the SWSB-63 large- moment medium-pressure hydraulic motor* (in Polish). Scientific research project, Gdańsk University of Technology, Gdańsk 1972

3. Balawender A.: *Physical and mathematical models of losses in hydraulic motors*. In: Developments in Mechanical Engineering, Chapter 19, ed. Barylski, A., Ciesliński, J. T. Wydawnictwo Politechnika Gdańska (Gdańsk University of Technology Publishing House), Gdańsk 2005

4. Maczyszyn A.: *Assessment of losses in hydraulic motor on the example of SWSB-63 motor tests* (in Polish). A chapter of the monograph on „Research, designing, manufacturing and operating of hydraulic systems" (in Polish), ed. Klich A., Kozieł A., Palczak E. The library „Cylinder". Centrum Mechanizacji Górnictwa „Komag" (Mining Industry Mechanization Centre), Gliwice 2010

5. Paszota Z.: *Aspects energetiques des transmissions hydrostatiques*. Wydawnictwo Politechnika Gdańska (Gdańsk University of Technology Publishing House), Gdańsk 2002

6. Paszota Z.: *Model of pressure losses in displacement pump used in hydrostatic drive* (in Polish). Materials of the 8th Scientific Conference „ Ship Technology and Ocean Engineering" on „Development prospects of transport systems". Międzyzdroje, 7-9 June 2006. Szczecin Technical University Publishing House, Szczecin 2006

7. Paszota Z.: *Model of volumetric losses in displacement pump of variable capacity used in hydrostatic drive* (in Polish). In: Napędy i Sterowanie 2006 (Drives and Control). The Scientific Technical Seminar "TECHNICON'06" accompanying the Fairs for Producers, Sub-contractors and Sellers of Drive Units and Control Systems, Gdańsk, 25 October 2006

8. Paszota Z.: *The power of energy losses in elements of hydrostatic drive system - definitions, relations, variability ranges, energy efficiences, Part I. Hydraulic motor* (in Polish). Napędy i Sterowanie, No. 11(103), November 2007

9. Paszota Z.: *Graphical presentation of the power of energy losses and power developed in elements of hydrostatic drive and control system, Part I -Rotational hydraulic motor speed series throttling control and volumetric control systems* (in Polish). A chapter of the monograph on „Research, designing,

manufacturing and operating of hydraulic systems" (in Polish), ed. Klich A., Kozieł A., Palczak E., The library „Cylinder". Centrum Mechanizacji Górnictwa „Komag" (Mining Industry Mechanization Centre), Gliwice 2008

10. Paszota Z.: *Graphical presentation of the power of energy losses and power developed in the elements of hydrostatic drive and control system, Part II - Rotational hydraulic motor speed parallel throttling control and volumetric control systems* (in Polish). A chapter of the monograph on „Research, designing, manufacturing and operating of hydraulic systems" (in Polish), ed. Klich A., Kozieł A., Palczak E., The library „Cylinder". Centrum Mechanizacji Górnictwa „Komag" (Mining Industry Mechanization Centre), Gliwice 2008

11. Paszota Z.: *Direction of power flux increase in hydrostatic drive and control system. Graphical presentation of the power of energy losses and the power developed in elements of the system, Part I. - Rotational hydraulic motor speed series throttling control and volumetric control systems* (in Polish). Napędy i Sterowanie, No. 10 (114), October 2008

12. Paszota Z.: *Direction of power flux increase in hydrostatic drive and control system. Graphical presentation of the power of energy losses and the power developed in elements of the system, Part II. - Rotational hydraulic motor speed parallel throttling control and volumetric control systems* (in Polish). Napędy i Sterowanie, No. 11 (115), November 2008

13. Paszota Z.: *Graphical presentation of the power of energy losses and power developed in the elements of hydrostatic drive and control system. Part I – Rotational hydraulic motor speed series throttling control systems*. Polish Maritime Research 3 (57), Vol. 15, 2008

14. Paszota Z.: *Graphical presentation of the power of energy losses and power developed in the elements of hydrostatic drive and control system. Part II – Rotational hydraulic motor speed parallel throttling control and volumetric control systems*. Polish Maritime Research 4 (58),Vol. 15, 2008

15. Paszota Z.: *The operating field of hydrostatic drive system (in Polish). A chapter of the monograph on „Research, designing, manufacturing and operating of hydraulic systems"* (in Polish), ed. Klich A., Kozieł A., Palczak E., The library „Cylinder". Centrum Mechanizacji Górnictwa „Komag" (Mining Industry Mechanization Centre), Gliwice 2009

16. Paszota Z.: *Parameters of efficiency investigations of hydraulic pumps and motors. Operating field of hydrostatic drive* (in Polish). Napędy i Sterowanie, No. 11 (127), November 2009

17. Paszota Z.: *The operating field of a hydrostatic drive system parameters of the energy efficiency investigations of pumps and hydraulic motor*. Polish Maritime Research 4 (62), Vol. 16, 2009

18. Paszota Z.: *Energy losses in hydraulic displacement motor - definitions and relations for assessing efficiency of hydrostatic motor and drive (in Polish). A chapter of the monograph on „Research, designing, manufacturing and operating of hydraulic systems"* (in Polish), ed. Klich A., Kozieł A., Palczak E., The library „Cylinder". Centrum Mechanizacji Górnictwa „Komag" (Mining Industry Mechanization Centre), Gliwice 2010

19. Paszota Z.: *Theoretical and mathematical models of mechanical losses in rotational hydraulic motor used in hydrostatic drive (in Polish). A chapter of the monograph on „Research, designing, manufacturing and operating of hydraulic systems"* (in Polish), ed. Klich A., Kozieł A., Palczak E., The library „Cylinder". Centrum Mechanizacji Górnictwa „Komag" (Mining Industry Mechanization Centre), Gliwice 2010.

CONTACT WITH THE AUTHOR

Agnieszka Maczyszyn, M. Sc.
Faculty of Ocean Engineering
and Ship Technology,
Gdańsk University of Technology
Narutowicza 11/12
80-233 Gdańsk, POLAND
e-mail: agnieszka.maczyszyn@pg.gda.pl

A concept of drive and control system of a novel device for people evacuating from large passenger ships

Czesław Dymarski, Prof.
Gdansk University of Technology

ABSTRACT

Year-after-year increasing number and size of sea-going passenger ships make it necessary to search for novel methods of evacuation of passengers from such large objects or to improve those which have been applied so far. This paper presents a concept of one of the original methods, in which, a.o., chain lifts have been applied to hold up life boats during voyage as well as to launch them in case of evacuation. Technical assumptions and requirements as well as schematic diagram of the hydraulic drive and control system of the lift, is presented.

Keywords: ship deck equipment; ship evacuating systems; life saving appliances systems; hydraulic drive and control system

USE OF THE ELABORATED CONCEPT OF THE DEVICE

The presented concept of evacuation method of people from a large passenger ship was elaborated by this author for the passenger ship Queen Mary 2 in the frame of the European project SAFECRAFTS. This choice has been based on the fact that the ship has been so far one of the most modern and largest passenger ships intended for shipping on North Atlantic route.

Fig. 1. The ship Queen Mary 2 with visible life boats placed on ship's side [7, 8]

The main technical and operational parameters of the ship are as follows:

Length: 345 m
Breadth: 41 m
Draught: 10 m
Overall height (keel-chimney): 72 m
Displacement: 150 000 t
Maximum speed: ~30 knots
Power: 115,4 MW
Drive: 4 pod propellers of 21,5 MW power each, two of them azimuthal
Number of passengers and crew members:
2620 + 1253 = 3873

GENERAL CONCEPT OF THE DEVICE

The general concept of the evacuation device is presented in Fig. 2. It consists in location of life boats not on ship sides as until now, but aft in two (or more) casings placed symmetrically.

On each side of walls of the casing are located two chain lifts fitted with special suitably spaced catches on which life boats pointing aft are placed horizontally. In emergency, people embark on all the boats simultaneously through doors close to aft parts of the boats. In the same time the stern ramp opens gravitationally. After taking seats in the boats and closing the doors the releasing system of hooks keeping the boats is triggered remotely from the boats or a ship control post, and then the system of stabilized gravitational launching the boats is put in operation. The boats launched one by one, in the instant of getting support on the slipway rollers, are automatically released out of the chain lift catches and drive down the slipway and ramp into water. The presented device is equipped with a line hoisting winch located in the fore upper part of the slipway. It is intended for the hoisting of successive boats out of water, e.g. after tests of the device, through the ramp to the extreme fore position on the slipway, from which each boat is lifted up on the catches of the chain lift unit under operation. As a result of an analysis it was concluded that the particular units of the system, i.e. the chain lift, stern ramp as well as line hoisting winch should be driven hydraulically,
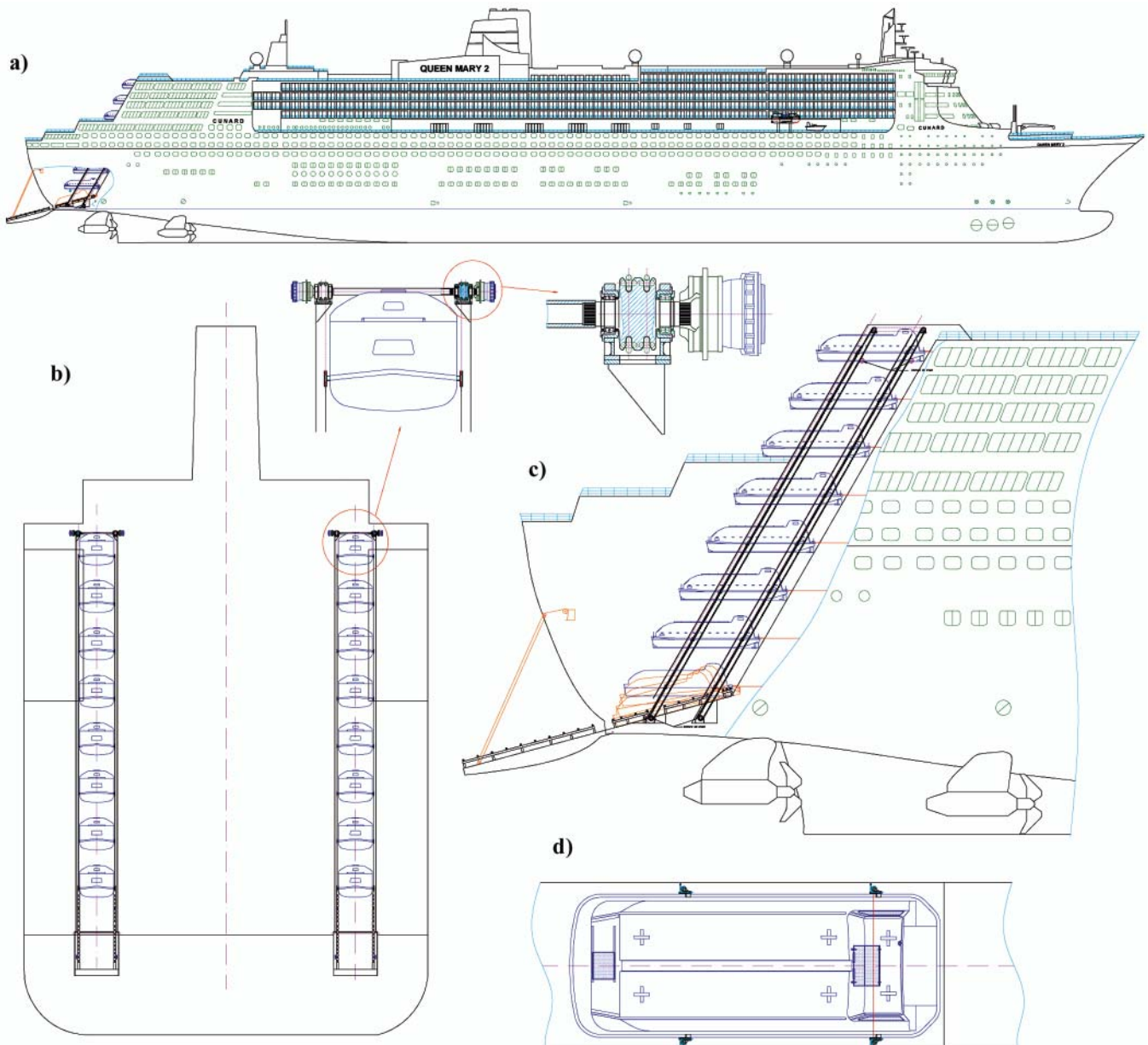
Fig. 2. *General concept of the device for evacuation of people:* **a)** *side view of the ship with the device installed on it;* **b)** *aft view of the ship with visible elements of drive system;* **c)** *cross-section through the casing with chain lifts and life boats;* **d)** *top view of the life boat placed on the chain lift in the casing*

in view of expected large variable loading, small speeds and a necessary high precision of motion.

DESCRIPTION OF OPERATIONAL PRINCIPLE OF THE EVACUATING SYSTEM

As mentioned above, the designed evacuating system consists of two independent devices contained in special casings located aft, behind the profitable space of the ship. In each casing four chain lifts mechanically coupled to each other, two on each side wall, are placed. In the lower part of the casing the slipway fitted with rollers is located. The casing is open from aft. Only the lower aft part of the casing can be closed by means of a simple ramp fitted, at its inner side, with a frame with rollers; this way after opening the ramp the frame can serve as an extension of the slipway as far as under water level. To the chains of the lift the catches suitably spaced to support closed life boats, are fixed. During voyage the lift's drive is kept blocked mechanically. Also, the location of the life boats on the lift's catches is blocked by means of the so called slip hooks which are also equipped with a hydraulic release, apart from a typical mechanical release. Owing to this in the case of sinking the ship its life boats are able to free themselves automatically. In view of the shape and location of the casings, eight life boats per each casing are provided for the ship as large as the Queen Mary 2. Number of life boats is limited by ship's height [depth] as well as a required spacing between successive boats; the boats are rather large, of the capacity of 120 or 150 persons. The spacing between the boats is to be such as to prevent possible collisions during evacuation. Specificity of the presented concept consists in that it makes it possible to evacuate all people on board simultaneously and to remotely start launching operation also from inside of a life boat. The this - way triggered evacuation process will be continued automatically until the last boat is launched. When the first launched boat is already placed in the slipway and starts driving on the rollers in uniformly accelerated motion, the successive boat on the chain lift is approaching the preceding one. For this reason it is very important to keep an appropriate spacing between the boats.

A favourable feature of the solution in question is that persons embark the boat when it is stiffly connected with ship's hull. This way, in the presented solution, the problem of movement of the boat against the ship, that usually occurs in the case of embarking the boat hanging along ship side, was eliminated. Owing to this, people are not exposed to stress and fear which is a typical reaction to the sight of rough sea in the gap between the boat and ship side during embarkment on the boats launched in the traditional way by means of side boat davits. There are no impacts of the boat against ship side and in consequence no impact loads on the boat and passengers as well, which usually happen during lowering the life boats hanging on lines along side of the ship rolling in waves, especially in heavy weather conditions. In the discussed solution the process of lowering and launching the boats is fully controlled and free of any sudden accelerations and panting against water surface as it is in the case of evacuation systems based on free-fall lifeboats. Engine of the boat is started up during its going down along the slipway. As during launching the boat moves in opposite direction relative to the ship, therefore, being already in water, it continues the motion and sails away from the endangered ship. The above mentioned features are of special importance for older and handicapped persons for which both stress and sudden accelerations could be dangerous. Structure of the boats used in the presented solution contains some features of both free-fall boats and life boats lowered with the use of side davits. Like free-fall boats, they have specifically formed sides adjusted to going down on rollers. Because of their launching mode which causes much smaller dynamic loads they do not need to be as much resistant to loads as the free-fall boats. Their proportions are similar to those of free-fall boats, namely, they are more slender and longer than the side lifeboats. This makes it possible to save a part of expensive usable space of ship. The launching mode consists in lowering the boats at a controlled speed by using the chain mechanism. The motion takes place as a result of gravity forces and its speed is limited by means of a two-way flow controller installed in the hydraulic lift system, or a centrifugal brake. The boats are horizontally placed on the lift both during ship voyage and lowering process. In the lower part of the casing the boat, while settling on the rollers fastened to the frame inclined by 15° against the deck level, releases itself from the chain lift. In the initial, fore part of the slipway three rollers are placed very close to each other to provide a greater comfort during the transient phase of evacuation when the boat changes its angular position. The boat travels its final path along the slipway inside the ship hull and next the stern ramp, developing uniformly accelerated motion and freely going down on rollers so as to enter the water at a relatively small slope angle. It highly moderates dynamics of its contact with water and lowers accelerations acting on the boat and people inside.

In the proposed solution a simple ramp was used. It consists of a main segment built of steel plating, a number of stiffeners and frames, which provide sufficient stiffness and strength of the ramp in heavy sea conditions. On the outer surface of the ramp there is a metal frame made of square cross-section pipes to which rollers are fixed so that after opening the ramp the structure serves as an extension of the slipways, along which the boats go down to water.

The drive of the ramp consists of a double-drum line hoisting winch and double pulley block system on both sides of the ramp. The motor of the winch is fitted with a blocking brake equipped with a hydraulic release. The lowering of the ramp is realized gravitationally at a speed stabilized and controlled by means of a two-way flow controller and centrifugal brake, if necessary. The drive and control system of the ramp is rather complex. It contains additional elements which serve to pull closer and block the ramp in the voyage position, and – in the case of a variant solution – units for automatic adjusting the angle of its opening depending on ship's draught and trim. As the system is multi-variant and complex the authors have resigned from publishing its description in detail in this paper.

The ramp together with the line hoisting winch located in the ship's hull just before the ramp constitutes a system for hoisting the boats out of water after evacuation trials. The boats are pulled one by one onto the ramp and further onto the slipway where they are placed on the chain lift catches and after that the lift is put into motion. In the instant when a boat is displaced upward the casing to a level assigned on the scale of boat arrangement, which is controlled by sensors, the chain lift is automatically stopped until a successive boat is taken out of water and placed on the catches, and then the mechanism is put in operation, the process is repeated again and again up to the last boat.

For driving the mutually coupled chain lifts, four winches fitted with double chain wheel and high-torque hydraulic motor equipped with blocking brake, hydraulic release and, if necessary, additional centrifugal brake, are used. Boat's lowering speed is stabilized and controlled by a two-way flow controller. A schematic diagram of the hydraulic drive

and control system is presented in the next section. Fast and efficient evacuation of people from all decks of the ship is ensured by an appropriate form of staircases and a visual and acoustic system for directing the people to the life boats. The concept is based on that the doors leading from the staircases are located just opposite the entrances to the boats. Moreover, an emergency passage connecting successive levels, placed just behind the casing, is provided to facilitate people displacing in emergency. And, in this area anti-slipping materials are used to prevent people from slipping and falling down.

HYDRAULIC DRIVE AND CONTROL SYSTEM FOR CHAIN LIFTS

The hydraulic drive and control system for the chain lifts is presented below in Fig. 3.

The main task of the system in question is to ensure that all the boats with embarked people, placed on the chain lift, can be lowered with an appropriate, possibly constant speed in the conditions of no electric supply from ship's power plant. And, it was assumed that it should be possible to stop and start again the boat lowering operation from a post on board the ship. Moreover the system should be capable of hoisting all the boats without people but with full standard equipment. In the presented system the boat lowering operation will be performed gravitationally at switched-off electric motor (4). Pressure in the accumulator (7) should be checked before starting-up the operation. The accumulator is hydraulically connected (R) with the drive system of the stern ramp whose operation of opening, executed earlier, automatically triggers the accumulator charging. To be on the safe side, the small hand-pump (3) by which the accumulator can be charged, is added. The starting-up of the chain lifts with boats is executed by switching over the distributors (8) and (7) to the right, remotely - from the upper boat or locally - from the control post. This makes oil to flow from the accumulator (7) to the
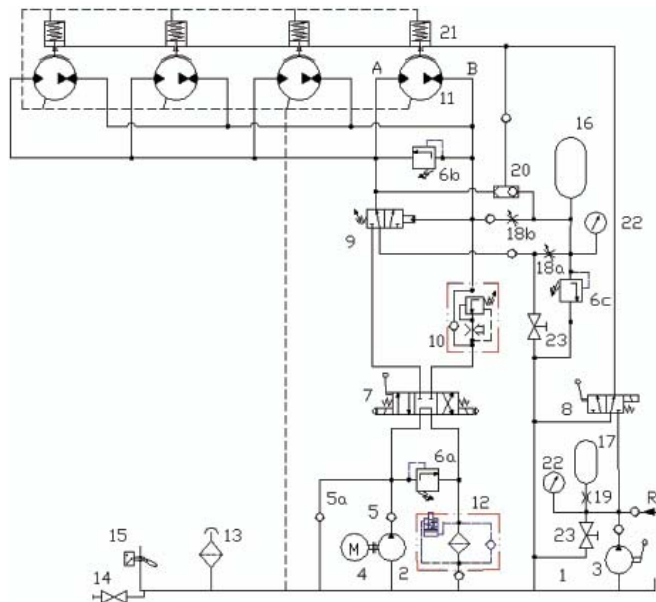
Fig. 3. Schematic diagram of the hydraulic drive and control system for the life-boat chain lift. Notation: 1), 13), 14) and 15) oil tank with equipment; 2) and 4) pump and electric motor; 3) hand-pump; 5) check valves; 6) overflow valve; 7) four–way three-position distributor; 8) and 9) three-way two-position distributors; 10) two-way flow controller; 11) hydraulic motors of constant absorbing capacity; 12) oil filter; 16) and 17) hydraulic-gas accumulators; 18) and 19) throttle valves; 20) pressure control valves; 21) hydraulic brake release; 22) manometers; 23) cut-off valves; A, B – stands for main circuit branches; R – stands for oil inflow from stern-ramp drive system

hydraulic brake releases (21) causing a sudden rise of pressure in the right branch (B) of motor circuit due to external load. In consequence the distributor (9) is then switched over to the left making this way oil to flow from the tank (1) through the distributor (7) and (9) to the motors (11) due to their pumping work resulting from the load of the boats with people. Speed of the motion is stabilized by the two-way flow controller (10). In the first phase of the process the motion will be somewhat faster because of the high oil pressure dependent on the load as well as due to the fact that a part of the oil pressed from the branch pipe (B) is gradually drained from the branch (B) through the throttle valve (18b) to the accumulator (16). The accumulator is aimed at making the lowering motion fluent also during placing the last boat on the rollers and releasing it from the catches when the external load of the motors (11) is too low to overcome friction forces in the system and ensure their pumping work. When the oil pressure in the branch (B) drops down to its threshold level set by the spring of the distributor (9), it will be switched over to the position of connecting the accumulator (16) with the charging branch (A) of the motors (11), that will ensure continuous work of the chain lift.

FEATURES OF THE SYSTEM

The crucial features which characterize various aspects of the elaborated concept are the following:
1. Safety of the proposed evacuating system from the point of view of passengers:
   • simple and safe access to life boats (appropriately formed staircases leading straight to boats, on every deck level a boat can be find),
   • stiff connection of boat and gangway relative to the ship (there are no mutual displacements of boat and ship; rough sea is not visible during embarkation on boats),
   • a relatively lower load exerted on people,
   • a gentle acceleration effect to people inside the boat (neither panting of boat against ship side nor slamming against water occurs),
2. Safety and reliability of the system in question:
   • easiness of simultaneous control of readiness of all boats (access openings or doors fitted with sight glasses are provided for in casing walls to make it possible to reach the boats,
   • collision-free launching (the boats are placed on the chain mechanism supports, with keeping safe mutual distance so as to make the just launched boat going far away possible until the successive boat is in water),
   • easy and safe launching the boats (the applied system of rollers located in the end part of the casing makes it possible to gently transfer the boats from the lowering mechanism onto the slipway equipped with rollers, due to which the boat is able to slide into water automatically)
   • safe contact of boat with water (for the time of evacuation the slipway located in the end part of the casing, can be extended by the length of the ramp partly immersed in water, due to which the boat goes bows-on into water under a small entrance angle; its engine is started in advance on the slipway, and, the boat departs just after launching in the direction opposite to that of ship's motion),
   • the system in question does not require any large number of operators nor special skill,
   • the boat lowering process runs automatically under gravity forces,

- the launching can be performed to water area behind the stern of the ship under motion, free of ice floats and possible contaminations, i.e. in the conditions that can not be ensured at the side of ship,

3. Quickness of evacuation:
   - on average a shorter distance is to be covered by evacuating persons,
   - simultaneous access to all boats from particular decks of ship,
   - less confusion than during evacuation by using a boat system having side boat davits when all passengers gather on one and the same deck,
   - a shorter evacuation process as all the boats are lowered simultaneously after starting up only one common driving system (the starting-up of the driving system which lowers the boats is preceded by the simultaneous lifting-up of all gangways and releasing the hooks (releases) of the mechanisms blocking the boats during ship voyage).

4. Technical merits:
   - less number of mechanisms than in the case of side evacuation systems using side boat davits,
   - a great simplicity of mechanisms, hence a higher reliability,
   - low cost of devices.

5. Analysis of the applied boats:
   - the boats applied in the proposed solution are of a smaller breadth and a little greater length than the side boats, and their form is rather similar to the free-fall boats,
   - their structure is adjusted to going down on rollers,
   - their strength is not required to be as big as that of free-fall boats because dynamic loads applied to them are much smaller (comparable to loads exerted to classical boats launched by using side davits, or even smaller).

6. Possible automatic freeing the boats in case of sinking the ship:
   - this is fully possible as the casing is open from the ship stern side, and only in its lower part there is the gravitationally openable ramp closed during voyage; the releasing system of ramp clamping devices is integrated with that of hooks keeping the boats in their voyage position as well as with the system for folding the gangways after embarkation of people on boats, which is automatically triggered by the hydrostatic release.

7. Procedure of hoisting the boats after evacuation trials and fastening the boats during voyage:
   - the double-drum line-hoisting winch is so located in ship's hull that it does not interfere in ship's image and esthetic merits,
   - the voyage position of boats on the chain lifts is blocked by slip hooks, like in the systems for free-fall boats.

8. Overall merits:
   - the system simultaneously operates on all decks,
   - the whole evacuation system occupies a relatively small area because the boats are placed one over the other,
   - the location of the system is favourable because it does not occupy the expensive hotel space fitted with windows.

- more safe and comfortable operation of people embarking on boats,
- a smaller resistance of ship to motion,
- a more esthetic image of ship,
- during ship sinking the freeing of boats is fully possible.

9. Disadvantage:
   - Possible blockage of even only one boat causes the chain lift stopping and necessessity of emptying the boat and next removing it off the chain lift by using a line hoist (not shown in the drawing) installed on both walls of the casing, and placing the boat onto the slipway fitted with rollers, that unfortunately will make the evacuation process longer. A more detailed description of the blocked boat removing system is rather extensive, hence it could be presented in a separate paper.

BIBLIOGRAPHY

1. Dymarski Cz., Dymarski P.: *Shipboard life saving and rescue equipment – R&D projects* (in Polish). Materials of 10th International Scientific Technical Conference „ Safety at Sea and Marine Environment". 5th Maritime Forum, Koszalin - Kołobrzeg 2006, Ed. NOT, Koszalin 2006.
2. Dymarski Cz., Łubiński P.: *Safe evacuation of people from ships – research performed in the frame of the European Research Project SAFECRAFTS* (in Polish). Materials of 8th Conference on Shipbuilding and Ocean Technology, „Development prospects of transport systems", Międzyzdroje, June 2006. Publ. Szczecin University of Technology, Szczecin 2006
3. Dymarski Cz., Kraskowski M., Sperski M.: *Investigation of motion of the lifeboat lowered from ship's deck.* Polish Maritime Research. - Vol. 13, no. 3, 2006
4. Dymarski Cz., Dymarski P.: *A system for evacuation of people from multi-deck ship, passenger ship in particular* (in Polish). Patent application No. P 379355, dated 3 April 2006
5. Dymarski Cz., Łubiński P., Dymarski P.: *Ramp and chain-lift-launched lifeboats - radical concepts for evacuating cruise ships.* Naval Architect, October 2006
6. Dymarski Cz.: *A concept of drive and control system of a novel device for people evacuating from large passenger ship. Research and construction* (in Polish). Materials of the Conf. on „Wytwarzanie i Eksploatacja Układów Hydraulicznych" CYLINDER 2009 (Production and Operation of Hydraulic Systems), Szczyrk, 23÷25 August 2009, Publ. Centrum Mechanizacji Górnictwa KOMAG.
7. Stareńczak P.: *The Queen Mary 2 - a new queen of oceans* (in Polish). Budownictwo Okrętowe, nr 1 (534), January 2004
8. http://www.marinetraffic.com/ais/pl/showallphotos.aspx?mmsi=235762000.

CONTACT WITH THE AUTHOR

Prof. Czesław Dymarski
Faculty of Ocean Engineering
and Ship Technology,
Gdańsk University of Technology
Narutowicza 11/12
80-233 Gdańsk, POLAND
e-mail: cpdymars@pg.gda.pl

Analysis of fracture toughness of modified timber

Part II
Mathematical description

Lesław Kyzioł, Ph. D.
Polish Naval Academy in Gdynia

ABSTRACT

This paper presents results of fracture toughness tests on DCB specimens made of natural and modified pine wood. The energy release coefficients G_a were calculated for both the materials under TL and RL crack propagation modes and the 1st mode of loading. Relations between the energy release coeffcients G_{aI} and the stress intensity factors K_{aI} have been determined. The obtained test results are presented in the form of tables and diagrams.

Keywords: anisotropic material; energy release coefficient; stresss intensity factor; anisotropic material cracking

INTRODUCTION

In the earlier phase of tests the critical stress intensity factor K_{Ic} [5, 6] was used for description of wood fracture toughness. Finally, the critical energy release coeffcient G_{Ic} was applied to describe wood cracking [4, 7, 8].

In the 1960s were made the first attempts to determining wood fracture toughness which consisted in testing the pine wood specimens under 1st mode of loading at TL and RL crack propagation modes, [4]. To the tests the DCB cantilever specimens were used to determine critical values of the energy release coeffcient G_{Ic}. By making use of the earlier obtained results of the tests on specimens of geometrical dimensions only a little different from the laboratory specimens, intended for describing wood fracture toughness, it was stated that the minor differences in dimensions did not affected values of the determined critical coeffcient G_{Ic}. Moreover it was observed that at both the considered modes only minor differences appeared in values of the critical coeffcient G_{Ic}. Many conducted tests have demonstrated that for the modes RL and TL the fracture toughness is multifold greater than for other modes, and it was the reason that in this work the fracture toughness tests of modified wood and, for comparison, also natural wood have been undertaken for both the mentioned modes.

This work has been aimed at determining fracture toughness of modified wood in contrast to natural wood. Results of the tests have been expected to show impact of modification of wood on its fracture toghness. The earlier performed tests on modified wood demonstrated significant increase of its strength properties both statical and dynamical in contrast to natural wood [1], therefore the determining of fracture toughness of the material has been deemed purposeful.

RESULTS OF THE TESTS

The tests of modified and natural wood were performed on 10 specimens at RL and LT crack propagation modes. On the basis of the tests (whose description was in detail presented in Part I) the below presented results were achieved.

In Tab. 1 are presented the example results of crack propagation run in the tested specimen C1 of natural wood in the direction of RL mode, and in Fig. 1 - the collective diagram which presents crack development in function of loading at the RL mode.

Fig. 1. *Collective diagram of the displacement δ in function of the load P for the specimens at RL crack propagation mode, with depicted value of critical load determined by using the P(δ) method (natural wood)*

Time [s]	Length of developed crack [mm]	Axial force [N]
0.540	0.01	6.0
5.745	0.11	8.0
10.050	0.20	10.0
15.054	0.29	12.0
20.059	0.40	18.0
25.064	0.49	20.4
30.069	0.60	25.0
35.074	0.70	30.0
40.079	0.80	34.0
45.084	0.90	44.0
50.089	0.99	54.0
55.094	1.10	58.0
60.098	1.20	60.0
…	…	…
325.057	6.50	200.0
330.062	6.60	195.0
335.067	6.70	190.0
340.072	6.80	187.0
345.076	6.90	186.0
350.081	7.00	185.0
355.086	7.10	178.0
360.091	7.21	163.0

In Fig. 2 is below presented the collective diagram of crack development run for structural natural wood in the TL crack propagation direction.
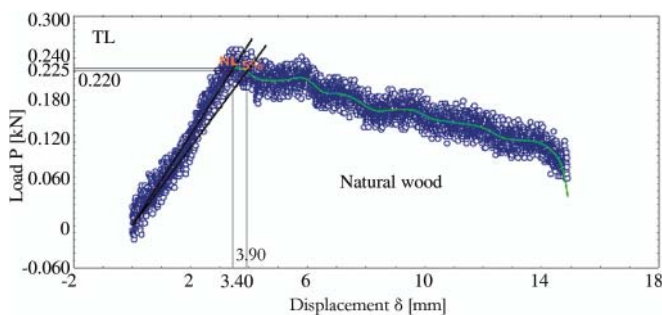
Fig. 2. Collective diagram of the displacement δ in function of the load P for the specimens at TL crack propagation mode, with depicted value of critical load determined by using the P(δ) method (natural wood)

Analysis of the crack propagation in natural wood specimens (Fig. 1 and 2) demonstrated that for the TL mode the values of critical load and relevant displacement according to the P(δ) method were only a little greater. It results from the structure of wood being an orthotropic material.

As results from the available subject-matter literature no fracture toughness tests of modified wood have been performed so far.

The modification of wood consisted in introducing a synthetic polymer to wood structure, and then its thermal polymerization. As a result of the process the material of properties different from its components was obtained [1].

In Fig. 3 and 4 are presented the collective diagrams of crack propagation run for the tested specimens of modified pine wood at the TL and RL direction modes.
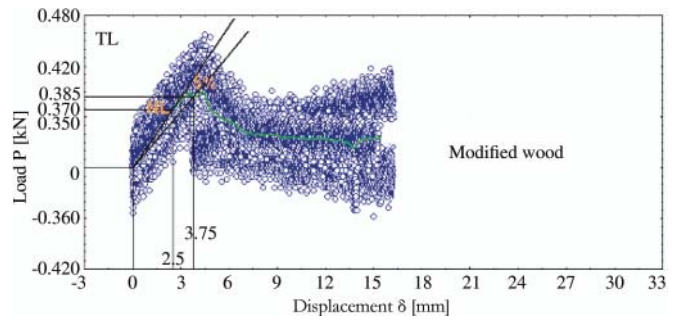
Fig. 3. Collective diagram of the displacement δ in function of the load P for the specimens at RL crack propagation mode, with depicted value of critical load determined by using the P(δ) method (modified wood)

Initial fracture toughness tests of modified wood have made it possible to determine loss of integrity of the composite depending on crack propagation mode. Like in the case of natural wood the tests were performed for the radial-longitudinal mode RL and tangential – longitudinal mode TL. The tested cases were characterized by single cracks which were developing up to exceedance of allowable stresses. In the tangential-longitudinal mode TL the crack propagated in the direction almost parallel to the material fibres, and in the radial-longitudinal one RL - along the material fibres.
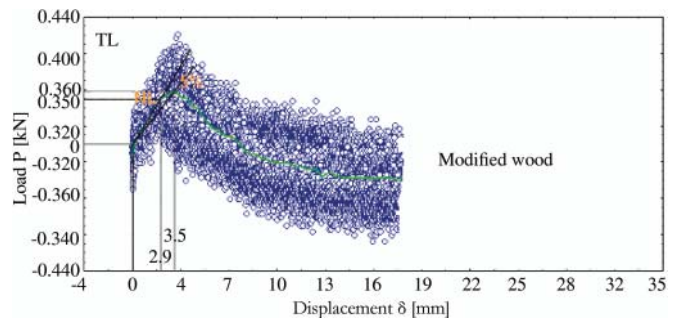
Fig. 4. Collective diagram of the displacement δ in function of the load P for the specimens at TL crack propagation mode, with depicted value of critical load determined by using the P(δ) method (modified wood)

The selected results of the tests on structural wood specimens loaded in accordance with the 1st mode at the TL and RL crack propagation modes, are presented in Tab. 2 (natural wood) and Tab. 3 (modified wood).

The analysis of the cracking of modified wood specimens, performed on the basis of the results given in Fig, 3 and 4, has demostrated that the critical loads and the displacements corresponding to them, according to the applied method P(δ), showed greater values than for natural wood. As results, the modified wood is more tough against cracking. The increase of strength properties and fracture toughness of the modified wood is due to the strengthening of the porous structure of wood by filling it with the polymer. As a result of polymerization of the monomer introduced to wood structure a new material of improved properties as compared with natural wood, was achieved. The results of the fracture toughness tests of the modified wood confirmed the positive influence of the polymer on improving mechanical properties of wood [1].

As follows from the test results presented in tab. 2 and 3, the similar values of the critical coefficients G_{Ic} were obtained for both the analyzed crack propagation modes (TL and RL). And, the values of the coefficients for the modified wood are more than twice greater than for the natural wood. This confirms

Tab. 2. *Results of the tests on natural wood specimens loaded in accordance with the 1st mode at the RL and TL crack propagation modes*

No. of specimen	$2h_i$ [mm]	Humidity [%]	δ_i [mm]	P_i [N]	B_i [mm]	n	G_i [J/m²]
C1RL	19.9		3.15	215	20.1		589
C2RL	20.1		2.35	208	19.9		429
C3RL	19.9		1.95	195	19.8		336
C4RL	20.1		2.05	185	20.1		330
C5RL	20.2		2.15	198	19.9		374
C6RL	19.7		1.97	187	20.2		319
C7RL	19.9		2.56	201	20.3		443
C8RL	20.1		1.97	197	20.3		334
C9RL	19.6		2.08	200	19.8		367
C10RL	19.8		1.98	189	20.1		325
Mean value		12.8	**2.22**	**197**		2.80	**384**
C1TL	20.0		3.55	215	20.2		661
C2TL	20.2		3.08	200	20.1		536
C3TL	19.9		1.97	189	20.3		320
C4TL	20.2		1.75	198	20.6		294
C5TL	19.9		2.06	187	20.1		335
C6TL	20.1		1.97	179	20.2		305
C7TL	19.8		2.05	207	19.6		378
C8TL	20.2		2.38	178	19.5		380
C9TL	19.9		1.95	194	20.1		330
C10TL	20.2		2.56	197	19.8		445
Mean value			**2.33**	**194**			**398**

Tab. 3. *Results of the tests on modified wood specimens loaded in accordance with the 1st mode at the RL and TL crack propagation modes*

No. of speci-men	$2h_i$ [mm]	Humidity [%]	δ_i [mm]	P_i [N]	B_i [mm]	n	G_i [J/m²]
CM1RL	20.1		3.50	360	20.1		1097
CM2RL	20.2		3.45	350	19.9		1061
CM3RL	19.9		2.98	347	20.2		895
CM4RL	19.8		3.45	298	20.1		895
CM5RL	20.0		2.98	267	20.3		686
CM6RL	20.1		2.45	245	20.2		520
CM7RL	19.9		2.16	305	20.1		573
CM8RL	20.1		3.05	276	20.2		729
CM9RL	20.0		3.14	301	19.8		819
CM10RL	19.9		2.94	298	20.2		759
Mean value		8.80	**3.01**	**304**		2.80	**803**
CM1TL	19.9		3.75	385	20.4		1238
CM2TL	20.1		3.15	320	20.2		873
CM3TL	19.8		2.56	300	20.3		662
CM4TL	19.9		2.78	298	20.4		710
CM5TL	20.1		3.05	276	20.2		729
CM6TL	19.9		3.14	305	20.3		825
CM7TL	20.0		2.87	309	19.9		779
CM8TL	20.1		3.05	298	20.4		779
CM9TL	19.8		3.07	287	20.1		767
CM10TL	20.0		2.78	298	19.9		728
Mean value			**3.02**	**307**			**809**

the earlier obtained results showing that the modification of wood by using methyl polymethacrylate greatly improves its fracture toughness.

ANALYSIS OF RESULTS OF THE TESTS

The general relation between the energy release coefficients G_α, and the stress intensity factors K_α is expressed as follows:

$$G_\alpha = c_\alpha \cdot K_\alpha^2 \quad \alpha = I, II, III \tag{1}$$

By making use of the relations between G_α and K_α acc. [10] for wood being an orthotropic material under the 1st mode of loading, the following is obtained for the TL crack propagation mode:

$$G_I = K_I^2 \cdot \sqrt{\frac{1}{2E_L E_T}} \left[\sqrt{\frac{E_L}{E_T}} + \frac{E_L}{2G_{LT}} - \nu_{LT} \right]^{\frac{1}{2}} \tag{2}$$

and for the RL crack propagation mode:

$$G_I = K_I^2 \cdot \sqrt{\frac{1}{2E_L E_R}} \left[\sqrt{\frac{E_L}{E_R}} + \frac{E_L}{2G_{LR}} - \nu_{LR} \right]^{\frac{1}{2}} \tag{3}$$

On substitution of material constants appropriate for the natural pine wood and the modified pine wood, the following relations between the energy release coefficients $G_{\alpha I}$ and the stress intensity factors $K_{\alpha I}$ are obtained:

• at the TL crack propagation mode:
  - for the natural wood:

$$G_I = 4.26367 \cdot 10^{-9} \cdot K_I^2 \cdot Pa^{-1} \tag{4}$$

  - for the modified wood:

$$G_I = 1.6881 \cdot 10^{-9} \cdot K_I^2 \cdot Pa^{-1} \tag{5}$$

• at the RL crack propagation mode:
  - for the natural mode:

$$G_I = 3.88915 \cdot 10^{-9} \cdot K_I^2 \cdot Pa^{-1} \tag{6}$$

  - for the modified wood:

$$G_I = 1.63856 \cdot 10^{-9} \cdot K_I^2 \cdot Pa^{-1} \tag{7}$$

At the TL mode: $G_{Ic} = 398$ J/m² for the natural wood, and $G_{Ic} = 809$ J/m² for the modified wood, whereas at the RL mode: $G_{Ic} = 384$ J/m² for the natural wood, and $G_{Ic} = 803$ J/m² for the modified wood.

If the relations (4) ÷ (7) are taken into account the critical values of the coefficients K_{Ic} at the TL mode are equal to $K_{Ic} = 305.5$ Pa·m$^{1/2}$ for the natural wood, and $K_{Ic} = 692.3$ Pa·m$^{1/2}$ for the modified wood, whereas at the RL mode $K_{Ic} = 314.2$ Pa·m$^{1/2}$ for the natural wood and $K_{Ic} = 700.0$ Pa·m$^{1/2}$ for the modified wood. On the basis of the literature sources [2, 3] for pine wood at the TL mode the value of the coefficient $K_{Ic} = 430 ÷ 450$ Pa·m$^{1/2}$, whereas at the RL mode: $K_{Ic} = 500$ Pa·m$^{1/2}$. The results obtained for the natural wood demonstrate lower values as compared with those found in the literature sources. This may result from many reasons, one of them may be an origin of such wood which grows on various continents and in various climatic zones. Wood reveals different density and consequently different properties. Moreover used determination methods of critical loads may be different. In present for the determining of values of the critical loads the acoustic emission method is used.

The performed tests on cracking the natural and modified wood showed significant differences in values of the displacement **δ** for the same values of the crack length **a**. The tested modified wood showed smaller values of the displacement than the natural wood. The fracture of the modified wood specimens occurred under loads of geater values than for the natural wood at both the tangential-longitudinal crack propagation mode TL and the radial-longitudinal one, RL. Therefore it results that the wood-polymer composite shows greater fracture toughness than the natural wood.

The displacement values in function of the energy release coefficient for both the crack propagation modes were close to each other. Values of the energy release coefficient were increasing up to the instant of reaching the critical load value and then dropping (Fig. 5 ÷ 8). As results, after reaching the critical value of the energy release coeffcient the integrity losing process has been triggered off in the tested specimens.
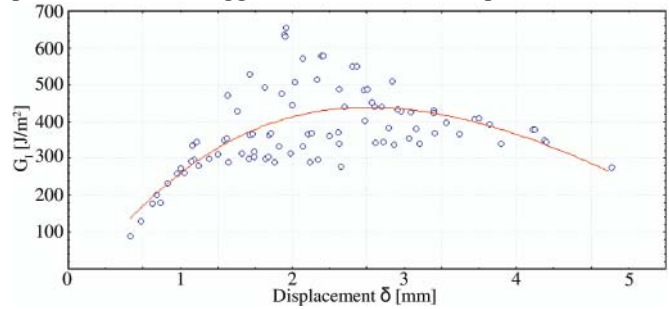
Fig. 5. *The energy release coeffcent in function of the displacement at the TL crack propagation mode (natural wood)*
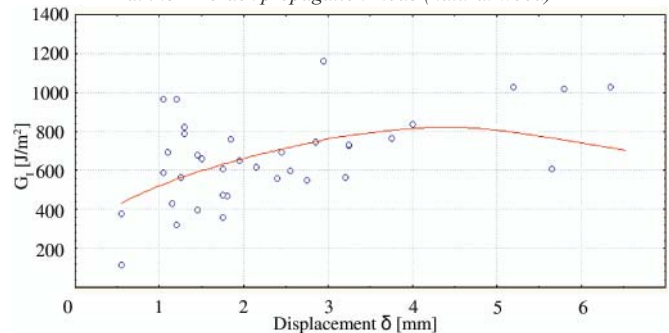
Fig. 6. *The energy release coeffcent in function of the displacement at the TL crack propagation mode (modified wood)*
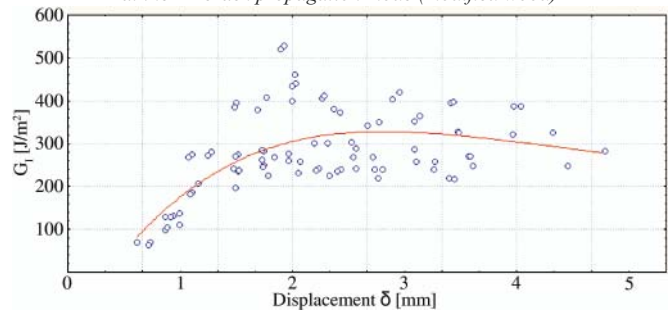
Fig. 7. *The energy release coeffcent in function of the displacement at the RL crack propagation mode (natural wood)*
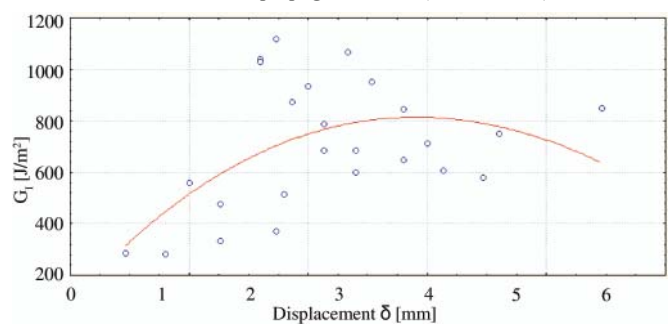
Fig. 8. *The energy release coeffcent in function of the displacement at the RL crack propagation mode (modified wood)*

FINAL CONCLUSIONS

Structural timber being an orthotropic material of different properties in different planes is difficult in testing.

In the performed tests of structural wood the impact of polymer on fracture toughness of the wood-polymer composite was determined as well as the ways of determining the critical load were highlighted. The material integrity loss under the 1st mode load acting perpendicularly to gap plane was discussed in detail.

The performed fracture toughness tests on natural and modified pine wood revealed essential differences in behaviour of the materials under testing. Critical values of the coefficients G_{Ic} and stress intensity factors $K_{\alpha I}$ are deemed the parameters which show how large is fracture toughness of a material. On the basis of the performed tests similar values of the critical coeffcients G_{Ic} were obtained for the both analyzed crack propagation modes (TL and RL). And, the values of the coefficients for the modified wood are more than twice greater than for the natural wood. This confirms the earlier obtained results showing that the modification of wood by means of methyl polymethacrylate greatly improves its strength properties. The values of the displacement δ showed quantitatively that the tested modified wood exhibited smaller displacement values than the natural wood. Fractures of the modified wood occurred under greater load values than in the case of the natural wood both at the tangential - longitudinal crack propagation mode TL and radial-longitudinal one, RL. Therefore it can be concluded that the wood-polymer composite is characterized by a greater fracture toughness than the natural wood.

BIBLIOGRAPHY

1. Kyzioł L.: *Analysis of properties of structural wood of MM polymer- saturated surface* (in Polish). Akademia Marynarki Wojennej (Polish Naval Academy), Gdynia, 2004.
2. Patton-Mallory M., Cramer S.M.: *Fracture Mechanics: A Tool for Predicting Wood Component Strength*. Forest Products Journal, Vol. 37, 1987.
3. Green D. W., Winandy J. E., Kretschman D. E.: *Wood Handbook – Wood as an Engineering Material. Chapter 4. Mechanical Properties of Wood*, U. S. Department of Agriculture, Forest Service, Forest Products Laboratory, Madison, 1999.
4. Debaise G. R., Porter A. W., Pentoney R. E.: *Morphology and Mechanics of Wood Fracture.* Materials Research & Standards, Vol. 6, 1966.
5. Wu E. M.: *Application of Fracture Mechanics to Anisotropic Plates*. Journal of Applied Mechanics, Vol. 34, 1967.
6. Ando H., Ohta M.: *Relationships between the Morphology of Micro-Fractures of Wood and the Acoustic Emission Characteristics*. Mokuzai Gakkaishi, Vol. 41, 1995.
7. Kossakowski P.: *Fracture Toughness of Wood.* 2nd International Conference, Fracture Mechanics of Materials and Structural Integrity, Lviv, 1999.
8. Kossakowski P.: *Fracture toughness of wood* (in Polish). VII Krajowa Konferencja Mechaniki Pękania (7th National Conference on Fracture Mechanics), Kielce/Cedzyna, 1999.

CONTACT WITH THE AUTHOR

Lesław Kyzioł, Ph.D.
Faculty of Mechanical and Electrical Engineering
Institute of Basic Engineering
Polish Naval Academy in Gdynia
Śmidowicza 69
81-103 Gdynia, POLAND
e-mail: L.Kyziol@amw.gdynia.pl

Identification of hydroacoustic wave sources of ship in motion

Eugeniusz Kozaczka, Prof.
Gdansk University of Technology
Naval Academy of Gdynia
University of Technology and Life Sciences in Bydgoszcz
Jacek Domagalski, Ph. D.
Naval Academy of Gdynia

ABSTRACT

This paper deals with results of identification tests of acoustic field spectrum of underwater noise generated by ship in motion. The field is connected with acoustic activity of ship mechanisms and devices in operation. Vibration energy generated by the mechanisms and devices is transferred through ship structural elements to surrounding water where it propagates in the form of acoustic waves of a broad band of frequencies. In the publication results of identification tests of underwater noise generated by a ship in motion, are presented.

Keywords: Identification; propagation; hydroacoustics

INTRODUCTION

Every new-built naval ship, after capital repair or modernization work, is subjected to a series of complex tests carried out in testing and measuring trial areas of Polish Navy. In the frame of the tests, a.o., measurements of underwater noise generated by ships are conducted both in stationary and dynamic trial areas. The results of identification of acoustic wave sources, obtained from the tests performed in a stationary trial area have been presented in the previous publication [7, 8, 9, 10].

After the measurements carried out in the stationary trial area, were made measurements of underwater noise generated by a ship in motion. The tests were aimed at confirming the results of identification of acoustic wave sources determined in the stationary trial area (i.e. main engines, ship propellers, shaft lines, electric generating sets), as well as at determining theoretical relationships on the basis of which it would be possible to present frequencies of waves generated by propulsion systems operating at different ship speeds. The below presented results were obtained from the above mentioned complex tests of the ship. During the tests, hydroacoustic field measurements for all operational settings of propulsion systems, were performed. During its service a ship under testing crosses the control and measurement areas about once per two months. Since the complex measurements taken in 2004, the ship in question crossed the ranges 147 times (33 measurements recorded during the complex measurement tests and 114 control tests in service). Hence a vast body of information about noise emitted by the ship to surrounding water, has been collected in archives. In view of the rich amount of data obtained from the tests, only representative results are published in this paper.

During the hydroacoustic tests ships cross twice (with course angle: 180° and 0°) the measurement trial area at set operational parameters of their propulsion systems. The set ship parameters are reached at the distance of 300 m at least before the trial area and maintained over the distance of 600 m at least (300 m behind the buoys). Most data were recorded by a hydrophone located 1 m over the sea bed. The continuous recording of acoustic pressure measurements is made at a distance afore and astern the ship. The information obtained this way makes it possible to characterize underwater disturbances around the ship. In Fig. 1 is shown a schematic picture of the facility for hydroacoustic field control and measurements.

To compare results obtained from measurements performed in dynamic and stationary trial areas the common diagram of the spectra recorded during the trials was prepared as shown in Fig. 2.

As can be clearly observed in the presented spectra, both the noise records are quite similar in the frequency band up to 100 [Hz]. In this range the underwater noise records were analyzed in detail and compared to each other.

The signals recorded in the trial areas were processed with the use of PULS software. They were appropriately modified by using EXEL calculation sheet to make their presentation more clear. The spectra obtained from the tests are presented in Fig. 3. In the spectra can be observed a series of excitations which repeated during the tests of ship engines both under load and idle running.
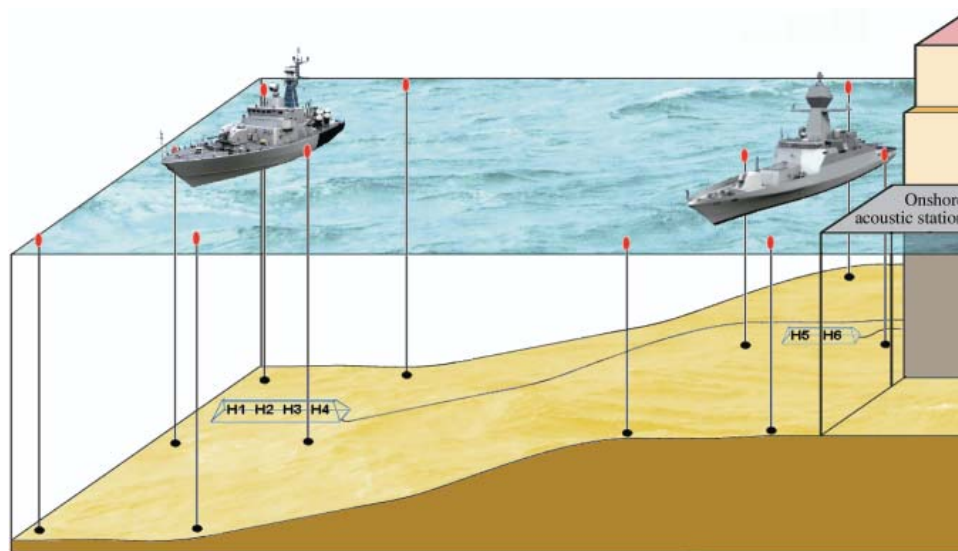
Fig. 1. *Schematic picture of a movable trial facility for underwater measurement of acoustic disturbances generated by ship in motion, where: H1, H2,... H6 – hydrophones*
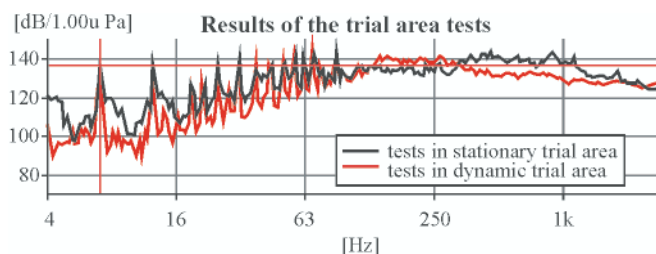
Fig. 2. *Acoustic pressure spectra recorded during the tests in dynamic and stationary trial areas*
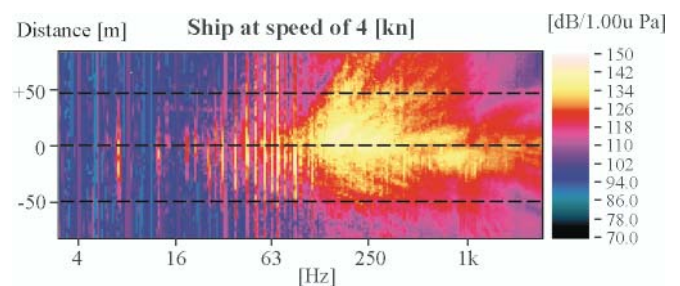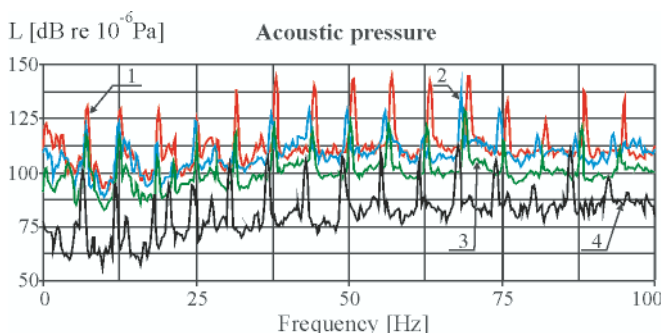
Fig. 3. *Underwater noise spectra of the tested ship. Signals recorded at the main engine speed n = 750 [rpm].* **Notation: 1.** *the underwater noise spectrum. Tests in stationary trial area (two engines under operation),* **2.** *the underwater noise spectrum (signal suppressed by 10[dB]). Tests in stationary trial area (left engine under operation),* **3.** *the underwater noise spectrum (signal suppressed by 20[dB]). Tests in stationary trial area (right engine under operation),* **4.** *the underwater noise spectrum (signal suppressed by 30[dB]). Tests in dynamic trial area (two engines under operation)*

When comparing the tests of acoustic field structure of the ship in motion with those performed in standstill it can be observed that in the band up to about 100 [Hz] the noise records are relatively similar.

The identifying was initiated from the analysis of acoustic fiel structure of the ship moving with 4-knot speed. Fig. 4 presents the spectrogram containing changes in acoustic pressure level and distance covered by the ship in function of frequency. The spectrogram is composed of 299 spectra recorded every 312 [ms], at 1/24 octave resolution in the frequency band from 3 [Hz] to 2.818 [kHz]. The dashed lines mark distances from the ship to the acoustic sensor.

Two distinct zones are seen in the spectrogram. The first zone contains frequencies up to about 100 [Hz]. In the zone

Fig. 4. *Acoustic field spectrogram of the ship moving at speed of 4 knots*

characteristic components resulting from operation of ship mechanisms can be distinguished. The second zone from 100 [Hz] to 2.8 [kHz] contains the continuous spectrum. The spectrum is associated with operation of cavitating screw propeller, turbulent flow through pipelines, water flow around the hull, air flow through fans etc.

To identify in detail the characteristic spectral components appearing in the first zone a spectrogram was prepared with the use of the same filters and settings which were applied during the ship's tests in the stationary trial area. The applied software (as well as the analyzer internal memory) made it possible to record 98.6 s - time interval of underwater noise of the ship crossing the trial area. The recording time interval made it possible to examine changes in hydroacoustic field of the ship over the distance of about 100 m before and behind the trial area.
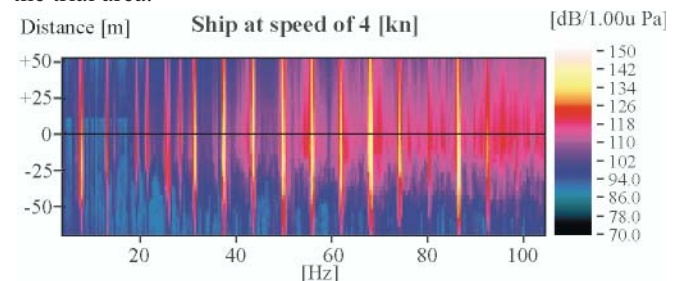
Fig. 5. *Acoustic field spectrogram of the ship moving at speed of 4 knots*

The spectrogram is consisted of 74 spectra recorded every 1.333 [s] with 0.25Hz – resolution in the band up to 100 [Hz]. From the figure was selected the spectrum when the ship's engine room was just over the acoustic sensor (the place is distinguished with black line on the spectrogram).
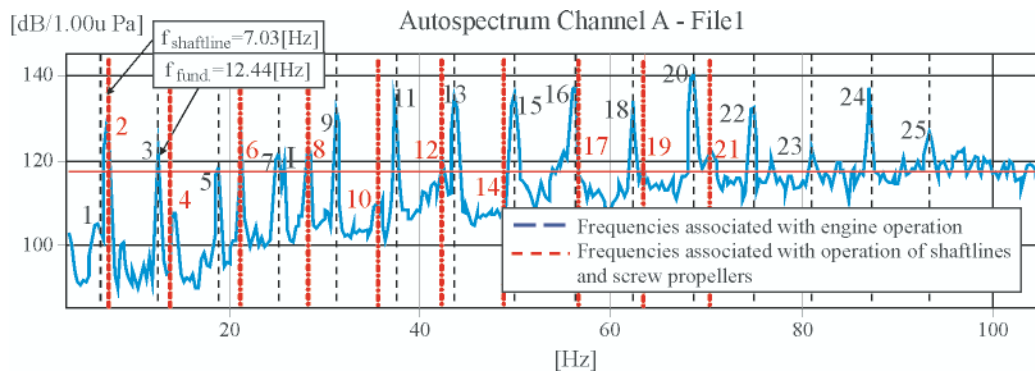
Fig. 6. *The acoustic field spectrum of the ship, prepared for the distance „0" marked in the spectrogram of Fig. 5*

In the figure are clearly seen the characteristic components resulting from operation of the main engines, shaft lines and screw propellers, as well as the single red stripe numbered „I" resulting form operation of the electric generating set. Each of the characteristic components is distinguished by a successive number whose green digits stand for components due to operation of the screw propellers and shaft lines, and black digits represent components due to operation of the main engines. The characteristic spectral components are additionally marked with dashed lines as follows: those in blue show frequencies associated with operation of the main engines, and those in black – frequencies associated with operation of the shaft lines and screw propellers.

As observed on the basis of the performed trials the frequencies associated with operation of the propulsion systems can be determined from the following relationships:

1. Frequencies associated with combustion process occurring in main engine cylinders:
   - fundamental frequencies of firing in particular cylinders of engines:
     $f_{z1} = f_o \cdot s$ - fundamental frequency of firing in one cylinder,
     $f_{z2} = 2f_o \cdot s$ - fundamental frequency of firing in two cylinders,
     $f_{z3} = 3f_o \cdot s$ - fundamental frequency of firing in three cylinders,
     ....
     $f_z = f_{z6} = 6f_o \cdot s$ - frequency of firing in six cylinders.

   - 2nd harmonic frequencies of firing in engine cylinders:
     $f_{IIz1} = f_{z1} + f_z$ - 2nd harmonic frequency of firing in one cylinder,
     $f_{IIz2} = f_{z2} + f_z$ - 2nd harmonic frequency of firing in two cylinders,
     $f_{IIz3} = f_{z3} + f_z$ - 2nd harmonic frequency of firing in three cylinders,
     ....
     $f_{IIz6} = 2f_z$ - 2nd harmonic frequency of firing in six cylinders,

   - 3rd harmonic frequencies of firing in engine cylinders:
     $f_{IIIz1} = f_{z1} + 2f_z$ - 3rd harmonic frequency of firing in one cylinder,
     $f_{IIIz2} = f_{z2} + 2f_z$ - 3rd harmonic frequency of firing in two cylinders,
     $f_{IIIz3} = f_{z3} + 2f_z$ - 3rd harmonic frequency of firing in three cylinders,
     ....
     $f_{IIIz6} = 3f_z$ - 3rd harmonic frequency of firing in six cylinders.

2. Frequencies associated with rotation of screw propellers:
   $f_{ś1} = f_o/1.77$ - fundamental frequency due to operation of one blade of screw propeller,
   $f_{ś2} = 2f_o/1.77$ - fundamental frequency due to operation of two blades of screw propeller,
   ....
   $f_ś = 4f_o/1.77$ - fundamental frequency due to operation of screw propeller.

   - 2nd harmonic frequencies associated with operation of screw propellers:
     $f_{IIś1} = f_o/1.77 + f_ś$ - 2nd harmonic frequency due to operation of one blade of screw propeller,
     $f_{IIś2} = 2f_o/1.77 + f_ś$ - 2nd harmonic frequency due to operation of two blades of screw propeller,
     ....
     $f_{IIś} = 4f_o/1.77 + f_ś$ - 2nd harmonic frequency due to operation of screw propeller,

   - 3rd harmonic frequencies associated with operation of screw propellers:
     $f_{IIIś1} = f_o/1.77 + f_{IIś}$ - 3rd harmonic frequency due to operation of one blade of screw propeller,
     $f_{IIIś2} = 2f_o/1.77 + f_{IIś}$ - 3rd harmonic frequency due to operation of two blades of screw propeller,
     ....
     $f_{IIIś} = 4f_o/1.77 + f_{IIś}$ - 3rd harmonic frequency due to operation of screw propeller.

3. Frequencies associated with rotation of shaft lines:
   $f_{LW1} = f_o/(2 * 1.77)$ - fundamental frequency due to rotation of shaft lines,
   $f_{LW2} = 2f_o/(2 * 1.77)$ - 2nd harmonic frequency due to rotation of shaft lines,
   $f_{LW3} = 3f_o/(2 * 1.77)$ - 3rd harmonic frequency due to rotation of shaft lines,
   $f_{LW4} = 4f_o/(2 * 1.77)$ - 4th harmonic frequency due to rotation of shaft lines;

where:
f_o – the fundamental frequency $f_o = n/60$,
n – number of rotations per one minute, [rpm],
s – stroke factor (0.5 – for four stroke engine),
1.77 – reduction ratio of ship reduction gear.

The calculation results obtained from the above given relationships are presented in Tab. 1.

The fundamental frequency resulting from unbalanced rotating elements of the main engines, $f_o = 12.44$ [Hz], was determined with the use of B&K PULSELABSHOP software. In an anlogous way were determined fundamental frequencies and their harmonics resulting from rotation of shaft lines ($f_{shaftline} = 7.03$[Hz]).

No.	f [Hz]	Frequencies of hydroacoustic wave sources
1.	6.00	Fundamental frequency of main engine firing (due to operation of one cylinder).
2.	7.00	Fundamental frequency due to rotation of shaft lines. Fundamental frequency due to operation of one blade of screw propellers
3.	12.50	Fundamental frequency of main engine firing (due to operation of two cylinders).
4.	14.00	2nd harmonic frequency due to rotation of shaft lines. Fundamental frequency due to operation of two blades of screw propellers.
5.	18.75	Fundamental frequency of main engine firing (due to operation of three cylinders).
6.	21.00	3rd harmonic frequency due to rotation of shaft lines. Fundamental frequency due to operation of three blades of screw propellers.
7.	25.00	Fundamental frequency of main engine firing (due to operation of four cylinders).
I.	25.25	Fundamental frequency due to rotation of electric generating set
8.	28.00	Fundamental frequency due to operation of four blades of screw propellers.
9.	31.00	Fundamental frequency of main engine firing (due to operation of five cylinders).
10.	35.25	2nd harmonic frequency due to operation of single blades of screw propellers
11.	37.25	Fundamental frequency of main engine firing (due to operation of six cylinders).
12.	42.25	2nd harmonic frequency due to operation of two blades of screw propellers
13.	43.50	2nd harmonic frequency of main engine firing (due to operation of one cylinder).
14.	49.25	2nd harmonic frequency due to operation of three blades of screw propellers.
15.	49.75	2nd harmonic frequency of main engine firing (due to operation of two cylinders).
16.	56.00	2nd harmonic frequency of main engine firing (due to operation of three cylinders).
17.	56.25	2nd harmonic frequency due to operation of two blades of screw propellers.
18.	62.00	2nd harmonic frequency of main engine firing (due to operation of four cylinders).
19.	63.25	2nd harmonic frequency due to operation of three blades of screw propellers.
20.	68.50	2nd harmonic frequency of main engine firing (due to operation of five cylinders).
21.	70.25	2nd harmonic frequency due to operation of four blades of screw propellers.
22.	74.75	2nd harmonic frequency of main engine firing (due to operation of six cylinders).
23.	81.00	3rd harmonic frequency of main engine firing (due to operation of one cylinder).
24.	87.00	3rd harmonic frequency of main engine firing (due to operation of two cylinders).
25.	93.25	3rd harmonic frequency of main engine firing (due to operation of three cylinders).

The frequencies of sources of waves being components of acoustic field structure of the ship in question, presented in Fig. 5, were unambiguously attributed to ship's mechanisms and devices under operation. Results of the tests showed that to identify, in water environment, waves resulting from propulsion system operation, in the frequency band up to 100 [Hz], is possible. The frequencies presented in Tab. 1 are in compliance with the theoretical relationships and measurement results obtained from the tests of the ship in the stationary trial area.

The insignificant differences in the particular frequencies of acoustic wave sources are caused by a little different rotational speeds of main engines. During the measurements the speeds was varying within the range from about 745 to about 760 [rpm].

The frequencies of operation of shaft lines and screw propellers obtained from the dynamic tests are also comparable with those obtained from the tests in the stationary trial area. The results are compared in Tab. 4.

Tab. 2. Set of frequencies obtained from the tests conducted both in stationary and dynamic trial area

Tests conducted in:	Frequencies due to operation of main engine at the rotational speed n = 750 [rpm] [Hz]			
	Left main engine $f_{fund.}$=12.43 [Hz] (right M.E. -stopped)	Right main engine $f_{fund.}$=12.68 [Hz] (left M.E. -stopped)	Left main engine $f_{fund.}$=12.53 [Hz]	Right main engine $f_{fund.}$=12.57 [Hz]
	One propulsion system under operation		Two propulsion systems under operation	
the stationary trial area	12.50, 18.75, 24.75, 31.00, 37.75, 43.50, 49.75, 56.00, 62.25, 68.25, 74.50, 80.75, 87.00, 93.25, 99.50.	12.75, 19.00, 25.25, 31.75, 38.00, 44.25, 50.50, 57.00, 63.25, 69.50, 76.00, 82.25, 88.50, 95.00.	12.50, 18.75, 25.00, 31.25, 37.50, 43.75, 50.25, 56.50, 62.75, 69.00, 75.25, 81.50, 87.75, 94.00.	12.50, 18.75, 25.00, 31.50, 37.75, 44.00, 50.50, 56.75, 63.00, 69.25, 75.50, 81.75, 88.00, 94.25.
the dynamic trial area	6.00, 12.50, 18.75, 25.00, 31.00, 37.25, 43.50, 49.75, 56.00, 62, 68.5, 74.75 81.00, 87.00, 93.25.			

Tab. 3. Set of frequencies obtained from the trial area tests and theoretical relationships

Source of hydroacoustic waves	Frequencies of hydrodynamic waves	
	obtained from the tests in dynamic trial area	calculated by using the presented theoretical relationships
Main engines	6.00, 12.50, 18.75, 25.00, 31.00, 37.25, 43.50, 49.75, 56.00, 62.00, 68.50, 74.75, 81.00, 87.00, 93.25.	6.22, 12.44, 18.66, 24.88, 31.10, 37.32, 43.54, 49.76, 55.98, 62.20, 68.42, 74.64, 80.86, 87.08, 93.30.
Ship screw propeller and shaftline	7.00, 14.00, 21.00, 28.00, 35.25, 42.25, 49.25, 56.25, 63.25, 70.25.	7.03, 14.07, 21.10, 28.14, 35.17, 42.20, 49.24, 56.27, 63.31, 70.34.

Tab. 4. Set of frequencies obtained from the tests conducted in dynamic trial area and standstill

Tests conducted in:	Frequencies due to operation of shaft lines and screw propellers at the main engines' rotational speed n = 750 [rpm] [Hz]			
	One propulsion system under operation		Two propulsion systems under operation	
	Left main engine (Right M.E. -stopped)	Right main engine (Left M.E. -stopped)	Left main engine	Right main engine
the stationary trial area	Fundamental frequencies of shaft lines and screw propellers			
	7.00, 28.50.	7.25, 28.50.	7.00, 28.50.	7.00, 28.50.
the dynamic trial area	7.00, 14.00, 21.00, 28.00, 35.25, 42.25, 49.25, 56.25, 63.25, 70.25.			

The presented results of the tests made both in the dynamic and stationary trial area for the rotational speed of main engines, n = 750 [rpm] in the band up to 100 [Hz] showed that to identify the sources of waves in water environment is possible.

Identification of acoustic field structure of a ship on which two main engines operate at near rotational speeds but so much different that the characteristic components generated by left and right engine can be detected in the frequency spectrum, is a very complex problem. Occurrence of the components could be observed during the testing of acoustic field structure of the ship propelled by two main engines under operation at the rotational speed n = 950 [rpm], and the propeller settings of 2°, 2.5°and 4.5°.

The ship with the above mentioned settings of its propeller developed the speed of 6, 8, 12 [kn], respectively. The spectrograms achieved during the tests are presented in Fig. 7.

When the ship was passing just over the sensors (the places distinguished by black lines in the spectrograms) the underwater noise spectra presented in Fig. 8, were recorded.

In the above presented figure the spectrum at the ship's speed of 8 [kn] was suppressed by 30 [dB], and that at the speed of 12 [kn] - by 60 [dB], in order to make their presentation more clear. The characteristic spectral components resulting from operating propulsion systems and electric generating sets appear at the same frequencies. From the analysis

were obtained exact values of the fundamental frequencies associated with rotation of unbalanced movable elements of engines. The fundamental frequency of the left engine was: $f_{fund.}$ = 15.49 [Hz] (929 [rpm]), and that of the right engine: $f_{fund.}$ = 15.78 [Hz] (947 [rpm]). Knowing rotational speed of the engines one can easily determine the remaining frequencies due to operation of the propulsion systems. Onto the spectra were introduced cursors - in black (for right engine) and in blue (for left engine) – associated with fuel oil combustion in the engines, as well as those in red – associated with operation of the screw propeller and shaft lines. In the spectra, above 30 [Hz] frequency, one can observed double components reflecting differences in rotational speeds of the main engines to appear. To each component a successive number was attributed. The set of the excitations is presented together with their description in Tab. 5.

The tests performed on the ship moving at the speed v = 6, 8, 12 [kn] in the dynamic trial area demonstrated that to identify, in water environment, acoustic waves resulting from operation of right and left propulsion system, is possible. The frequencies of sources of acoustic waves, experimentally obtained from the tests in the trial area, (Tab. 6), are in compliance with those calculated by using the theoretical relationships.

Tab. 5. Set of results obtained from the tests of the ship moving at the speed v = 6, 8 and 12 [kn], respectively, in dynamic trial area

No.	f [Hz]	Frequencies of sources of hydroacoustic waves
1.	8.00	Fundamental frequency of main engine firing (due to operation of single cylinder of right and left engine).
2.	8.75	Fundamental frequency of rotating shaft lines. Fundamental frequency of operation of single screw propeller blade.
3.	15.75	Fundamental frequency of main engine firing (due to operation of two cylinders of right and left engine).
4.	17.50	2nd harmonic frequency of rotating shaft lines. Fundamental frequency of operation of two screw propeller blades
5.	23.25	Fundamental frequency of main engine firing (due to operation of three cylinders of right and left engine).
I	25.25	Fundamental frequency of electric generating set
6.	26.25	3rd harmonic frequency of rotating shaft lines – left propulsion system. Fundamental frequency of operation of three screw propeller blades – left propulsion system.
7.	26.50	3rd harmonic frequency of rotating shaft lines – right propulsion system. Fundamental frequency of operation of three screw propeller blades – right propulsion system.
8.	31.25	Fundamental frequency of main engine firing (due to operation of four cylinders of left engine).
9.	31.50	Fundamental frequency of main engine firing (due to operation of four cylinders of right engine).
10.	35.00	Fundamental frequency of operation of four screw propeller blades – left propulsion system.
11.	35.50	Fundamental frequency of operation of four screw propeller blades – right propulsion system.
12.	38.75	Fundamental frequency of main engine firing (due to operation of five cylinders of left engine).
13.	39.50	Fundamental frequency of main engine firing (due to operation of five cylinders of right engine).
14.	46.50	Fundamental frequency of main engine firing (due to operation of six cylinders of left engine).
15.	47.25	Fundamental frequency of main engine firing (due to operation of six cylinders of right engine).
II	50.25	2nd harmonic frequency of electric generating set and supply network
16.	54.25	2nd harmonic frequency of main engine firing (due to operation of single cylinder of left engine).
17.	55.25	2nd harmonic frequency of main engine firing (due to operation of six cylinders of right engine).
18.	62.00	2nd harmonic frequency of main engine firing (due to operation of six cylinders of left engine).
19.	63.00	2nd harmonic frequency of main engine firing (due to operation of two cylinders of right engine).
20.	69.75	2nd harmonic frequency of main engine firing (due to operation of three cylinders of left engine).
21.	71.00	2nd harmonic frequency of main engine firing (due to operation of three cylinders of right engine).
23.	78.75	2nd harmonic frequency of main engine firing (due to operation of four cylinders of right engine).
24.	85.25	2nd harmonic frequency of main engine firing (due to operation of five cylinders of left engine).
25.	86.75	2nd harmonic frequency of main engine firing (due to operation of five cylinders of right engine).
26.	93.00	2nd harmonic frequency of main engine firing (due to operation of six cylinders of left engine).
27.	94.50	2nd harmonic frequency of main engine firing (due to operation of six cylinders of right engine).
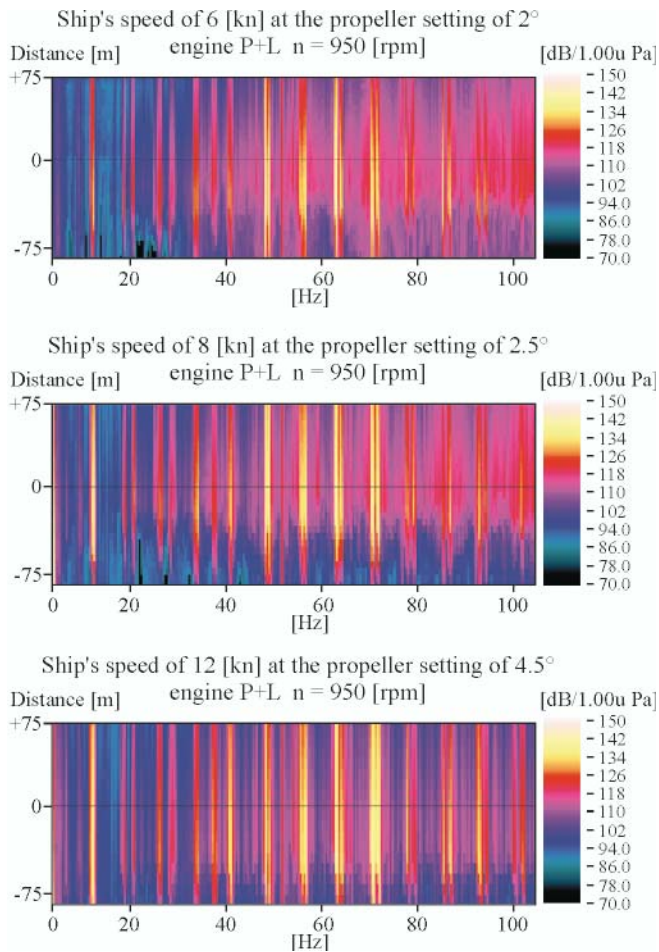
Fig. 7. Spectrograms achieved during the tests in dynamic trial area, at the rotational speed of main engines n = 950 [rpm] and the propeller setting of 2°, 2.5° and 4.5°, respectively

CONCLUSIONS

- As has been demonstrated in this publication, to identify hydroacoustic waves associated with operation of ship propulsion systems and auxiliary mechanisms is possible also in shallow water.
- The comprehensive tests conducted in measurement trial areas (both movable and stationary) demonstrated that on the basis of underwater noise measurements it is generally possible to identify, in ship hydroacoustic field structure, its characteristic components associated with operation of main engines, shaft lines and screw propellers as well as those resulting from operation of electric generating sets.
- The used identification method of hydroacoustic waves, consisting in simultaneous measuring vibrations and acoustic pressure, has made it possible to exactly determine frequencies of the waves. Knowing the frequencies appearing in the considered band up to 100 [Hz] one is able to unambiguously attribute them to a given propulsion system, and on this basis to determine type of a considered ship.
- The elaborated theoretical relationships have been confirmed by the results of the tests. Differences between the experimentally obtained results and those calculated by using the given relationships have not exceeded 0.25 [Hz], it means that the determined error has been contained in the frequency band of the filters applied to processing the signals.
- In the future a series of comprehensive tests should be performed with the aim of determining maximum distances at which identification of particular ships would be still possible. The tests should be conducted in a coastal acoustic station both in various sea state conditions and various noise levels of hydroacoustic background, and also in trial areas located in Gdansk Bay at various water depths.
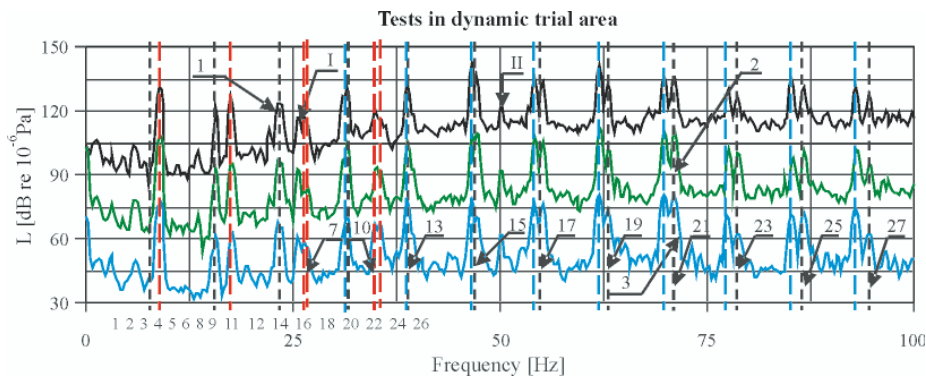
Fig. 8. Underwater noise spectra recorded during the tests in dynamic trial area at the rotational speed of main engines n = 950 [rpm].
Notation: 1. the tests made at the ship's speed v = 6 [kn] and the propeller setting of 2°, 2. the tests made at the ship's speed v = 8 [kn] and the propeller setting of 2.5° (signal suppressed by 30 [dB]), 3. the tests made at the ship's speed v = 12 [kn] and the propeller setting of 4.5° (signal suppressed by 60 [dB]

Tab. 6. Set of frequencies obtained from the trial area tests and theoretical relationships

Source of hydroacoustic waves	Frequencies of hydroacoustic waves	
	obtained from the tests in dynamic trial area	calculated by using the presented theoretical relationships
Right main engine	8.00, 15.75, 23.50, 31.50, 39.50, 47.25, 55.25, 63.00, 71.00, 78.75, 86.75, 94.50.	7.89, 15.78, 23.67, 31.56, 39.45, 47.34, 55.23, 63.12, 71.01, 78.90, 86.79, 94.68.
Left main engine	8.00, 15.75, 23.50, 31.25, 38.75, 46.50, 54.25. 62.00, 69.75, 77.50, 85.25, 93.00.	7.75, 15.49, 23.24, 30.98, 38.73, 46.47, 54.22, 61.96, 69,71, 77.45, 85.20, 92.94.
Screw propeller and right shaftline	8,75, 17.50, 26.50, 35.50.	8.92, 17.84, 26.76, 35.68.
Screw propeller and left shaftline	8,75, 17.50, 26.25, 35.00.	8.76, 17.51, 26.27, 35.03.

BIBLIOGRAPHY

1. Baranowska A Gloza I.: *Identification of underwater disturbance sources by using coherence functions* (in Polish). Materials of 48ᵗʰ Open Seminar on Acoustics, pp.245÷250, Wrocław 2001.
2. Gloza I., Malinowski S.: *Identification of ships underwater noise sources in the coastal region*. Hydroacoustics, Vol. 5/6, 9-16, 2003.
3. Gloza I., Domagalski J., Malinowski S.: *Identification of ships hydro-acoustic field sources in the near surrounding (in Polish)*, Materials of 49 ᵗʰ Open Seminar on Acoustics, pp. 407-412, Warszawa - Stare Jabłonki 2002.
4. Grelowska G., Bittner P., Gloza I.: *Experimental tests of noise generated by ship in motion* (in Polish). Materials of 9ᵗʰ Seminar on Hydro-acoustics, pp. 125-132, Gdynia-Jurata, 1992.
6. R. J. Urick: *Principles of Underwater Sound*, Mc Graw – Hill, New York 1975
7. Kozaczka E., Domagalski J., Gloza I.: *Investigation of the underwater noise produced by ships by means of intensity method,* Polish Maritime Research No 3(66) 2010 Vol 17
8. E. Kozaczka, I. Gloza, *Measurement of underwater noise produced by means of the intensity method*, Proceedings of EURONOISE 2009, Edinburgh, UK, 26-28 October 2009
9. E. Kozaczka, I. Gloza, *Determination of the ship signature in the very shallow water*, Proceedings of the 14th International Congress on Sound and Vibration, Cairns, 9-12 July 2007, 6 pp., CD
10. E. Kozaczka, G. Grelowska, *Shipping noise*, Archives of Acoustics vol. 29, 2, 169-176, (2004)
11. E. Kozaczka, S. Kozaczka, *Classification of underwater objects by means of an acoustic method*, Proceedings of the 13th International Congress on Sound and Vibration, Vienna, Austria, 2-6 July 2006

RESEARCH REPORTS

1. Kozaczka E, Kiciński W., Milanowski W.: *Identification tests of acoustic signals emitted into water environment, Stage II* Gdynia 1993.
2. Kozaczka E., Grelowska G., Bittner P., Baranowska A.,: *Experimental tests of ship hydro-acoustic field, Stage III* Gdynia 1993.
3. Kozaczka E., Grelowska G., Bittner P., Baranowska A., Kiciński W., Milanowski W.: *Spatial distribution of underwater noise emitted by ships to hemisphere, and its normalization* Gdynia 1997.
4. Kozaczka E., Grelowska G., Bittner P., Baranowska A., Milanowski W., Dobrzaniecki J.: *Spatial distribution of underwater noise emitted by ships to hemisphere, Stage II*, Gdynia 1992.
5. Kozaczka E., Grelowska G., Gloza I., Dobrzaniecki J., Przysowa T.: *Passive acoustic observation of coastal zone with the use of broad-band acoustic characteristics of ships*, Gdynia 1997.
6. Kozaczka E., Kiciński W., Nyszko G.: *Identification tests of acoustic signals emitted into water environment, Stage II* Gdynia 1995
7. Kozaczka E., Kiciński W., Nyszko G.: *Identification tests of acoustic signals emitted into water environment, Stage IV* Gdynia 1995.

CONTACT WITH THE AUTHORS

Eugeniusz Kozaczka, Prof.,
Faculty of Ocean Engineering
and Ship Technology
Gdansk University of Technology
Narutowicza 11/12
80-233 Gdansk, POLAND
fax: (058) 347-21-81,
e-mail: kozaczka@pg.gda.pl

Jacek Domagalski, Ph. D.
Faculty of Navigation and Naval Waeapons,
Polish Naval Academy
Śmidowicza 69
81-103 Gdynia POLAND

Bayesian methods in reliability of search and rescue action

Zbigniew Burciu, Assoc. Prof.
Gdynia Maritime University

ABSTRACT

This paper concerns the application of bayesian network to planning and monitoring life saving actions at sea. The presented bayesian network was formed a.o. on the basis of the determined life raft safety function. The proposed bayesian network makes it possible to determine reliability of conducted life saving action, with accounting for a large number of events which influence course of the action. Reliability control was proposed to be applied to search and rescue - SAR action in contrast to risk control. Reliability levels were defined to make the assessing of safety of conducted SAR action, possible.

Keywords: coordinator, SAR action, reliability, Bayesian network

INTRODUCTION

Life saving actions at sea constitute suitably coordinated operations undertaken with the use of avaliable forces and means necessary to provide effective help to people being in potential or real danger at sea. Success of such action is decided first of all by its appropriate coordination defined as an ordered action aimed at providing help to people in distress at sea.

Plannning and executing the action is carried out on the basis of limited information. Presently is observed a general trend of implementing the decision-aiding systems aimed at improving safety in sea shipping. The bayesian network proposed in this paper is a tool which may serve as an element of a decision- aiding system for SAR-action coordinator.

DESCRIPTION OF BAYESIAN NETWORK OF SAR ACTION

The operational reliability of SAR action, (R_{SAR}), is the reliability of executors, subjects and elements of the action, measured by the probability of task realization within a given time interval Δt or given hydrometeorological conditions – wind velocity [3, 4, 5].

General assumptions of bayesian methods [8]:
- by making use of Bayes theorem, results of observations are combined with a priori information by using which a posteriori distribution of an estimated parameter can be obtained,
- decision concerning choice of an estimator for a parameter in question is made in such a way as to make expected losses resulting from the decision as small as possible:

$$P(A_i \mid B) = \frac{P(A_i)P(B \mid A_i)}{\sum\limits_{i=1}^{n} P(A_i)P(B \mid A_i)}$$

where:
A – original event
B – secondary event

The Bayes theorem enables the action coordinator to combine a priori information with results of past SAR actions. The SAR action coordinator having experience and skill acquired from SAR actions previously coordinated by him, is equipped with knowledge necessary for estimating probability of such action elements which change the values have been so far at hand.

The tests performed by the CTO [2, 12] and Aeronautical Institute [2, 13] made it possible to determine the wind leeway [2], and safety function – the life raft reliability R_{tr} [5, 6].

$$R(x) = P_r\{Z_{tr} > x\} \tag{1}$$

The safety function – life raft reliability [5, 6] is as follows:

$$R(x) = P(Z_{tr} > x) = 1 - \int\limits_{0}^{x} f_Z(z)\,dz =$$

$$= 1 - \frac{\lambda_1^{\alpha_1}\lambda_2^{\alpha_2}}{3^{\alpha_1}2^{\alpha_2}B(\alpha_1,\alpha_2)} \int\limits_{0}^{x} \frac{z^{\alpha_2-1}}{(\frac{\lambda_1}{3}+\frac{\lambda_2}{2}z)^{\alpha_1+\alpha_2}}\,dz \quad z > 0 \tag{2}$$

where:
$R(x)$ – life raft reliability, safety function
Z_{tr} – maximum value of life raft speed (wind leeway),

x – wind velocity,
y – speed of life raft expressed numerically,
a, b – mean values of the independent non-negative random variables A, B
A – random variable of the gamma distribution $G(\alpha_1, \lambda_1)$
B – random variable of the gamma distribution $G(\alpha_2, \lambda_2)$

The reliability function values determined from Eq. (2) are presented in Tab. 1.

Tab. 1. Values of the reliability function for 6-person life raft [5, 6]

Wind velocity x [kn]	Life raft without drift anchor 6-1 pers.	Life raft without drift anchor 6-6 pers.	Life raft with drift anchor 6-1 pers.	Life raft with drift anchor 6-6 pers.
	R(x)	R(x)	R(x)	R(x)
40	0.999996	0.9999999	0.99998	0.9999999997
44	0.9991	0.9999997	0.9982	0.9999997
48	0.9712	0.99992	0.9546	0.9998
52	0.7785	0.9962	0.7122	0.9943
56	0.3895	0.9474	0.3128	0.9311
60	0.1046	0.7405	0.0717	0.6947
64	0.0151	0.3945	0.0088	0.3434
68	0.0012	0.1304	0.0006	0.1037
72	0.00006	0.0267	0.00003	0.0193
76	2.23971×10^{-6}	0.0035	8.1781×10^{-7}	0.0023

The survival probability of object in water, $S_p(t)$, is presented in Fig. 1.
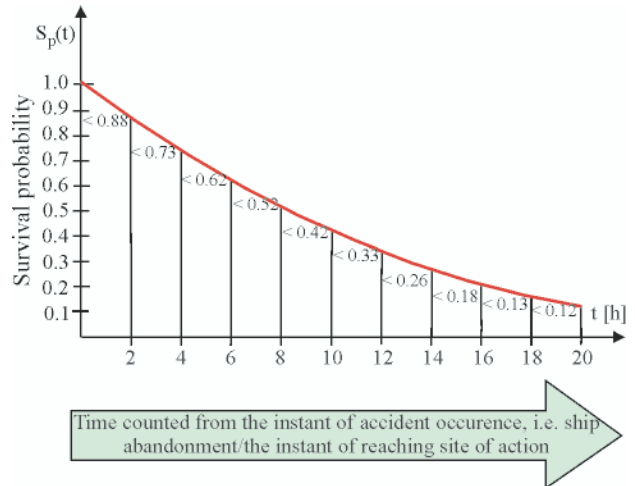
Fig. 1. The survival probability of object in water, $S_p(t)$, in function of time, at 20°C water temperature, elaborated acc. [1]

$$S_p(t) = e^{-0.1654\,t^{1.3213}\,e^{-0.071 \cdot tw}}$$

where:
tw – water temperature

The defined parameters $R_{(x)}$, $S_p(t)$ independent of coordinator of SAR action make it possible to form a bayesian network.

The determined reliability parameters of particular elements of SAR action system enable to perform reliability analysis of SAR action by using the bayesian network.

The bayesian network for one search ship and one searched for object, elaborated with the use of Hugin Program, v. 7.3
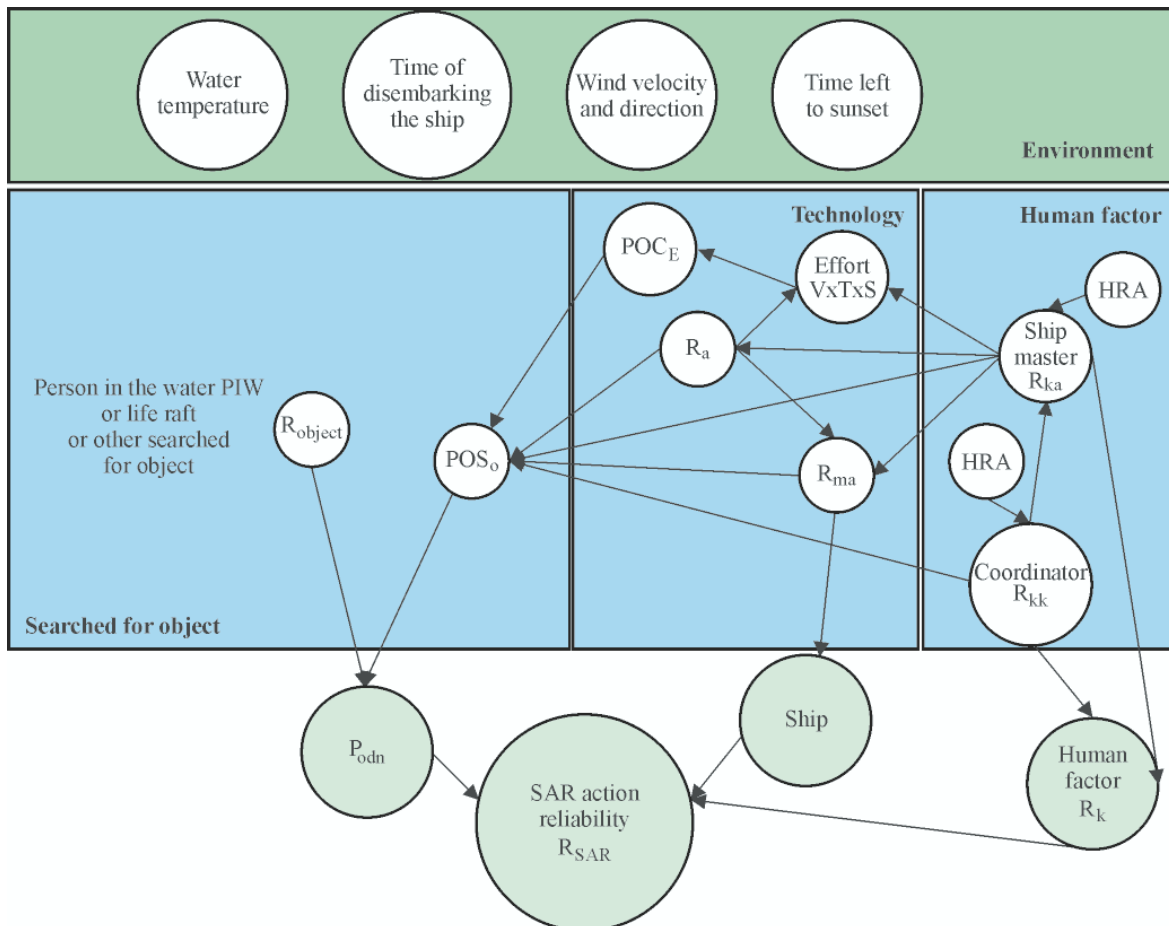
Fig. 2. The bayesian network for one search ship and one searched for object

Tab. 2. *Events, descriptions and states of bayesian network of SAR action*

Item	Description	State	
P_{odn}	probability of finding the searched object	high	low
R_a	technical operational reliability of the search ship (a)	technically serviceable/ stable	lack of technical serviceability /lack of stability on searching courses
POC_E	probability of containment of the object within a given search area (complying with an available effort of search ship)	location of the object complies with the assumed capability (effort) of the search ship	location of the object lies above the assumed capability (effort) of the search ship
R_E	effort aimed at possible finding the search object by the search ship	possibility of coping with the task	lack of possibility
POS_o	probability of reaching success in finding the searched for object	success	lack of success
R_{ka}	reliability of ship master and crew (experience, knowledge etc)	[sufficient] training acquired at sea	lack of sea training
R_{kk}	reliability of SAR action coordinator (experience, knowledge, practice etc)	experienced [enough]	lack of experience
R_{object}	reliability of life raft, a searched for object	[sufficient] reliability	unreliability
R_{ma}	reliability of the ship (a) assigned to SAR action	[sufficient] seaworthiness	lack of seaworthiness
HRA	human reliability assessment,	lack of errors /lack of stress	errors/stress
S_p	probability of survival in water (PIW)	reliability	unreliability

INFLUENCE OF POC ON RELIABILITY OF SAR ACTION

Search area [10, 11] may be determined for:
1) capabilities of the search ships (a + b + c).
The available effort of search ship is as follows:

$$Z = V \cdot T \cdot W$$

where:
Z – available effort of search ship
V – speed of the ship sweeping a given area,
T – assumed time for SAR action, time left to sunset
W – sweep band width

2) the assumed probability of containment of searched for object, POC, [2, 10, 11].
The detection probability equation in relation to a detector under monotonous motion is expressed as follows [7, 9]:

$$p(x) = 1 - e^{-\frac{2kh_O}{Vx^2}}$$

where:
k – detection factor
h_O – location height of observer
x – transverse distance between observer and sensor

By integrating the above given function it is possible to determine the sweep width W, [7, 9]:

$$W = \int_{-\infty}^{+\infty} 1 - e^{-\frac{2kh_O}{Vx^2}} dx = 2\sqrt{\frac{2\pi kh_O}{V}}$$

Example
SAR action has to be undertaken for the following searched for objects: 6-person life rafts and a person in the water (PIW)

in the following hydrometeorological conditions: cloud ceiling of 300 m, 7-9°B, water temperature of 20°C, visibility up to 5 NM, wave height of 1÷1,5 m. Time left to sunset of 4 h. Three ships: (a), (b) and (c) are engaged in the action;. the search area A_o = 100 [NM²]

Areas for Z values - the available efforts of the search ships (a), (b) and (c):
- for the ship (a) at V=16 kn:

$$Z = V \cdot T \cdot W = 16 \cdot 4 \cdot 0.25 = 16.0 \text{ [NM}^2\text{]}$$

$POC_a = 0.71$

- for the ship (b) at V=9 kn:

$$Z = V \cdot T \cdot W = 9 \cdot 4 \cdot 0.25 = 9.0 \text{ [NM}^2\text{]}$$

$POC_b = 0.58$

- for the ship (c) at V=4 kn:

$$Z = V \cdot T \cdot W = 4 \cdot 4 \cdot 0.25 = 4.0 \text{ [NM}^2\text{]}$$

$POC_c = 0.27$

where:
T – assumed time for SAR action, time left to sunset

The sweep band width determined for PIW:
- acc. Table N-4 – Sweep width for merchant vessels 0.5 NM, [10, 11]
- acc. Table N-7 – Weather correction factors for all types of search facilities 0.5 [10, 11]

For the area swept by the search ship (a):

$$Z = V \cdot T \cdot W = 16 \cdot 4 \cdot 0.25 = 16.0 \text{ [NM}^2\text{]}$$

(Expanding square search pattern acc. to IAMSAR [10, 11])

The total probability of SAR action reliability under the made assumptions:

- **POC$_a$ = 0.71**
- influence of human factor: $R_{kk} = 0.85$
- influence of search ship: $R_{ma} = 0.81$
- influence of finding- the- object parameter: $P_{odn} = 0.48$

  R_{SAR} = 0.57

For the area swept by the search ship (b):

$$Z = V \cdot T \cdot W = 9 \cdot 4 \cdot 0.25 = 9.0 \; [NM^2]$$

(Expanding square search pattern)

The total probability of SAR action reliability under the made assumptions:
- **POC$_b$ = 0.58**
- influence of human factor: $R_{kk} = 0.85$
- influence of search ship: $R_{ma} = 0.81$
- influence of finding- the- object parameter: $P_{odn} = 0.45$

  R_{SAR} = 0.53

For the area swept by the search ship (c):

$$Z = V \cdot T \cdot W = 4 \cdot 4 \cdot 0.25 = 4.0 \; [NM^2]$$

(Expanding square search pattern)

The total probability of SAR action reliability under the made assumptions:
- **POC$_c$ = 0.27**
- influence of human factor: $R_{kk} = 0.85$
- influence of search ship: $R_{ma} = 0.81$
- influence of finding- the- object parameter: $P_{odn} = 0.36$

  R_{SAR} = 0.49

The probabilities POC$_a$, POC$_b$, POC$_c$, are decisive for the reliability R_{SAR}
- POC = 0.99 R_{SAR} = 0.67 (for search area A_o = 100 [NM^2])
- POC$_a$ = 0.71 R_{SAR} = 0.57 for the ship (a)
- POC$_b$ = 0.58 R_{SAR} = 0.53 for the ship (b)
- POC$_c$ = 0.27 R_{SAR} = 0.49 for the ship (c)

0.00%	0.00%	0.01%	0.03%	0.06%	0.06%	0.03%	0.01%	0.00%	0.00%
0.00%	0.02%	0.09%	0.24%	0.38%	0.38%	0.24%	0.09%	0.02%	0.00%
0.01%	0.09%	0.38%	1.00%	1.61%	1.61%	1.00%	0.38%	0.09%	0.01%
0.03%	0.24%	1.00%	2.60%	4.19%	4.19%	2.60%	1.00%	0.24%	0.03%
0.06%	0.38%	1.61%	4.19%	6.76%	6.76%	4.19%	1.61%	0.38%	0.06%
0.06%	0.38%	1.61%	4.19%	6.76%	6.76%	4.19%	1.61%	0.38%	0.06%
0.03%	0.24%	1.00%	2.60%	4.19%	4.19%	2.60%	1.00%	0.24%	0.03%
0.01%	0.09%	0.38%	1.00%	1.61%	1.61%	1.00%	0.38%	0.09%	0.01%
0.00%	0.02%	0.09%	0.24%	0.38%	0.38%	0.24%	0.09%	0.02%	0.00%
0.00%	0.00%	0.01%	0.03%	0.06%	0.06%	0.03%	0.01%	0.00%	0.00%

H
(10×10)

Fig. 3. *Location of a searched for object, under assumption of normal distribution [10, 11]*

The faultlessly performed SAR action consists in:
- lack of stress, highly experienced ship master: $R_{ka} = 1.0$, and highly experienced coordinator of the action: $R_k = 1.0$,
- high technical operational effectiveness: $R_a = 1.0$, and high seaworthiness of the search ship: $R_{ma} = 1.0$
- maximum possible effort for sweeping the assigned area, POC = 0.71.

In the case of a faultlessly performed SAR action (for POC = 0.71) the initial reliability POS$_o$ = 0.62 increases to POS$_o$ = 0.76.

PROBABILITY OF FINDING A SEARCHED FOR OBJECT DURING SAR ACTION

The search area A_o constitutes a part of water area limited by a circle determined by its centre placed in the reference point P_o, and the optimum sweeping radius R_o within which the probability of containment of searched for object is equal to POC = 0.999.

According to IAMSAR [10, 11]:
- The optimum search area (in case of its circular form):

$$A_o = 4 \cdot R_o^2$$

- The search area cover factor:

$$C = Z/A_o$$

- The SAR action success probability acc. IAMSAR [10, 11]:

$$POS = POD \cdot POC$$

The SAR action success probability POS is the product of the detection probability POD and the probability of containment of the object within a given area, POC.

The detection probability POD, [10, 11], depends on the area cover factor C.

The detection probability POD [7]:

$$POD = 1 - e^{-C}$$

where:
A$_o$ – search area
POS – success probability
POC – containment probability of the object within a given search area
R$_o$ – search area radius
C – search area cover factor
POD – detection probability

In the presented bayesian network the probability of finding the searched for object, P_{odn}, depends on reaching success of the SAR action conducted within a given area and reliability of the searched for object:

$$P_{odn} = R_{object} \cdot POS_o$$

The probability of success in sweeping the search area POS$_o$ (bayesian network) takes into account the coordinator reliability R_k, ship master reliability R_{ka}, ship's technical operational reliability R_a, its seaworthiness R_{ma}, probability of containment of searched for object within a given area, POC$_E$.

The probability of finding the searched for object P$_{odn}$ (bayesian network) takes into account the reliability of the searched for object (S_p and R_{object}), as well as the probability of success in sweeping a given area, POS$_o$, in contrast to the IAMSAR recommendations [8, 9], in which the area cover factor C = Z/A$_o$ and POC appear.

SAR ACTION RELIABILITY CONTROL

The elaborated bayesian network which enables to determine the SAR action reliability R_{SAR}, may be used to control reliability. Obviously, SAR action coordinator will not be able to influence all events of the bayesian network. There will appear such parameters as the life raft safety function – the reliability R_{tr} or the survival probability of object- in- water, S_p, on which he would have only a minor influence since a properly planned action resulting in shortening duration time of the action would improve the reliability S_p in contrast to the R_{tr} which is directly affected by wind velocity.

The approach based on the control of reliability of subjects and elements of SAR action system is composed of the following phases:
1. Determination of reliability of subjects and elements of SAR action system.
2. Reliability estimation:
   a. assessment and determination of limit reliability parameters enabling SAR operations
3. Selection and hire of SAR subjects for SAR action with taking into account their reliability values.
4. Current control of reliability parameters of SAR action subjects and elements:
   a. changes in the planning and executing of SAR action system aimed at improving reliability of the elements whose reliability really lowers the whole action reliability R_{SAR}
5. Elimination of such SAR action subjects whose reliability parameters could lead to hazardous situation – break down of SAR action.
6. Monitoring the reliability parameters of SAR action elements.

The general principles of reliability evaluation are proposed as follows:
- low risk if: $R_{SAR} \geq 0.7$
  - SAR action should be monitored (admissible level)
- moderate risk if: $0.7 \geq R_{SAR} \geq 0.5$
  - reliability of an element/elements which lower SAR action reliability should be improved (admissible level, reservedly)
- high risk if: $R_{SAR} \leq 0.5$

- this level should not be allowed to happen. Such drop will make the action dangerous, i.e. causing hazards to SAR action personnel and sea environment, and leading to loss of rescue ships. SAR action will end without any success (inadmissible level).
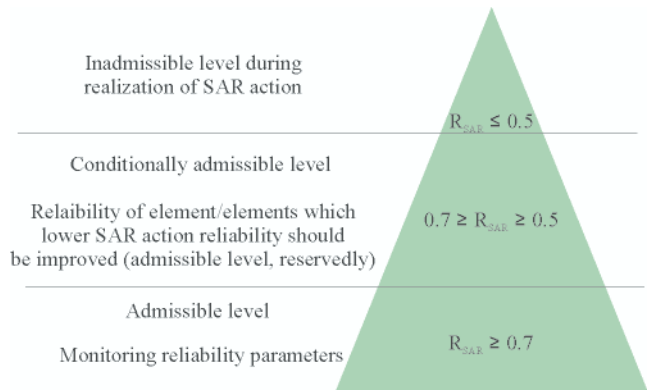
Fig. 5. *Scheme of the application of the reliability principles to SAR action*

To improve the reliability $\mathbf{R_{SAR}}$ the following steps should be made:
− to estimate the reliability parameters,
− to select only such elements which are able to bring effectively and fast a definite improvement of reliability,
− to decide whether the changes introduced to the system are realistic and capable of improving its reliability.
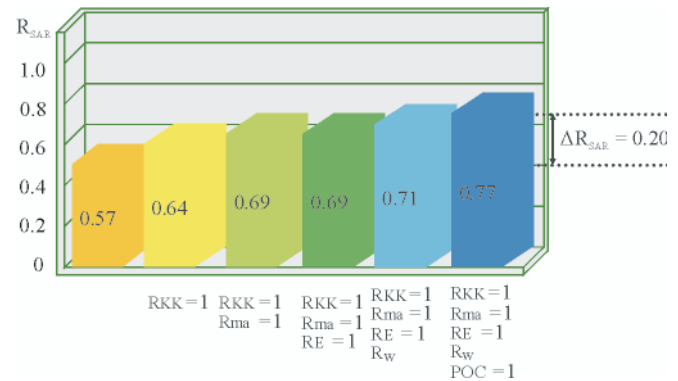
Fig. 6. *The reliability increase $\Delta R_{SAR} = 0.20$ by improving reliability of selected elements of SAR action (an example of reliability control)*
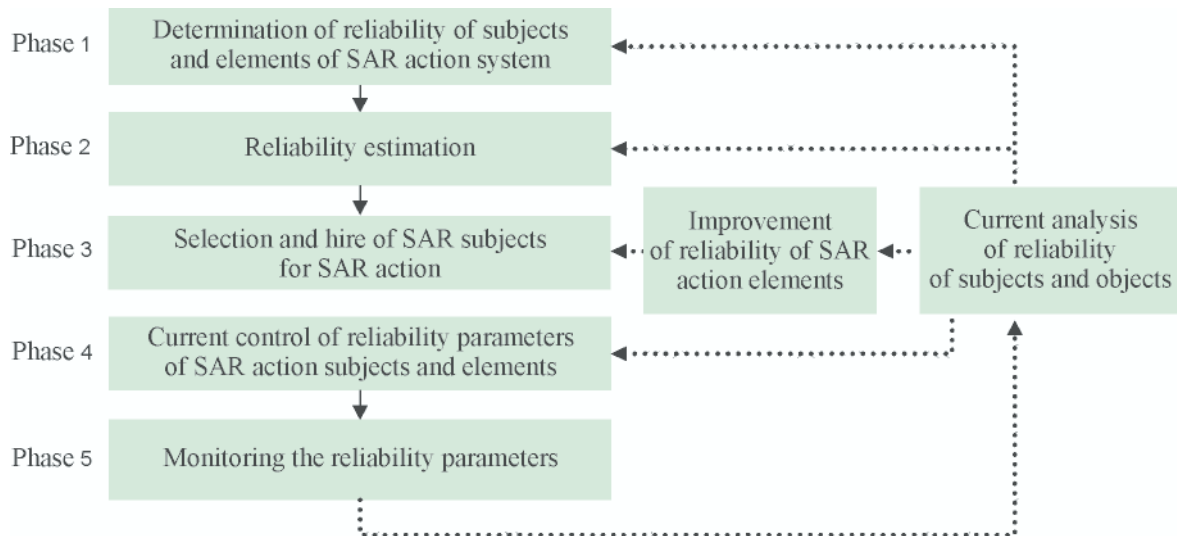
Fig. 4. *SAR action reliability control diagram*

The improvement of reliability of the selected elements of SAR action system as a result of the reliability control will improve the SAR action reliability R_{SAR}, up to its admissible level: $\mathbf{R_{SAR} = 0.77}$. Hence the action should be continued.

Tab. 3. Influence of reliability of ship master and SAR action coordinator on the SAR action reliability R_{SAR}

R	Description	[-]	[-]	[-]	[-]	[-]	[-]	[-]
R_k	SAR action coordinator reliability	**0.89**	0	0.54	**0**	1.0	0.93	**1.0**
R_{ka}	Ship master reliability	**0.87**	0.48	0	**0**	0.92	1.0	**1.0**
R_{SAR}	SAR action reliability	**0.57**	0.26	0.16	**0.1**	0.61	0.61	**0.64**

The following results from Tab. 3:
- The lack of sea practice and experience in qualifications of ship master and SAR action coordinator results in that the planned SAR action is from the very beginning doomed to failure as $\mathbf{R_{SAR} = 0.1}$.
- The drop in the SAR action coordinator reliability R_{kk} results in the drop of the ship master reliability R_{ka} and vice versa the drop in the ship master reliability lowers the drop in SAR action coordinator reliability (lack of communication).
- The high level of experience/sea practice in qualifications of ship master or coordinator makes mutually the coordinator's or ship master's reliability increasing (good communication, understanding) that leads to $\mathbf{R_{SAR} = 0.64.}$

Example

A$_1$ — the event consisting in that the ship master takes decision on searching for a castaway in an assigned area,

A$_2$ — the event consisting in that the coordinator takes decision on locating a castaway in the same area as that assigned by the ship master,

B — the event consisting in finding a castaway in the assigned area,

$\overline{B}$ — the event consisting in not finding a castaway in the assigned area: P(B) = 0.6, P($\overline{B}$) = 0.4

$P(A_1|B) = 0.6$ - probability of correctness of the ship master's inference concerning location of a castaway,

$P(A_1|\overline{B}) = 0.5$ - probability of incorrectness of the ship master's inference concerning location of a castaway,

$P(A_2|B) = 0.7$ - probability of correctness of the coordinator's inference,

$P(A_2|\overline{B}) = 0.5$ - probability of that the castaway is not located within the area assigned by the coordinator (incorrect assumption made by the coordinator).

By using Bayes theorem the following values of the probability of finding the castaway within the area assigned by the ship master and coordinator, are obtained:

$$P(B|A_1) = \frac{P(B)P(A_1|B)}{P(B)P(A_1|B) + P(\overline{B})(P(A_1|\overline{B})} =$$

$$= \frac{0.6 \cdot 0.6}{0.6 \cdot 0.6 + 0.4 \cdot 0.5} = \frac{36}{56} = \frac{9}{14} = 0.6428$$

$$P(B|A_2) = \frac{P(B)P(A_2|B)}{P(B)P(A_2|B) + P(\overline{B})(P(A_2|\overline{B})} =$$

$$= \frac{0.6 \cdot 0.7}{0.6 \cdot 0.7 + 0.4 \cdot 0.5} = \frac{42}{62} = \frac{21}{31} = 0.6774$$

It can be assumed that the events A_1 and A_2 do not depend to each other. Then on the basis of the Bayes formula the probabilities of finding the castaway can be estimated if only the opinions of both the ship master and coordinator have been accounted for simultaneously:

$$P(B|A_1 \cap A_2) = \frac{P(B)P(A_1 \cap A_2|B)}{P(B)P(A_1 \cap A_2|B) + P(\overline{B})P(A_1 \cap A_2|\overline{B})} =$$

$$= \frac{P(B)P(A_1|B)P(A_2|B)}{P(B)P(A_1|B)P(A_2|B) + P(\overline{B})P(A_1|\overline{B})P(A_2|\overline{B})}$$

$$P(B|A_1 \cap A_2) = \frac{0.6 \cdot 0.6 \cdot 0.7}{0.6 \cdot 0.6 \cdot 0.7 + 0.4 \cdot 0.5 \cdot 0.5} =$$

$$= \frac{252}{362} = 0.7159$$

The example shows that accounting for two opinions may increase probability of success of SAR action.

In planning and executing SAR action, an additional information, e.g. provided by ship master, introduced to the Bayes theorem, leads to a higher accuracy of evaluation of a planned and executed SAR action.

CONCLUSIONS

- The determined reliability measure of SAR action based on the elaborated bayesian network will allow for influencing safety of to-be-rescued people and rescueing personnel.
- Bayesian network elaborated by a SAR action coordinator would be subjective. However, if elaborated on the basis of experience and sea practice of the coordinator aided by a team of advisors (e.g. by brain storming), it will be capable of reflecting reality of a realized SAR action.
- Every SAR action planned by its coordinator should be aided by an appropriate bayesian network which makes it possible to evaluate reliability of a planned and executed SAR action.
- During execution of coordinated SAR action it will be possible to monitor and control its reliability.
- The bayesian network makes it possible to account for more parameters and thus becomes more reliable for SAR action coordinator, that is especially important in the case of action realized on the basis of incomplete and uncertain information.

BIBLIOGRAPHY

1. Arden C. Turner: Survival of Distressed Mariners. United States Coast Guard, Research and Development Center Groton, Connecticut. Seatechweek Brest 2008.
2. Burciu Z.: Search domain modelling in the aspect of transport safety of people at sea (in Polish). Prace Naukowe (Scientific Bulletin), Transport No.50, Oficyna Wydawnicza Politechniki

Warszawskiej (Publishing House of Warsaw University of Technology), Warsaw 2003

3. Burciu Z.: The disturbances of the life raft leeway induced by the fluctuations of wind direction in the life raft coordinate system. Polish Maritime Research No.S2/2007

4. Burciu Z.: The influence of south Baltic hydro-meteorological conditions on determining the survivors search domain. Polish Maritime Research No. 3/2003

5. Burciu Z.: Safety in shipping by sea Search and rescue (SAR) (in Polish). A monograph (to be published)

6. Burciu Z., Grabski F.: The experimental and theoretical study on the reliability of life rafts. Submitted for publication in Reliability Engineering & System Safety, Elsevier

7. Frost J.R., Principles of Search Theory. 2000. Principles%20of% 20Search%20Theory.pdf

8. Grabski F., Jaźwiński J.: Metody Bayesian methods in reliability and diagnostics (in Polish).Wydawnictwo Komunikacji i Łączności (Transport and Telecommunication Publishing House),Warsaw 2001

9. Koopman B.O.: Search and Screening. Military Operations Research Society, Alexandria, Virginia 1999

10.IMO/ICAO: International Aeronautical and Maritime Search and Rescue Manual. Vol. II. London/Montreal 1999

11.IMO/ICAO: IAMSAR - International Aeronautical and Maritime Search and Rescue Manual, Volume II, Mission Co-Ordination. 2008 Edition (incorporating 2001, 2002, 2003, 2004, 2005, 2006 and 2007 amendments), London/Montreal 2008

12.Resistance tests of three life rafts (in Polish). Delivery-acceptance act, Contract No. RH/862-20/2000, Centrum Techniki Okrętowej(Ship Design and Research Centre) Gdańsk 2000

13.Aerodynamical tests of inflatable life rafts in the wind tunnel of 5m - diameter (in Polish). Research report No.168/BA/2000/D, Instytut Lotnictwa (Aeronautical Institute),Warsaw 2000.

CONTACT WITH THE AUTHOR

Zbigniew Burciu, Assoc. Prof.
Faculty of Navigation,
Gdynia Maritime University
Aleja Jana Pawła II 3
81-345 Gdynia, POLAND
e-mail: zbj@am.gdynia.pl

The Ship Handling Research and Training Centre at Ilawa is owned by the Foundation for Safety of Navigation and Environment Protection, which is a joint venture between the Gdynia Maritime University, the Gdansk University of Technology and the City of Ilawa.

Two main fields of activity of the Foundation are:

➲ Training on ship handling. Since 1980 more than 2500 ship masters and pilots from 35 countries were trained at Iława Centre. The Foundation for Safety of Navigation and Environment Protection, being non-profit organisation is reinvesting all spare funds in new facilities and each year to the existing facilities new models and new training areas were added. Existing training models each year are also modernised, that's why at present the Centre represents a modern facility perfectly capable to perform training on ship handling of shipmasters, pilots and tug masters.

➲ Research on ship's manoeuvrability. Many experimental and theoretical research programmes covering different problems of manoeuvrability (including human effect, harbour and waterway design) are successfully realised at the Centre.

The Foundation possesses ISO 9001 quality certificate.

Why training on ship handling?

The safe handling of ships depends on many factors - on ship's manoeuvring characteristics, human factor (operator experience and skill, his behaviour in stressed situation, etc.), actual environmental conditions, and degree of water area restriction.

Results of analysis of CRG (collisions, rammings and groundings) casualties show that in one third of all the human error is involved, and the same amount of CRG casualties is attributed to the poor controllability of ships. Training on ship handling is largely recommended by IMO as one of the most effective method for improving the safety at sea. The goal of the above training is to gain theoretical and practical knowledge on ship handling in a wide number of different situations met in practice at sea.

For further information please contact:
The Foundation for Safety of Navigation and Environment Protection

Head office:
36, Chrzanowskiego Street
80-278 GDAŃSK, POLAND
tel./fax: +48 (0) 58 341 59 19

Ship Handling Centre:
14-200 IŁAWA-KAMIONKA, POLAND
tel./fax: +48 (0) 89 648 74 90
e-mail: office@ilawashiphandling.com.pl
e-mail: office@portilawa.com

GDANSK UNIVERSITY OF TECHNOLOGY

is the oldest and largest scientific and technological academic institution in the Pomeranian region. The history of Gdansk University of Technology is marked by two basic dates, namely: October 6, 1904 and May 24, 1945.

The first date is connected with the beginning of the technical education at academic level in Gdansk. The second date is connected with establishing of Gdansk University of Technology, Polish state academic university. Gdansk University of Technology employ 2,500 staff, 1,200 whom are academics. The number of students approximates 20,000, most of them studying full-time. Their career choices vary from Architecture to Business and Management, from Mathematics and Computer Science to Biotechnology and Environmental Engineering, from Applied Chemistry to Geodesics and Transport, from Ocean Engineering to Mechanical Engineering and Ship Technology, from Civil Engineering to Telecommunication, Electrical and Control Engineering. Their life goals, however, are much the same - to meet the challenge of the changing world. The educational opportunities offered by our faculties are much wider than those of other Polish Technical universities, and the scientific research areas include all of 21st Century technology. We are one of the best schools in Poland and one of the best known schools in Europe – one that educates specialists excelling in the programming technology and computer methods used in solving complicated scientific, engineering, organizational and economic problems.

THE FACULTY OF OCEAN ENGINEERING AND SHIP TECHNOLOGY

The Faculty of Ocean Engineering and Ship Technology (FOEST) as the only faculty in Poland since the beginning of 1945 has continuously been educating engineers and doctors in the field of Naval Architecture and Marine Technology.

The educational and training activities of FOEST are supported by cooperation with Polish and foreign universities, membership in different international organizations and associations, as well as participation in scientific conferences and symposia. Hosting young scientists and students from different countries is also a usual practice in FOEST.

The activities of Faculty departments are related to: mechanics and strength of structures, hydromechanics, manufacturing, materials and system quality, power plants, equipment and systems of automatic control, mostly in shipbuilding, marine engineering and energetic systems.

FOEST is a member of such organizations like WEGEMT; The Association of Polish Maritime Industries and the co-operation between Nordic Maritime Universities and Det Norske Veritas. The intensive teaching is complemented and supported by extensive research activities, the core of which is performed in close collaboration between FOEST staff and industry. We take great care to ensure that the applied research meet both the long term and short term needs of Polish maritime industry. FOEST collaborates with almost all Polish shipyards. Close links are maintained with other research organizations and research institutions supporting the Polish maritime industry, such as Ship Design and Research Centre and Polish Register of Shipping, where several members of the Faculty are also members of the Technical Board.

The Faculty of Ocean Engineering and Ship Technology is a unique academic structure, which possesses numerous highly qualified and experienced staff in all above mentioned specific research areas. Moreover, the staff is used to effective co-operation and exchange of ideas between specialists of different detailed areas. This enables a more integrated and comprehensive treatment of research and practical problems encountered in such a complicated field of activity as naval architecture, shipbuilding and marine engineering.

The staff of the Faculty has strong international links worldwide, being members or cooperating with international organizations like International Maritime Organization IMO, International Towing Tank Conference ITTC, International Ship and Offshore Structures Congress ISSC, International Conference on Practical Design of Ship and other floating Structures PRADS just to name a few.

GDANSK UNIVERSITY OF TECHNOLOGY
Faculty of Ocean Engineering and Ship Technology
11/12 Narutowicza Street, 80-952 Gdansk, Poland
Tel (+48) 58 347 1548 ; Fax (+48) 58 341 4712
e-mail: sekoce@pg.gda.pl

www.oce.pg.gda.pl